Vol. 9, no. 3, 2025 eISSN 2587-8999
PEER-REVIEWED SCIENTIFIC AND THEORETICAL JOURNAL

Computational Mathematics and Information Technologies

Computational Mathematics

Mathematical Modelling

Information Technologies

www.cmit-journal.ru
DOI 10.23947/2587-8999

Computational Mathematics and Information Technologies

Peer-reviewed scientific and theoretical journal

eISSN 2587–8999

Published since 2017

Periodicity — 4 issues per year

DOI: 10.23947/2587–8999

Founder and Publisher — Don State Technical University (DSTU), Rostov-on-Don, Russian Federation

The journal "Computational Mathematics and Information Technologies" publishes reviews, original articles and short reports on mathematical modeling, numerical methods and information technologies for solving complex and topical problems of science and modern technology. Research areas include continuum mechanics, fluid dynamics, Earth sciences, chemistry, biology, image processing and pattern recognition, parallel computing theory and its applications, big database and artificial intelligence technologies, etc.

The journal "Computational Mathematics and Information Technologies" accepts scientific and review articles for publication in accordance with the sections:

1. Computational Mathematics
2. Mathematical Modelling
3. Information Technologies

Registration:	Mass media registration certificate ЭЛ № ФС 77–66529 dated July 21, 2016 issued by the Federal Service for Supervision of Communications, Information Technology and Mass Media
Indexing and Archiving:	RISC, Crossref, Cyberleninka
Website:	https://cmit-journal.ru
Address of the Editorial Office:	1, Gagarin sq., Rostov-on-Don, 344003, Russian Federation
E-mail:	CMIT-EJ@yandex.ru
Telephone:	+7 (863) 273–85–14
Date of publication No. 3, 2025:	30.09.2025

Computational Mathematics and Information Technologies

Рецензируемый научно-теоретический журнал

eISSN 2587–8999

Издается с 2017 года

Периодичность — 4 выпуска в год

DOI: 10.23947/2587–8999

Учредитель и издатель — Федеральное государственное бюджетное образовательное учреждение высшего образования «Донской государственный технический университет» (ДГТУ), г. Ростов-на-Дону, Российская Федерация

Журнал «Computational Mathematics and Information Technologies» публикует обзоры, оригинальные статьи и краткие сообщения, посвященные математическому моделированию, численным методам и информационным технологиям для решения сложных и актуальных проблем науки и современной технологии. Область применения исследований — это механика сплошных сред, гидроаэродинамика, науки о Земле, химия, биология, обработка изображений и распознавание образов, теория параллельных вычислений и ее приложения, технологии больших баз данных и искусственного интеллекта и т. д.

Журнал «Computational Mathematics and Information Technologies» принимает к публикации научные и обзорные статьи в соответствии с разделами:

1. Вычислительная математика
2. Математическое моделирование
3. Информационные технологии

Регистрация:	Свидетельство о регистрации средства массовой информации ЭЛ № ФС 77 – 66529 от 21 июля 2016 г., выдано Федеральной службой по надзору в сфере связи, информационных технологий и массовых коммуникаций
Индексация и архивация:	РИНЦ, CrossRef, CyberLeninka
Сайт:	https://cmit-journal.ru
Адрес редакции:	344003, Российская Федерация, г. Ростов-на-Дону, пл. Гагарина, 1
E-mail:	CMIT-EJ@yandex.ru
Телефон:	+7 (863) 273–85–14
Дата выхода № 3, 2025 в свет:	30.09.2025

Contents

COMPUTATIONAL MATHEMATICS

Multistage Grid-Characteristic Method of Increased Order of Accuracy for Acoustic Problems 7
Xin Mi, Vasily I. Golubev

Approximation of Boundary Conditions of the Second and Third Types in Convection–Diffusion Equations with Applications to Environmental Hydrophysics 16
Alexander I. Sukhinov, Valentina V. Sidoryakina

Modelling Circulation in Blood Vessel Aneurysms 30
Natalya K. Volosova, Konstantin A. Volosov, Aleksandra K. Volosova, Mikhail I. Karlov, Dmitriy F. Pastukhov, Yuriy F. Pastukhov

MATHEMATICAL MODELLING

Adaptive Grid Techniques for the Efficient Simulation of Shallow Coastal Systems 44
Alexander I. Sukhinov, Sofia V. Protsenko, Elena A. Protsenko

Application of Neural Networks to Steady-State Oscillations 56
Alexander V. Galaburdin

Содержание

ВЫЧИСЛИТЕЛЬНАЯ МАТЕМАТИКА

Многостадийный сеточно-характеристический метод повышенного порядка точности для задач акустики 7
С. Ми, В.И. Голубев

Аппроксимация граничных условий второго и третьего рода в краевых задачах для уравнений конвекции-диффузии с приложением к экологической гидрофизике 16
А.И. Сухинов, В.В. Сидорякина

Моделирование циркуляции в аневризмах кровеносных сосудов 30
Н.К. Волосова, К.А. Волосов, А.К. Волосова, М.И. Карлов, Д.Ф. Пастухов, Ю.Ф. Пастухов

МАТЕМАТИЧЕСКОЕ МОДЕЛИРОВАНИЕ

Адаптивные сеточные методы для эффективного моделирования динамики мелководных прибрежных систем 44
А.И. Сухинов, С.В. Проценко, Е.А. Проценко

Применение нейронных сетей для решения задачи об установившихся колебаниях 56
А.В. Галабурдин

COMPUTATIONAL MATHEMATICS
ВЫЧИСЛИТЕЛЬНАЯ МАТЕМАТИКА

UDC 519.6

Original Empirical Research

https://doi.org/10.23947/2587-8999-2025-9-3-7-15

Multistage Grid-Characteristic Method of Increased Order of Accuracy for Acoustic Problems

Xin Mi[1] ✉, **Vasily I. Golubev**[1,2]

[1] Moscow Institute of Physics and Technology, Dolgoprudny, Russian Federation

[2] Scientific Research Institute for System Analysis of the National Research Centre "Kurchatov Institute", Moscow, Russian Federation

✉ xinawafe@gmail.com

Abstract

Introduction. Seismic exploration is a widely used technology for locating hydrocarbon deposits. An important stage of this process is the simulation of seismic wave propagation in a geological model of the medium with specified physical characteristics. Due to the high computational cost of this problem, the acoustic approximation is widely used in practice, allowing for the correct description of longitudinal wave propagation. The most common approach to seismic modeling is the use of finite-difference schemes on staggered Cartesian computational grids. Despite their simplicity of implementation and high computational efficiency, such methods exhibit insufficient accuracy when modelling complex geological structures, including curvilinear interfaces between geological layers. A promising direction is the development of new high-order computational methods on curvilinear computational grids. This paper presents a stable fifth-order grid-characteristic method successfully applied to solving the problem of acoustic wave propagation in the two-dimensional case.

Materials and Methods. The study employs a grid-characteristic method with a fifth-degree interpolation polynomial constructed on an extended spatial stencil. A class of curvilinear grids is identified that makes it possible to retain the accuracy achieved when solving a one-dimensional problem. Furthermore, the use of a multistage splitting method allows the preservation of the scheme's order in both time and space for multidimensional formulations.

Results. The formulas of the computational algorithm are presented, the achievement of the declared convergence order is empirically confirmed, and wavefield patterns of the dynamic process are calculated.

Discussion. The results demonstrate lower numerical dissipation of the proposed computational algorithm. The trade-off for this improvement is a significant increase in computation time.

Conclusion. The developed computational algorithm ensures high accuracy in calculating seismic fronts, which is critically important for seismic exploration tasks in layered geological massifs.

Keywords: seismic exploration, seismic waves, mathematical modelling, curvilinear grids, acoustic medium, grid-characteristic method, operator splitting

Funding. The work was carried out within the framework of the state task of the NRC "Kurchatov Institute" — SRISA on the topic No. FNEF–2024–0002 "Mathematical modeling of multi-scale dynamic processes and virtual environment systems" (1023032900401–5–1.2.1). Mi Xin's research work was supported by a scholarship from the China Scholarship Council.

For Citation. Mi X., Golubev V.I. Multistage Grid-Characteristic Method of High Order of Accuracy for Acoustic Problems. *Computational Mathematics and Information Technologies*. 2025;9(3):7–15. https://doi.org/10.23947/2587-8999-2025-9-3-7-15

Оригинальное эмпирическое исследование

Многостадийный сеточно-характеристический метод повышенного порядка точности для задач акустики

С. Ми[1] ✉, **В.И. Голубев**[1,2]

[1] Московский физико-технический институт, г. Долгопрудный, Российская Федерация

[2] Федеральное государственное автономное учреждение «Федеральный научный центр Научно-исследовательский институт системных исследований Национального исследовательского центра «Курчатовский институт»,
г. Москва, Российская Федерация

✉ xinawafe@gmail.com

Аннотация

Введение. Сейсмическая разведка является широко применяемой технологией поиска месторождений углеводородов. Важным этапом данного процесса является расчёт распространения сейсмических волн в геологической модели среды с заданными физическими характеристиками. Ввиду высокой вычислительной сложности задачи на практике активно используется акустическое приближение, позволяющее корректно описать распространение продольных волн. Наиболее часто для сейсмического моделирования используются конечно-разностные схемы на сдвинутых кубических расчётных сетках. Несмотря на простоту их реализации и высокую вычислительную эффективность, такие подходы демонстрируют недостаточную точность при моделировании сложных геологических структур, включая криволинейные границы раздела геологических слоёв. Перспективным направлением является разработка новых вычислительных методов высокого порядка точности на криволинейных расчётных сетках. В настоящей работе представлен устойчивый сеточно-характеристический метод пятого порядка аппроксимации, успешно применённый для решения задачи о распространении акустических волн в двумерной постановке.

Материалы и методы. Используется сеточно-характеристический метод с интерполяционным полиномом пятой степени, построенном на расширенном пространственном шаблоне. Выделен класс криволинейных сеток, позволяющий сохранить достигнутую при решении одномерной задачи точность расчёта. При этом с помощью метода многошагового расщепления удается сохранить порядок схемы по времени и по пространству в многомерной постановке.

Результаты исследования. Представлены формулы вычислительного алгоритма, эмпирически подтверждено достижение заявленного порядка сходимости, рассчитаны волновые картины динамического процесса.

Обсуждение. Результаты расчётов демонстрируют меньшую численную диссипацию предложенного вычислительного алгоритма. Платой за это является значимое увеличение времени расчёта.

Заключение. Разработанный расчётный алгоритм обеспечивает высокую точность расчёта сейсмических фронтов, что критически важно в задачах сейсморазведки в слоистых геологических массивах.

Ключевые слова: сейсмическая разведка, сейсмические волны, математическое моделирование, криволинейные сетки, акустическая среда, сеточно-характеристический метод, операторное расщепление

Финансирование. Работа выполнена в рамках государственного задания НИЦ «Курчатовский институт» — НИИСИ по теме № FNEF–2024–0002 «Математическое моделирование многомасштабных динамических процессов и системы виртуального окружения» (1023032900401–5–1.2.1). Исследования Ми Синь были поддержаны Китайским советом по стипендиям.

Для цитирования. Ми С., Голубев В.И. Многостадийный сеточно-характеристический метод повышенного порядка точности для задач акустики. *Computational Mathematics and Information Technologies*. 2025;9(3):7–15. https://doi.org/10.23947/2587-8999-2025-9-3-7-15

Introduction. Computer simulation of wavefields in heterogeneous media is widely used in geophysical research and plays a key role in solving problems of migration and inversion of seismic exploration data [1, 2]. Many different numerical methods applicable to solving the dynamic deformation problem of geological media have been developed by various research groups: the finite-difference method [3], the finite-element method [4], the discontinuous Galerkin method [5], and the spectral element method [6]. Among them, the finite-difference method remains the most frequently used in practice due to its ease of implementation and high computational efficiency.

One of the actively developing methods is the grid-characteristic method [7], which is used in the present work. In recent years, active development of modifications of the grid-characteristic method has been carried out on various types of computational grids: unstructured tetrahedral [8, 9], Cartesian [10–13], curvilinear structured [14], chimeric overlapping [15–17] for solving practical problems of seismic exploration [8, 10, 11, 15, 16], seismic resistance [12, 14], non-destructive testing of composite materials [18], and calculation of vibrations of railway tracks [13, 17].

In marine seismic exploration, seismic waves propagate both in an acoustic medium (water layer) and in an elastic medium (sea bottom and underlying geological massif). If the interface between the media is curvilinear, the finite-difference method encounters significant difficulties when attempting to correctly calculate the travel times of waves reflected from the bottom [19]. One possible way to improve the accuracy of specifying the geometry of the interface is to reduce the grid step, but this leads to a significant increase in the computational complexity of the problem [20]. To achieve a compromise between the increase in computational costs and a decrease in the accuracy of modelling, it is possible to combine the finite difference method with the coordinate transformation technique [21]. This approach is based on mapping a curvilinear computational grid coinciding with the layer boundary into a computationally convenient orthogonal grid using a sufficiently smooth coordinate transformation.

In this paper, we consider the problem of seismic wave propagation in an acoustic medium containing curvilinear layer interfaces. Using the inverse transformation from curvilinear to Cartesian coordinates allows us to apply a grid-characteristic method of increased accuracy order on an extended spatial stencil for a special class of computational grids. To eliminate the effect of reducing the order of approximation of a two-dimensional computational algorithm in time due to the use of coordinate-wise splitting, the method of multi-step operator splitting is used [22]. The computational experiments conducted confirm the high accuracy of calculations and the stability of the scheme when the standard Courant condition is met.

Materials and Methods. The dynamic behavior of a homogeneous acoustic medium under small deformations and in the absence of external volumetric forces is described by a hyperbolic system of equations of the form:

$$\begin{cases} \rho\dfrac{\partial\vec{v}}{\partial t}+\nabla p=\vec{0}, \\ \dfrac{\partial p}{\partial t}+\rho c^2\nabla\cdot\vec{v}=0. \end{cases}$$

The following notations are used here: ρ is the medium density; c is the P-wave propagation velocity; $p(x,y,z,t)$ is the pressure, $\vec{v}(x,y,z,t)=(u,v,w)^T$ is the velocity vector at the considered point of the acoustic medium. In the two-dimensional formulation of the problem considered in this paper, all the sought functions do not depend on the third spatial variable: $\dfrac{\partial\vec{v}}{\partial z}=\vec{0},\dfrac{\partial p}{\partial z}=0.$ Let the integration domain initially be covered by some curvilinear structural computational grid so that its sufficiently smooth mapping onto a uniform square computational region is possible (Fig. 1). Let the relationship between the original Cartesian coordinates x and y and transformed coordinates ξ and η is set explicitly as

$$\begin{cases} x=x(\xi,\eta), \\ y=y(\xi,\eta). \end{cases}$$

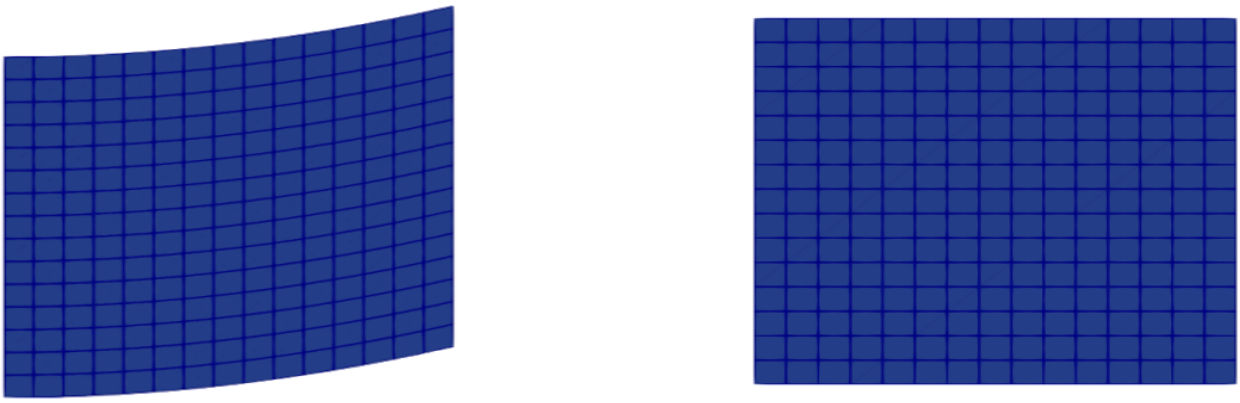

Fig. 1. The original curvilinear computational grid (x, y) (left) and the transformed square grid (ξ, η) (right)

By transitioning to new coordinates in the original system of equations, we obtain that

$$\frac{\partial p}{\partial t}+\rho c^2\frac{1}{|J|}\left[\left(\frac{\partial u}{\partial\xi}\frac{\partial y}{\partial\eta}-\frac{\partial u}{\partial\eta}\frac{\partial y}{\partial\xi}\right)\right]+\rho c^2\frac{1}{|J|}\left[\left(\frac{\partial v}{\partial\eta}\frac{\partial x}{\partial\xi}-\frac{\partial v}{\partial\xi}\frac{\partial x}{\partial\eta}\right)\right]=0,$$

$$\frac{\partial u}{\partial t}+\frac{1}{\rho}\frac{1}{|J|}\left(\frac{\partial p}{\partial \xi}\frac{\partial y}{\partial \eta}-\frac{\partial p}{\partial \eta}\frac{\partial y}{\partial \xi}\right)=0,$$

$$\frac{\partial v}{\partial t}+\frac{1}{\rho}\frac{1}{|J|}\left(\frac{\partial p}{\partial \eta}\frac{\partial x}{\partial \xi}-\frac{\partial p}{\partial \xi}\frac{\partial x}{\partial \eta}\right)=0,$$

where a new notation $|J|=\begin{vmatrix}\frac{\partial x}{\partial \xi} & \frac{\partial y}{\partial \xi}\\ \frac{\partial x}{\partial \eta} & \frac{\partial y}{\partial \eta}\end{vmatrix}$ is the Jacobi matrix.

This system of equations can be rewritten in canonical form:

$$\vec{q}_t+A_\xi\vec{q}_\xi+A_\eta\vec{q}_\eta=0.$$

The following additional notations are introduced here:

$$\vec{q}=(p,u,v)^T,$$

$$A_\xi=\begin{pmatrix}0 & \rho c^2\frac{1}{|J|}\frac{\partial y}{\partial \eta} & -\rho c^2\frac{1}{|J|}\frac{\partial x}{\partial \eta}\\ \frac{1}{\rho}\frac{1}{|J|}\frac{\partial y}{\partial \eta} & 0 & 0\\ -\frac{1}{\rho}\frac{1}{|J|}\frac{\partial x}{\partial \eta} & 0 & 0\end{pmatrix},$$

$$A_\eta=\begin{pmatrix}0 & -\rho c^2\frac{1}{|J|}\frac{\partial y}{\partial \xi} & \rho c^2\frac{1}{|J|}\frac{\partial x}{\partial \xi}\\ -\frac{1}{\rho}\frac{1}{|J|}\frac{\partial y}{\partial \xi} & 0 & 0\\ \frac{1}{\rho}\frac{1}{|J|}\frac{\partial x}{\partial \xi} & 0 & 0\end{pmatrix}.$$

To construct a numerical solution to this two-dimensional system of equations, one can use the method of splitting by spatial directions, thereby reducing the problem to a sequential solution of two one-dimensional problems

$$\vec{q}_t+A_\xi\vec{q}_\xi=0,$$

$$\vec{q}_t+A_\eta\vec{q}_\eta=0.$$

In this case, the solution of the first system of equations is the initial condition for solving the second system of equations. Note that this procedure allows us to construct a converging computational algorithm, which, however, in the general case has only the first order of approximation in time. This is due to the non-permutability of the operators associated with the matrices A_ξ and A_η.

Note that each of the one-dimensional systems with matrix $A_j(j=\xi,\eta)$ is hyperbolic and can be represented as follows:

$$A_j=\Omega_j^{-1}\Lambda_j\Omega_j,$$

$$\Lambda_\xi=\frac{1}{|J|}\sqrt{\left(\frac{\partial x}{\partial \eta}\right)^2+\left(\frac{\partial y}{\partial \eta}\right)^2}\,(c,-c,0),$$

$$\Lambda_\eta=\frac{1}{|J|}\sqrt{\left(\frac{\partial x}{\partial \xi}\right)^2+\left(\frac{\partial y}{\partial \xi}\right)^2}\,(c,-c,0).$$

The solution of a one-dimensional hyperbolic system with constant coefficients can be reduced to the solution of a spatial interpolation problem by transitioning to Riemann invariants according to the formula:

$$\vec{\omega}=\Omega_j\vec{q}.$$

For clarity, let us consider the procedure for constructing a solution to the problem along the direction ξ. Performing left multiplication of a system of equations by a matrix Ω_ξ and substituting the expressions obtained above into the original system of equations, under the conditions of independence Ω_ξ from ξ, we obtain, that

$$\vec{\omega}_t + \Lambda_\xi \vec{\omega}_\xi = 0.$$

For each equation from this system of one-dimensional independent transport equations with constant coefficients, according to their characteristic properties, the value at the next time layer is exactly determined by the following expression:

$$\vec{\omega}\left(\xi_m, t^n + \tau\right) = \vec{\omega}\left(\xi_m - \Lambda_\xi \tau, t^n\right).$$

When calculating the right-hand side of this equality, the procedure of interpolation by polynomials of a given degree on a fixed spatial stencil is used. In this work, a grid-characteristic scheme of the fifth order of approximation is used, constructed on a seven-point template using an interpolation polynomial of the fifth order [23]. Then the desired vector function $\vec{q} = (p,u,v)^T$, on the next time layer can be calculated using the formula (due to the non-degeneracy of the transformation):

$$\vec{q} = \Omega_\xi^{-1} \vec{\omega}.$$

Note that the structure of the matrix of eigenvectors can be written compactly in tensor form. We introduce the following notations for the directions corresponding to the axes ξ, η:

$$\overset{r}{n}_0 = \frac{1}{\sqrt{\left(\frac{\partial x}{\partial \eta}\right)^2 + \left(\frac{\partial y}{\partial \eta}\right)^2}} \begin{pmatrix} \frac{\partial y}{\partial \eta} \\ -\frac{\partial x}{\partial \eta} \end{pmatrix},$$

$$\overset{r}{n}_1 = \frac{1}{\sqrt{\left(\frac{\partial x}{\partial \xi}\right)^2 + \left(\frac{\partial y}{\partial \xi}\right)^2}} \begin{pmatrix} -\frac{\partial y}{\partial \xi} \\ \frac{\partial x}{\partial \xi} \end{pmatrix}.$$

Then the transition to Riemann invariants has the form:

$$\omega_{1,2} = \frac{1}{2}\vec{n}_0 \cdot \vec{v} \pm \frac{p}{2\rho c}, for\, \xi,$$

$$\omega_{1,2} = \frac{1}{2}\vec{n}_1 \cdot \vec{v} \pm \frac{p}{2\rho c}, for\, \eta.$$

As noted earlier, the use of this splitting method reduces the order of approximation of the two-dimensional scheme in time. To solve this problem, this paper uses multi-step operator splitting based on the use of fractional time steps [24]. In general, this calculation algorithm for each time step can be represented as follows:

for *i* in 1 ,..., *s*:

solve step along ξ: step $\xi\left(\alpha_i^\xi \tau\right)$,

solve step along η: step $\eta\left(\alpha_i^\eta \tau\right)$.

Coefficients $\alpha_i^j, i \in (1,2,...,s), j \in (\xi,\eta)$, defining the values of fractional time steps, uniquely determine the multi-step splitting scheme. It should be noted that it is possible to construct a non-unique scheme of a given order of approximation with a given number of stages. In this paper, a 5th-order multi-step splitting scheme with 7 stages was used [24]. Its coefficients are presented in Table 1.

Table 1

Coefficients of the used 5th order multi-step splitting scheme

i	α_i^ξ	α_i^η
1	0.475018345144539497	–0.402020995028838599
2	0.021856594741098449	0.345821780864741783
3	–0.334948298035883491	0.400962967485371350

End of table 1

i	α_i^{ξ}	α_i^{η}
4	0.512638174652696736	0.980926531879316517
5	–0.011978701020553904	–1.362064898669775624
6	–0.032120004263046859	0.923805029000837468
7	0.369533888781149572	0.112569584468347105

Results. The constructed two-dimensional grid-characteristic scheme was applied to model the process of propagation of a plane *P*-wave. The problem statement typical for the field of seismic exploration in a subhorizontal layered geological massif was considered. The computational domain was covered by a curvilinear computational grid specified by the following coordinate transformation:

$$\begin{cases} x = \xi, \\ y = \eta + \gamma\xi^2, \end{cases}$$

where $\gamma = 5 \cdot 10^{-4}$.

The advantage of this parameterization method is the independence of the eigenvectors and eigenvalues of the problem for steps along (ξ, η) of (ξ, η) accordingly. This allows you to bring a matrix Ω_j under the sign of differentiation with respect to the coordinate and construct an exact solution to the one-dimensional problem. The initial area of interest in Cartesian coordinates occupied a square with a side of 600 m. The acoustic characteristics of the medium were set equal to the following values: the density of the medium $\rho = 1000$ kg/m^3, *P*-wave velocity $c = 2000$ m/s. The initial disturbance was set at a distance of 400 m from the lower boundary directed vertically downwards. Totally, 50ms of physical time were calculated. The time step was selected from the Courant stability condition for the intermediate step of the computational algorithm, corresponding to the maximum coefficient by modulus α_5^{η}.

To confirm the achievement of the declared increased order of convergence by this scheme, a series of calculations were carried out on successively refined curvilinear computational grids. The results of the empirical assessment of the order of convergence according to the norms L_1 and L_∞ are presented in Table 2.

Table 2

Study of the order of convergence of the constructed scheme. The problem with a vertical *P*-wave

h	Error in L_1	Error in L_∞	Order in L_1	Order in L_∞
2.000	2.6081E+09	9.0030E+05	–	–
1.000	1.0736E+09	3.6153E+05	1.281	1.316
0.500	1.1051E+08	4.3919E+04	3.280	3.041
0.250	4.3173E+06	1.6748E+02	4.678	4.713
0.125	1.3778E+05	5.3186E+01	4.970	4.977

The calculation was performed using the standard method of splitting by spatial directions. The results are presented in Table 3.

Table 3

Study of the order of convergence of the scheme with standard splitting. The problem with a vertical *P*-wave

h	Error in L_1	Error in L_∞	Order in L_1	Order in L_∞
2.000	1.7314E+09	5.9920E+05	–	–
1.000	4.3286E+08	1.6200E+05	2.000	1.887
0.500	3.5098E+07	1.9527E+04	3.624	3.052
0.250	5.6940E+06	3.8921E+03	2.624	2.327
0.125	1.3951E+06	9.6667E+02	2.029	2.009

Note that the propagation of the wavefront along one of the lines of the computational grid, as it happened in the test presented above, is not an essential requirement for maintaining the order of convergence by the scheme. Under the conditions described above, the problem of propagation of a *P*-wave at a fixed angle $\beta = -5°$ was solved. The results of the empirical assessment of the order of convergence for two norms are presented in Table 4.

Table 4

Study of the order of convergence of the constructed scheme. Problem with an inclined *P*-wave

h	Error in L_1	Error in L_∞	Order in L_1	Order in L_∞
2.000	2.1279E+09	8.9108E+05	–	–
1.000	8.7694E+08	3.5489E+05	1.279	1.328
0.500	8.8829E+07	4.2314E+04	3.303	3.068
0.250	3.4498E+06	1.6029E+03	4.686	4.722
0.125	1.1013E+05	5.0870E+01	4.969	4.978

The calculation was performed using the standard method of splitting by spatial directions. The results are presented in Table 5.

Table 5

Study of the order of convergence of the standard splitting scheme. The problem with an inclined *P*-wave

h	Error in L_1	Error in L_∞	Order in L_1	Order in L_∞
2.000	1.4481E+09	5.9613E+05	–	–
1.000	3.6522E+08	1.6221E+05	1.987	1.878
0.500	3.6355E+07	2.4925E+04	3.329	2.702
0.250	7.3132E+06	5.4214E+03	2.314	2.201
0.125	1.8012E+06	1.3417E+03	2.022	2.015

Of greatest interest is the calculation of the process of seismic wave propagation in a medium consisting of geological layers with different mechanical characteristics (sandstones, clays, carbonates). To test the possibility of using the developed numerical scheme to solve this type of problem, the following computational experiment was conducted. Three computational grids were considered, covering three geological layers occupying a physical area of 90×150 m. The computational grid in the middle area was set as curvilinear with the parameter $\gamma = 5 \cdot 10^{-4}$. This leads to the formation of a curvilinear upper and lower boundaries. Then, the computational grids in the upper and lower regions were set with a gradually changing parameter γ so that the upper boundary of the upper grid and the lower boundary of the lower grid remained horizontal. A test was performed for the absence of significant reflections from "virtual" geological boundaries caused only by dividing the entire computational grid into three subregions. For this purpose, the same acoustic parameters were used in each of the layers.

The seismic signal source was a plane *P*-wave propagating downwards at a distance of 20 m from the upper boundary of the upper subdomain. The spatial grid step was 0.5 m, the time step was 100μs, which satisfies the Courant stability condition. Spatial pressure distributions in the entire computational domain at a fixed time T = 50 ms, obtained using the widely used third-order approximation grid-characteristic scheme and standard splitting scheme, and using the fifth-order approximation grid-characteristic scheme and multi-step splitting scheme described in the work are presented in Fig. 2. The amplitude of the original wave is more accurately preserved and there are no significant reflections.

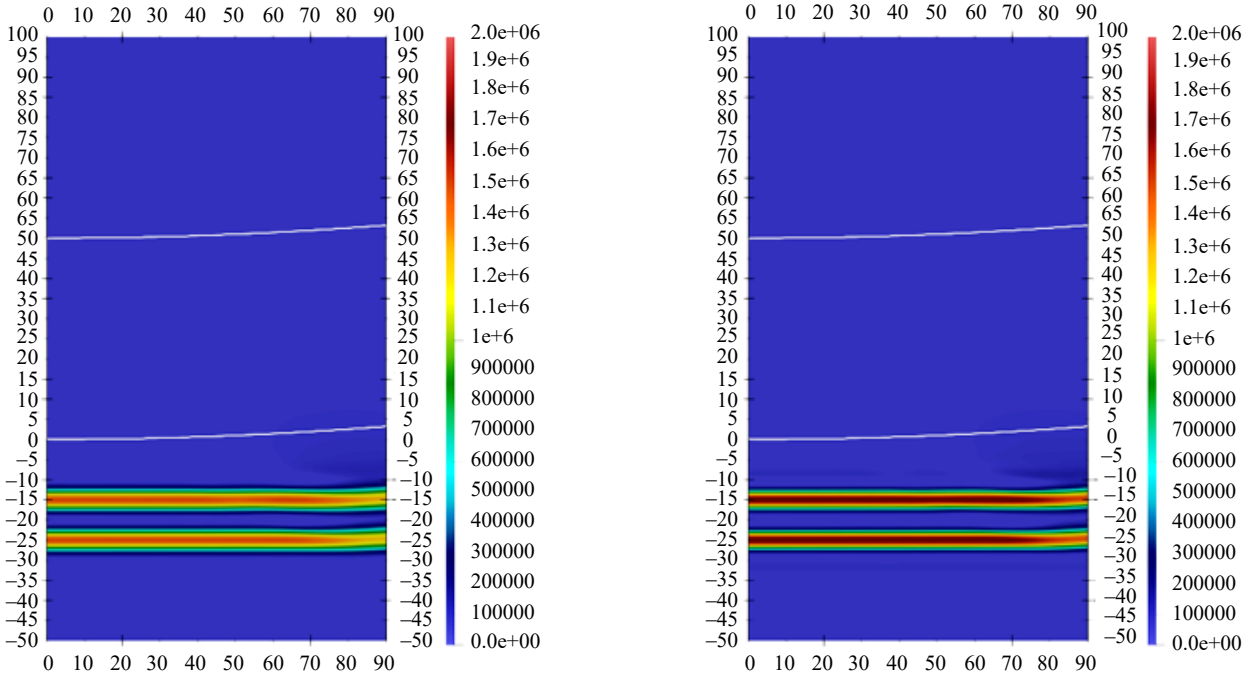

Fig. 2. Acoustic field in a three-layer medium. The following are used: a one-dimensional scheme of the third order of approximation and the usual spatial splitting (left) and the scheme proposed in this paper (right)

Discussion. In this paper, a new two-dimensional grid-characteristic scheme on curvilinear structural computational grids is presented. It is based on the application of the multistep splitting method to preserve the high order of approximation in time and uses the properties of the hyperbolic system of equations to reduce the solution of a one-dimensional hyperbolic problem to the procedure of spatial polynomial interpolation on a fixed seven-point template. The behavior of the obtained numerical solution to the problem of plane wave propagation in the computational domain covered by a special curvilinear grid is systematically investigated. The claimed 5th order of convergence in both coordinate and time is shown to be achieved. Note that in the case of impossibility of analytical calculation of the Jacobian of the transition between computational grids or the dependence of the operators of one-dimensional problems on the coordinate, the following modifications can be used. First, the Jacobian of the transition can be calculated with a given degree of accuracy by the finite-difference method. Secondly, the dependence of one-dimensional operators on the coordinate can be considered by using appropriate solvers of higher order of approximation for the one-dimensional hyperbolic problem.

The paper demonstrates the possibility of using the constructed simulation algorithm for modelling the seismic exploration process in a layered geological medium with curvilinear boundaries. To describe the horizontality of the daylight surface, a calculation grid is used that gradually levels out with distance from the interface. The comparison of the obtained acoustic wavefields with another calculation scheme showed the possibility of increasing the accuracy of preserving the amplitudes of propagating waves together with the absence of significant numerical artifacts at the contact boundaries.

Conclusion. Thus, it seems possible to apply the described approach to solving practical problems of seismic exploration. Promising areas of further research are:

1. Generalization of the simulation algorithm to more complex models of geological media: elastic, elastoplastic, elastoviscoplastic models;
2. Generalization of the calculation algorithm to three-dimensional problem statements to increase its universality and engineering applicability.

References

1. Kallivokas L.F., Fathi A., Kucukcoban S., Stokoe II K.H., Bielak J., Ghattas O. Site characterization using full waveform inversion. *Soil Dynamics and Earthquake Engineering*. 2013;47:62–82. http://dx.doi.org/10.1016/j.soildyn.2012.12.012

2. Yun Zhao, Xiaotao Wen, Chunlan Xie, Bo Li, Chenlong Li, Xiao Pan, et al. Simultaneous seismic inversion of effective stress parameter, fluid bulk modulus, and fracture density in TTI media. *Petroleum Science*. 2025. https://doi.org/10.1016/j.petsci.2025.04.002.

3. Samarskiy A.A., Nikolaev E.S. *Methods for solving grid equations*. Moscow: Nauka; 1978. 592 p. (In Russ.)

4. Matzen R. An efficient finite element time-domain formulation for the elastic second-order wave equation: A non-split complex frequency shifted convolutional PML. *International Journal for Numerical Methods in Engineering*. 2011;88(10):951–973. https://doi.org/10.1002/nme.3205

5. Antonietti P.F., Mazzieri I., Migliorini F. A discontinuous Galerkin time integration scheme for second order differential equations with applications to seismic wave propagation problems. *Computers & Mathematics with Applications*. 2023;134:87–100. https://doi.org/10.48550/arXiv.2112.01792

6. Komatitsch D., Tromp J. Introduction to the spectral element method for three-dimensional seismic wave propagation. *Geophysical Journal International*. 1999;139(3):806–822. https://doi.org/10.1046/J.1365-246X.1999.00967.X.

7. Magomedov K.M., Kholodov A.S. *Grid-characteristic numerical methods: textbook for universities*. 2nd ed., ispr. and add. Moscow: Yurait Publishing House; 2025. 313 p. (In Russ.)

8. Petrov I.B., Favorskaya A.V., Muratov M.V., Biryukov V.A., Sannikov A.V. Grid-characteristic method on unstructured tetrahedral grids. *Doklady Mathematics*. 2014;90:781–783. https://doi.org/10.1134/S1064562414070254

9. Favorskaya A.V., Petrov I.B. A study of high-order grid-characteristic methods on unstructured grids. *Numerical Analysis and Applications*. 2016;9:171–178. https://doi.org/10.1134/S1995423916020087

10. Favorskaya A.V., Zhdanov M.S., Khokhlov N.I., Petrov I.B. Modelling the wave phenomena in acoustic and elastic media with sharp variations of physical properties using the grid-characteristic method. *Geophysical Prospecting*. 2018;66(8):1485–1502. https://doi.org/10.1111/1365–2478.12639

11. Favorskaya A.V., Petrov I.B. The use of full-wave numerical simulation for the investigation of fractured zones. *Mathematical Models and Computer Simulations*. 2019;11:518–530. https://link.springer.com/article/10.1134/S2070048219040069

12. Favorskaya A.V., Petrov I.B. Inverse Problem of Determining the Strength Characteristics of Multi-Story Buildings on Piles. *Lobachevskii Journal of Mathematics*. 2025;46(1):202–213. https://doi.org/10.1134/S1995080224608555

13. Kozhemyachenko A.A., Petrov I.B., Favorskaya A.V., Khokhlov N.I. Boundary conditions for modeling the impact of wheels on railway track. *Computational Mathematics and Mathematical Physics*. 2020;60:1539–1554. https://link.springer.com/article/10.1134/S0965542520090110

14. Favorskaya A.V., Khokhlov N.I., Petrov I.B. Grid-characteristic method on joint structured regular and curved grids for modeling coupled elastic and acoustic wave phenomena in objects of complex shape. *Lobachevskii Journal of Mathematics*. 2020;41:512–525. https://doi.org/10.1134/S1995080220040083

15. Khokhlov N., Favorskaya A., Stetsyuk V, Mitskovets I. Grid-characteristic method using Chimera meshes for simulation of elastic waves scattering on geological fractured zones. *Journal of Computational Physics*. 2021;446:110637. https://doi.org/10.1016/j.jcp.2021.110637

16. Khokhlov N.I., Favorskaya A., Furgailo V. Grid-characteristic method on overlapping curvilinear meshes for modeling elastic waves scattering on geological fractures. *Minerals.* 2022;12(12):1597. https://doi.org/10.3390/min12121597

17. Pesnya E., Kozhemyachenko A.A., Favorskaya A.V. Vibration Analysis of Frost Heaving of the Ice Lens Type on Railways by a Grid-Characteristic Method. *Lobachevskii Journal of Mathematics*. 2025;46(1):317–325. https://doi.org/10.1134/S1995080224608270

18. Petrov I., Vasyukov A., Beklemysheva K., Ermakov A., Favorskaya A. Numerical modeling of non-destructive testing of composites. *Procedia Computer Science*. 2016;96:930–938. https://doi.org/10.1016/j.procs.2016.08.272

19. Yao Gang, da Silva N.V., Debens H.A., Wu Di. Accurate seabed modeling using finite difference methods. Computational Geosciences. 2018;22:469–84. https://doi.org/10.1007/s10596-017-9705-5

20. van Vossen R., Robertsson J.O., Chapman C.H. Finite-difference modeling of wave propagation in a fluid-solid configuration. *Geophysics*. 2002;67(2):618–24. https://doi.org/10.1190/1.1468623

21. Sun Yaochong, Zhang Wei, Xu Jiankuan, Chen Xiaofei. Numerical simulation of 2-D seismic wave propagation in the presence of a topographic fluid–solid interface at the sea bottom by the curvilinear grid finite-difference method. *Geophysical Journal International*. 2017;210(3):1721–1738. https://doi.org/10.1093/gji/ggx257

22. Golubev V.I., Shevchenko A.V., Petrov I.B. Raising convergence order of grid-characteristic schemes for 2D linear elasticity problems using operator splitting. *Computer Research and Modeling*. 2022;14(4):899–910. https://doi.org/10.20537/2076-7633-2022-14-4-899-910

23. Mi Xin, Golubev V. Two-Dimensional Grid-Characteristic Schemes for Acoustic Wave Simulations. Lobachevskii Journal of Mathematics. 2025;46:283–291. https://doi.org/10.1134/S199508022460852X

24. Auzinger W., Hofstätter H., Ketcheson D., Koch O. Practical splitting methods for the adaptive integration of nonlinear evolution equations. Part I: Construction of optimized schemes and pairs of schemes. *BIT. Numerical Mathematics.* 2017;57:55–74. https://doi.org/10.1007/s10543-016-0626-9

About the Authors:

Xin Mi, PhD Student at the Department of Computer Science and Computational Mathematics of the Moscow Institute of Physics and Technology (9, Institutskii lane, Dolgoprudny, 141701, Russian Federation), ORCID, xinawafe@gmail.com

Vasily I. Golubev, Professor at the Department of Computer Science and Computational Mathematics of the Moscow Institute of Physics and Technology (9, Institutskii lane, Dolgoprudny, 141701, Russian Federation), ORCID, SPIN-code, ScopusID, golubev.vi@mipt.ru

Contributions of the authors:

M Xin: making calculations; drawing conclusions; text preparation; working with sources; making graphic materials.

Golubev V.I.: basic concept formulation; research objectives and tasks computational analysis; conclusions correction; text revision.

Conflict of Interest Statement: **the authors declare no conflict of interest.**

All authors have read and approved the final manuscript.

Об авторах:

Синь Ми, аспирант кафедры информатики и вычислительной математики Московского физико-технического института (141701, Российская Федерация, Московская область, г. Долгопрудный, Институтский переулок, 9), ORCID, xinawafe@gmail.com

Василий Иванович Голубев, профессор кафедры информатики и вычислительной математики Московского физико-технического института (141701, Российская Федерация, Московская область, г. Долгопрудный, Институтский переулок, 9), ORCID, SPIN-код, ScopusID, golubev.vi@mipt.ru

Заявленный вклад авторов:

Синь Ми: проведение расчетов; формулирование выводов; подготовка текста; оформление научной статьи; работа с источниками; оформление графических материалов.

В.И. Голубев: формирование основной концепции; цели и задачи исследования; анализ результатов исследований; корректировка выводов; доработка текста.

Конфликт интересов: ***авторы заявляют об отсутствии конфликта интересов.***

Все авторы прочитали и одобрили окончательный вариант рукописи.

Received / **Поступила в редакцию** 27.06.2025
Revised / **Поступила после рецензирования** 24.07.2025
Accepted / **Принята к публикации** 15.08.2025

COMPUTATIONAL MATHEMATICS
ВЫЧИСЛИТЕЛЬНАЯ МАТЕМАТИКА

UDC 519.6

Original Theoretical Research

https://doi.org/10.23947/2587-8999-2025-9-3-16-29

Approximation of Boundary Conditions of the Second and Third Types in Convection–Diffusion Equations with Applications to Environmental Hydrophysics

Alexander I. Sukhinov, Valentina V. Sidoryakina✉
Don State Technical University, Rostov-on-Don, Russian Federation
✉ cvv9@mail.ru

Abstract

Introduction. A finite-difference scheme approximating a boundary value problem for a parabolic-type equation in a three-dimensional setting with boundary conditions of the first-third types is considered. This paper is a continuation of the authors' previous works devoted to the numerical solution of one of the pressing problems of hydrophysics in shallow marine zones — the problem of transport, deposition, and transformation of suspended matter. The approximation of this class of problems inside the domain leads to schemes converging at a rate of $O(\tau + h^2)$, where $h^2 = h_x^2 + h_y^2 + h_z^2$, h_x, h_y, h_z and τ are the steps of the difference grid along the spatial coordinates x, y, z and time, respectively. However, the case of boundary conditions requires careful treatment, since an inaccurate approximation may reduce the overall order of accuracy of the finite-difference scheme. The methods proposed by the authors for approximating boundary conditions ensure the convergence of the finite-difference scheme at the rate of $O(\tau + h^2)$.

Materials and Methods. The authors focused on approximating third-type boundary conditions (with second-type conditions considered as a particular case). The approach is based on the central difference approximation of boundary conditions on an extended grid and the elimination of suspended matter concentration values in ghost nodes (cells).

Results. Approximations of the second- and third-type boundary conditions were constructed for a boundary value problem describing suspended matter transport. These approximations guarantee convergence of the finite-difference scheme at the rate of $O(\tau + h^2)$.

Discussion. The study may be useful in convection–diffusion problems where achieving numerical solutions with acceptable accuracy is required.

Conclusion. Future research may focus on the analysis of the constructed finite-difference schemes under physically motivated constraints on the time step τ and the grid Peclet number.

Keywords: coastal marine systems, convection–diffusion problem, finite-difference scheme, second- and third-type boundary conditions, approximation error

Funding. The study was supported by the Russian Science Foundation grant No. 22–11–00295–П, https://rscf.ru/en/project/22-11-00295/

For Citation. Sukhinov A.I., Sidoryakina V.V. Approximation of Boundary Conditions of the Second and Third Types in Convection–Diffusion Equations with Applications to Environmental Hydrophysics. *Computational Mathematics and Information Technologies.* 2025;9(3):16–29. https://doi.org/10.23947/2587-8999-2025-9-3-16-29

Оригинальное теоретическое исследование

Аппроксимация граничных условий второго и третьего рода в краевых задачах для уравнений конвекции-диффузии с приложением к экологической гидрофизике

А.И. Сухинов, В.В. Сидорякина
Донской государственный технический университет, г. Ростов-на-Дону, Российская Федерация
✉ cvv9@mail.ru

Аннотация

Введение. Рассматривается разностная схема, аппроксимирующая краевую задачу для уравнения параболического типа в трехмерной постановке с условиями на границе I–III рода. Данная статья является дополнением к предыдущим работам авторов, посвященным численному решению одной из актуальных задач гидрофизики зон морского мелководья — задаче переноса, осаждения (транспорта) и трансформации взвешенного вещества. Аппроксимация указанного класса задач внутри области приводит к схемам, сходящимся со скоростью $O(\tau + h^2)$, где $h^2 = h_x^2 + h_y^2 + h_z^2$, h_x, h_y, h_z и τ — шаги разностной сетки по пространственным координатам x, y, z и времени соответственно. При этом требует аккуратного рассмотрения случай граничных условий, поскольку при неудачной их аппроксимации может понизиться порядок аппроксимации разностной схемы в целом. Предложенные авторами методы аппроксимации граничных условий обеспечивают сходимость разностной схемы со скоростью $O(\tau + h^2)$.

Материалы и методы. В своих исследованиях авторами сделан акцент на аппроксимации граничных условий третьего рода (аппроксимация граничных условий второго рода рассматривается как их частный случай). Ориентиром служит аппроксимация указанных граничных условий по формуле центральных разностей с последующим дифференцированием обеих частей уравнений диффузии-конвекции и исключением из полученных выражений функций решения в фиктивных узлах расширенной сетки.

Результаты исследования. Построены аппроксимации граничных условий II–III рода для краевой задачи, описывающей транспорт частиц взвешенного вещества, обеспечивающие сходимость разностной схемы со скоростью $O(\tau + h^2)$.

Обсуждение. Работа может быть полезна в задачах диффузии-конвекции, где необходимо добиться численного решения с приемлемой точностью.

Заключение. Дальнейшие исследования авторов могут быть направлены на исследование построенных разностных схем с учетом физически мотивированных ограничений на шаг временной сетки τ и сеточное число Пекле.

Ключевые слова: прибрежные морские системы, задача диффузии-конвекции, разностная схема, граничные условия второго и третьего рода, погрешность аппроксимации

Финансирование. Исследование выполнено за счет гранта Российского научного фонда № 22–11–00295–П, https://rscf.ru/project/22-11-00295/

Для цитирования. Сухинов А.И., Сидорякина В.В. Аппроксимация граничных условий второго и третьего рода в краевых задачах для уравнений конвекции-диффузии с приложением к экологической гидрофизике. *Computational Mathematics and Information Technologies*. 2025;9(3):16–29. https://doi.org/10.23947/2587-8999-2025-9-3-16-29

Introduction. We consider an initial–boundary value problem describing the transport of suspended matter of a multi-fractional composition, taking into account three spatial variables as well as the following physical parameters and processes: advective transport driven by the motion of the aquatic medium, microturbulent diffusion, and gravitational settling of suspended particles, along with the transition of particles from coarse granulometric fractions into finer ones (disintegration) and, conversely, the aggregation (coagulation) of particles of smaller fractions into larger ones [1–4].

For the continuous problem, the right-hand sides of the convection–diffusion–reaction equations governing the multi-fractional suspensions are transformed on a “lagged” time grid. Specifically, on a temporal mesh with step τ, the right-hand sides of the equations for suspended matter transport are modified as follows: for the concentration functions of fractions that enter the right-hand sides but do not belong to the fraction under consideration in the corresponding convection–diffusion–reaction equation, their values are taken from the previous time level. This approach significantly simplifies the subsequent numerical implementation of each convection–diffusion–reaction equation.

In the present study, we develop and analyze a finite-difference scheme approximating a boundary value problem for a parabolic-type equation in a three-dimensional setting with boundary conditions of the first through third types. This

paper extends the authors' previous research devoted to the numerical solution of one of the pressing problems in the hydrophysics of shallow marine areas — namely, the transport, deposition (settling), and transformation of suspended matter.

As is typical, the approximation of this class of problems within the computational domain leads to schemes converging at the rate of $O(\tau + h^2)$, where $h^2 = h_x^2 + h_y^2 + h_z^2$, h_x, h_y, h_z are the spatial mesh steps and τ is the time step. At the same time, the treatment of boundary conditions requires special care, since their inaccurate approximation can reduce the overall order of accuracy of the finite-difference scheme. The boundary approximation methods proposed by the authors ensure convergence of the finite-difference scheme at the rate of $O(\tau + h^2)$.

Materials and Methods. We assume that particles of suspended matter dispersed in the water column are divided into R fractions. The problem is formulated for the domain $\overline{G}$

$$\overline{G} = \left\{0 \le x \le L_x, 0 \le y \le L_y, 0 \le z \le L_z\right\}.$$

In the rectangular Cartesian coordinate system $Oxyz$, we consider the three-dimensional convection–diffusion–reaction equation for particle settling, expressed using a skew-symmetric representation of the convective transport operator [5–10]:

$$\frac{\partial c_r}{\partial t} + C_0 c_r = Dc_r + F_r,\ r = 1,...,R,\ (x,y,z) \in \overline{G},$$

$$C_0 c_r \equiv \frac{1}{2}\left[u\frac{\partial c_r}{\partial x} + v\frac{\partial c_r}{\partial y} + \frac{\partial c_r}{\partial z} + w'\frac{\partial (uc_r)}{\partial x} + \frac{\partial (vc_r)}{\partial y} + \frac{\partial (w_r' c_r)}{\partial z}\right],$$

$$Dc_r = \frac{\partial}{\partial x}\left(\mu_{hr}\frac{\partial c_r}{\partial x}\right) + \frac{\partial}{\partial y}\left(\mu_{hr}\frac{\partial c_r}{\partial y}\right) + \frac{\partial}{\partial z}\left(\mu_{vr}\frac{\partial c_r}{\partial z}\right), \tag{1}$$

$$F_1 = (\alpha_2 c_2 - \beta_1 c_1) + \gamma_1 c_1,\ F_R = (\beta_{R-1} c_{R-1} - \alpha_R c_R) + \gamma_R c_R,$$
$$F_r = (\beta_{r-1} c_{r-1} - \alpha_r c_r) + (\alpha_{r+1} c_{r+1} - \beta_r c_r) + \gamma_r c_r,\ r = 2,...,R-1,$$

where c_r, $c_r = c_r(x, y, z, t)$ is the particle concentration at time t, $t \in [0; T]$; u, v, w — are the components of the velocity vector of the aquatic medium $\vec{U}$; w_r', $w_r' = w + w_{g,r}$, $w_{g,r}$ is the particle settling velocity determined by hydraulic size; $\mu_{h,r}$, $\mu_{v,r}$ are the horizontal and vertical diffusion coefficients; F_r is a source term; α_r, β_r are the coefficients describing the transformation rate of particles from one fraction to another, $\alpha_r \ge 0$, $\beta_r \ge 0$; γ_r is the intensity of an external particle source.

Equation (1) is supplemented with the initial condition:

$$c_r(x,y,z,0) = c_{r,0}(x,y,z),\ (x,y,z) \in \overline{G} \tag{2}$$

and boundary conditions:

– on the lateral faces of the parallelepiped G:

$$c_r = c_r',\ \text{if}\ u_{\vec{n}} < 0, \tag{3}$$

$$\frac{\partial c_r}{\partial \vec{n}} = 0,\ \text{if}\ u_{\vec{n}} \ge 0$$

($u_{\vec{n}}$ is the projection of the velocity vector onto the outward normal $\vec{n}$ at the boundary, and c' are prescribed concentration values);

– on the upper and lower boundaries of the domain G, respectively:

$$\frac{\partial c_r}{\partial z} = 0, \tag{5}$$

$$\frac{\partial c_r}{\partial z} = -\frac{w_{g,r}}{\mu_{v,r}} c_r. \tag{6}$$

In problem (1)–(6), we introduce a transformation from the z-coordinate system to the θ-coordinate system. In this framework, a Cartesian system is retained in the horizontal plane, while the vertical coordinate is replaced with a dimensionless variable θ, $\theta \in [0; 1]$.

The transformation is defined by the relation:

$$\theta = \frac{z - \eta}{h},\ x_\theta = x,\ y_\theta = y \tag{7}$$

where h is the water depth, and η is the vertical coordinate measured relative to the free surface.

Using the methods described in [11], we apply a "lagged" transformation on the temporal grid $\overline{\omega}_\tau = \{t_n = n\tau, n = 0,1,...,N_t,\ N_t\tau = T\}$. As a result, we obtain a sequence of initial–boundary value problems, linked by the initial and final data at each time level.

Equation (1) is transformed as follows:

$$\frac{\partial c_r^n}{\partial t} + C_0 c_r^n = D c_r^n + F_r^n,\ t_{n-1} < t \le t_n,\ n = 1,2,...,N_t,$$
$$C_0 c_r^n \equiv \frac{1}{2}\left[u\frac{\partial c_r^n}{\partial x} + v\frac{\partial c_r^n}{\partial y} + w_r'\frac{1}{H}\frac{\partial c_r^n}{\partial \theta} + \frac{\partial\left(uc_r^n\right)}{\partial x} + \frac{\partial\left(vc_r^n\right)}{\partial y} + \frac{1}{H}\frac{\partial\left(w_r' c_r^n\right)}{\partial \theta}\right],$$
$$Dc_r^n = \frac{\partial}{\partial x}\left(\mu_{h,r}\frac{\partial c_r^n}{\partial x}\right) + \frac{\partial}{\partial y}\left(\mu_{h,r}\frac{\partial c_r^n}{\partial y}\right) + \frac{1}{H^2}\frac{\partial}{\partial \theta}\left(\mu_{v,r}\frac{\partial c_r^n}{\partial \theta}\right), \tag{8}$$
$$F_1^n = \left(\alpha_2 c_2^{n-1}(x,y,\theta,t_{n-1}) - \beta_1 c_1^n\right) + \gamma_1^n c_1^n,\ F_R^n = \left(\beta_{R-1} c_{R-1}^{n-1}(x,y,\theta,t_{n-1}) - \alpha_R c_R^n\right) + \gamma_R^n c_R^n,$$
$$F_r^n = \left(\beta_{r-1} c_{r-1}^{n-1}(x,y,\theta,t_{n-1}) - \alpha_r c_r^n\right) + \left(\alpha_{r+1} c_{r+1}^{n-1}(x,y,\theta,t_{n-1}) - \beta_r c_r^n\right) + \gamma_r^n c_r^n,\ r = 2,...,R-1.$$

with corresponding modifications of the initial and boundary conditions (2)–(6):

$$c_r^1(x,y,\theta,0) = c_{r,0},(x,y,\theta,0) \in \bar{G},$$
$$c_r^n(x,y,\theta,t_{n-1}) = c_r^{n-1}(x,y,\theta,t_{n-1}), n = 2,...,N_t,(x,y,\theta) \in G, \tag{9}$$

$$c_r^n = c',\ \text{if}\ u_{\vec{n}} < 0, \tag{10}$$

$$\frac{\partial c_r^n}{\partial \vec{n}} = 0,\ \text{if}\ u_{\vec{n}} \ge 0, \tag{11}$$

$$\frac{\partial c_r^n}{\partial \theta} = 0, \tag{12}$$

$$\frac{\partial c_r^n}{\partial \theta} = -\frac{w_{g,r}}{\mu_{v,r}} c_r^n. \tag{13}$$

It has been proved that the solutions of the transformed system converge to the solution of the original problem in the norm of the Hilbert space $L2(G)$ with accuracy $O(\tau)$ as $\tau \to 0$ [11].

To calculate the velocity field components of the aquatic medium, we employ a three-dimensional hydrodynamic model of bottom topography flow that accounts for bed friction and free-surface elevation [12–14].

Results. We assume the existence and continuity of the derivatives $\frac{\partial^2 u}{\partial x^2}$, $\frac{\partial^2 v}{\partial y^2}$, $\frac{\partial^2 w_r'}{\partial \theta^2}$, $\frac{\partial^2 \mu_{h,r}}{\partial x^2}$, $\frac{\partial^2 \mu_{h,r}}{\partial y^2}$, $\frac{\partial^2 \mu_{v,r}}{\partial \theta^2}$ a as well as the continuity of its second-order partial derivatives: $\frac{\partial^2 \mu_{h,r}}{\partial x^2}$, $\frac{\partial^2 \mu_{h,r}}{\partial y^2}$, $\frac{\partial^2 \mu_{v,r}}{\partial \theta^2}$. Additionally, we require that the mixed partial derivatives of c_r^n with respect to x, y, θ exist and are continuous up to the fifth order inclusively, while the mixed partial derivatives with respect to x, y, θ, t are continuous up to the second order. Furthermore, the mixed derivatives of the velocity field components u^n, v^n, $w_r'^n$ with respect to spatial variables x, y, θ are assumed continuous up to the second order inclusively.

To approximate problem (8)–(13), we introduce computational grids:

$$\omega = \omega_x \times \omega_y \times \omega_\theta \ \text{и}\ \bar{\omega} = \bar{\omega}_x \times \bar{\omega}_y \times \bar{\omega}_\theta,$$

where

$$\omega_x = \left\{x : x = ih_x;\ i = 1,...,N_x - 1;\ (N_x - 1)h_x \equiv L_x - h_x\right\},\ \bar{\omega}_x = \left\{x : x = ih_x;\ i = 0,1,...,N_x;\ N_x h_x \equiv L_x\right\},$$
$$\omega_y = \left\{y : y = jh_y;\ j = 1,...,N_y - 1;\ (N_y - 1)h_y \equiv L_y - h_y\right\},\ \bar{\omega}_y = \left\{y : y = jh_y;\ j = 0,1,...,N_y;\ N_y h_y \equiv L_y\right\},$$
$$\omega_\theta = \left\{\theta : \theta = kh_\theta;\ k = 1,...,N_\theta - 1;\ (N_\theta - 1)h_\theta \equiv 1 - h_\theta\right\},\ \bar{\omega}_\theta = \left\{\theta : \theta = kh_\theta;\ k = 0,1,...,N_\theta;\ N_\theta h_\theta \equiv 1\right\}.$$

In [15], a finite-difference scheme was obtained that approximates problem (8)–(13) at the internal nodes of the grid with second-order accuracy in spatial variables and first-order accuracy in time. The finite-difference scheme approximating equation (8) can be written as:

$$\frac{\bar{c}_r^n(x_i,y_j,\theta_k) - \bar{c}_r^{n-1}(x_i,y_j,\theta_k)}{\tau} + C\bar{c}_r^n = D\bar{c}_r^n + \bar{F}_r^n,\ r = 1,2,3,\ (x_i,y_j,\theta_k) \in \omega,\ t_n \in \bar{\omega}_\tau,$$
$$C\bar{c}_r^n = \frac{1}{2h_x}\left[u^n(x_i + 0.5h_x, y_j, \theta_k)\bar{c}_r^n(x_i + h_x, y_j, \theta_k) - u^n(x_i - 0.5h_x, y_j, \theta_k)\bar{c}_r^n(x_i - h_x, y_j, \theta_k)\right] +$$
$$+\frac{1}{2h_y}\left[v^n(x_i, y_j + 0.5h_y, \theta_k)\bar{c}_r^n(x_i, y_j + h_y, \theta_k) - v^n(x_i, y_j - 0.5h_y, \theta_k)\bar{c}_r^n(x_i, y_j - h_y, \theta_k)\right] +$$

$$+\frac{1}{2H(x,y)h_\theta}\left[w_r'^n\left(x_i,y_j,\theta_k+0.5h_\theta\right)\overline{c}_r^n\left(x_i,y_j,\theta_k+h_\theta\right)-w_r'^n\left(x_i,y_j,\theta_k-0.5h_\theta\right)\overline{c}_r^n\left(x_i,y_j,\theta_k-h_\theta\right)\right],$$

$$D\overline{c}_r^n=\frac{1}{h_x^2}\left[\mu_{h,r}\left(x_i+0.5h_x,y_j,\theta_k\right)\left(\overline{c}_r^n\left(x_i+h_x,y_j,\theta_k\right)-\overline{c}_r^n\left(x_i,y_j,\theta_k\right)\right)-\mu_{h,r}\left(x_i-0.5h_x,y_j,\theta_k\right)\cdot\right.$$

$$\left.\cdot\left(\overline{c}_r^n\left(x_i,y_j,\theta_k\right)-\overline{c}_r^n\left(x_i-h_x,y_j,\theta_k\right)\right)\right]+\frac{1}{h_y^2}\left[\mu_{h,r}\left(x_i,y_j+0.5h_y,\theta_k\right)\left(\overline{c}_r^n\left(x_i,y_j+h_y,\theta_k\right)-\overline{c}_r^n\left(x_i,y_j,\theta_k\right)\right)-\right.$$

$$\left.-\mu_{h,r}\left(x_i,y_j-0.5h_y,\theta_k\right)\left(\overline{c}_r^n\left(x_i,y_j,\theta_k\right)-\overline{c}_r^n\left(x_i,y_j-h_y,\theta_k\right)\right)\right]+\frac{1}{H^2\left(x_i,y_j\right)h_\theta^2}\left[\mu_{v,r}\left(x_i,y_j,\theta_k+0.5h_\theta\right)\cdot\right.$$

$$\left.\cdot\left(\overline{c}_r^n\left(x_i,y_j,\theta_k+h_\theta\right)-\overline{c}_r^n\left(x_i,y_j,\theta_k\right)\right)-\mu_{v,r}\left(x_i,y_j,\theta_k-0.5h_\theta\right)\left(\overline{c}_r^n\left(x_i,y_j,\theta_k\right)-\overline{c}_r^n\left(x_i,y_j,\theta_k-h_\theta\right)\right)\right],$$

$$\overline{F}_1^n=\left(\alpha_2\overline{c}_2^{n-1}(x,y,\theta,t_{n-1})-\beta_1\overline{c}_1^n\right)+\gamma_1^n\overline{c}_1^n;\ \overline{F}_R^n=\left(\beta_{R-1}\overline{c}_{R-1}^{n-1}(x,y,\theta,t_{n-1})-\alpha_R\overline{c}_R^n\right)+\gamma_R^n\overline{c}_R^n;$$

$$\overline{F}_r^n=\left(\beta_{r-1}\overline{c}_{r-1}^{n-1}(x,y,\theta,t_{n-1})-\alpha_r\overline{c}_r^n\right)+\left(\alpha_{r+1}\overline{c}_{r+1}^{n-1}(x,y,\theta,t_{n-1})-\beta_r\overline{c}_r^n\right)+\gamma_r^n\overline{c}_r^n,\ r=2,...,R-1.$$

$$\overline{F}_3^n=\left(\beta_2\overline{c}_2^{n-1}(x,y,\theta,t_{n-1})-\alpha_3\overline{c}_3^n\right)+\gamma_3^n\overline{c}_3^n,\ \left(x_i,y_j,\theta_k\right)\in\omega,\ t_n\in\overline{\omega}_\tau.$$

The overbar notation indicates that the quantities belong to the class of grid functions.

It is straightforward to verify that the approximation error $\psi^n\left(x_i,y_j,\theta_k\right)$ of the finite-difference scheme in the grid nodes $\overline{\omega}_\tau\times\omega$ satisfies the relation:

$$\psi^n\left(x_i,y_j,\theta_k\right)=O\left(\tau+h^2\right),\ n=0,1,...,N_t,$$

It should also be noted that the initial condition (9) is imposed on the temporal grid $\overline{\omega}_\tau\times\omega$ exactly.

We proceed to construct a finite-difference scheme of second-order accuracy for the transport problem of suspended matter at the boundary nodes.

We assume that the following conditions are satisfied:

$$k_{11}\le\frac{h_x}{h_y}\le k_{12},\ k_{21}\le\frac{h_\theta}{h_x}\le k_{22},\ k_{31}\le\frac{h_\theta}{h_y}\le k_{32},\tag{15}$$

where k_{11}, k_{12}, k_{21}, k_{22}, k_{31}, k_{32} are some positive constants.

To approximate the boundary conditions, we introduce an extended grid:

$$\overline{\omega}^+=\left\{\left(x_i,y_j,\theta_k\right),i=-1,0,...,N_x+1,j=-1,0,...,N_y+1,k=-1,0,...,N_\theta+1,x_i=ih_x;y_j=jh_y;\theta_k=kh_\theta,\right.$$

$$\left.N_xh_x=L_x;N_yh_y=L_y;N_\theta h_\theta=1\right\}.$$

For the nodes of the extended grid $\overline{\omega}^+\setminus\overline{\omega}$ the velocity vector components are assumed to vanish:

$$\overline{c}_r^n\left(x_i,y_j,\theta_k\right)=0,\ \text{if}\ \left(x_i,y_j,\theta_k\right)\in\overline{\omega}^+\setminus\overline{\omega}.\tag{16}$$

In addition, we assume the components of the velocity field and the hydraulic size of the suspended particles to be known at extended grid nodes $\overline{\omega}^+\setminus\overline{\omega}$ with fractional indices, i. e. at half-grid positions: $u^n\left(-0.5h_x,y_j,\theta_k\right)$, $u^n\left(L_x+0.5h_x,y_j,\theta_k\right)$, $v^n\left(x_i,-0.5h_y,\theta_k\right)$, $v^n\left(x_i,L_y+0.5h_y,\theta_k\right)$ and $w_r'^n\left(x_i,y_j,-0.5h_\theta\right)$, $w_r'^n\left(x_i,y_j,1+0.5h_\theta\right)$.

The boundary conditions (10) are approximated as follows:

$$\begin{cases}\overline{c}_r^n\left(0,y_j,\theta_k\right)=c_r',\ \text{если}\ u^n\left(0.5h_x,y_j,\theta_k\right)+u^n\left(-0.5h_x,y_j,\theta_k\right)>0,\\ \overline{c}_r^n\left(L_x,y_j,\theta_k\right)=c_r',\ \text{если}\ u^n\left(L_x-0.5h_x,y_j,\theta_k\right)+u^n\left(L_x+0.5h_x,y_j,\theta_k\right)<0,\ \left(x_i,y_j,\theta_k\right)\in\overline{\omega}^+,\end{cases}\tag{17}$$

$$\begin{cases}\overline{c}_r^n\left(x_i,0,\theta_k\right)=c_r',\ \text{если}\ v^n\left(x_i,0.5h_y,\theta_k\right)+v^n\left(x_i,-0.5h_y,\theta_k\right)>0,\\ \overline{c}_r^n\left(x_i,L_y,\theta_k\right)=c_r',\ \text{если}\ v^n\left(x_i,L_y-0.5h_y,\theta_k\right)+v^n\left(x_i,L_y+0.5h_y,\theta_k\right)<0,\ \left(x_i,y_j,\theta_k\right)\in\overline{\omega}^+.\end{cases}\tag{18}$$

The construction of finite-difference schemes for boundary conditions (11)–(13) is demonstrated on the example of the third-type (Robin) condition — condition (13). Since boundary conditions (11) and (12) (Neumann conditions) represent particular cases of condition (13), the construction of the corresponding finite-difference approximations can be carried out by analogous reasoning.

For $\theta_k=1$ the boundary condition (13) is equivalent to the following expression:

$$\frac{\partial c_r^n\left(x_i,y_j,1\right)}{\partial\theta}=-\frac{w_{g,r}}{\mu_{v,r}\left(x_i,y_j,1\right)}c_r^n\left(x_i,y_j,1\right).$$

On the grid $\overline{\omega}^+$ the nodes (x_i, y_j, 1) are interior.

The finite-difference scheme at the nodes (x_i, y_j, 1) of $\overline{\omega}^+$ is written as follows:

$$\frac{\overline{c}_r^n\left(x_i,y_j,1\right)-\overline{c}_r^{n-1}\left(x_i,y_j,1\right)}{\tau}+C\overline{c}_r^n\left(x_i,y_j,1\right)=D\overline{c}_r^n\left(x_i,y_j,1\right)+\overline{F}_r^n\left(x_i,y_j,1\right),\ n=1,...,N_t. \tag{20}$$

In what follows we base our reasoning on approximating the considered boundary condition by central differences on the extended grid and on eliminating from the resulting expression and from equation (20) the values of the function $\overline{c}_r^n$ in the ghost node (x_i, y_j, 1 + h_θ).

In equation (20) the function $\overline{c}_r^n\left(x_i,y_j,1+h_\theta\right)$ enters the following terms:

$$\frac{1}{2H\left(x_i,y_j\right)h_\theta}\left[w_r'^n\left(x_i,y_j,1+0.5h_\theta\right)\overline{c}_r^n\left(x_i,y_j,1+h_\theta\right)-w_r'^n\left(x_i,y_j,1-0.5h_\theta\right)\overline{c}_r^n\left(x_i,y_j,1-h_\theta\right)\right],$$

$$\frac{1}{H^2\left(x_i,y_j\right)h_\theta^2}\left[\mu_{v,r}\left(x_i,y_j,1+0.5h_\theta\right)\left(\overline{c}_r^n\left(x_i,y_j,1+h_\theta\right)-\overline{c}_r^n\left(x_i,y_j,1\right)\right)-\mu_{v,r}\left(x_i,y_j,1-0.5h_\theta\right)\cdot\right.$$

$$\left.\cdot\left(\overline{c}_r^n\left(x_i,y_j,1\right)-\overline{c}_r^n\left(x_i,y_j,1-h_\theta\right)\right)\right],$$

which we denote by $C_\theta\overline{c}_r^n\left(x_i,y_j,1\right)$ and $D_\theta\overline{c}_r^n\left(x_i,y_j,1\right)$ respectively.

Since on the considered boundary $w\big|_{(x,y,1)}\equiv 0$, the relation for $C_\theta\overline{c}_r^n\left(x_i,y_j,1\right)$ can be brought to the form:

$$\frac{w_{g,r}}{2H\left(x_i,y_j\right)h_\theta}\left[\overline{c}_r^n\left(x_i,y_j,1+h_\theta\right)-\overline{c}_r^n\left(x_i,y_j,1-h_\theta\right)\right].$$

Rewrite condition (19) in the form:

$$\frac{\overline{c}_r^n\left(x_i,y_j,1+h_\theta\right)-\overline{c}_r^n\left(x_i,y_j,1-h_\theta\right)}{2h_\theta}=-\frac{2w_{g,r}}{\mu_{v,r}\left(x_i,y_j,1+0.5h_\theta\right)+\mu_{v,r}\left(x_i,y_j,1-0.5h_\theta\right)}\overline{c}_r^n\left(x_i,y_j,1\right) \tag{21}$$

and from it we obtain:

$$\overline{c}_r^n\left(x_i,y_j,1+h_\theta\right)=\overline{c}_r^n\left(x_i,y_j,1-h_\theta\right)-\frac{4w_{g,r}h_\theta}{\mu_{v,r}\left(x_i,y_j,1+0.5h_\theta\right)+\mu_{v,r}\left(x_i,y_j,1-0.5h_\theta\right)}\overline{c}_r^n\left(x_i,y_j,1\right).$$

For a compact presentation of the subsequent reasoning we introduce the notation:

$$\varepsilon_r=\frac{2w_{g,r}}{\mu_{v,r}\left(x_i,y_j,1+0.5h_\theta\right)+\mu_{v,r}\left(x_i,y_j,1-0.5h_\theta\right)}$$

and then

$$\overline{c}_r^n\left(x_i,y_j,1+h_\theta\right)=\overline{c}_r^n\left(x_i,y_j,1-h_\theta\right)-2h_\theta\varepsilon_r\overline{c}_r^n\left(x_i,y_j,1\right). \tag{22}$$

Substituting the value of $\overline{c}_r^n\left(x_i,y_j,1+h_\theta\right)$ obtained by formula (22) into the expression for $C_\theta\overline{c}_r^n\left(x_i,y_j,1\right)$, we obtain the approximation:

$$C_\theta\overline{c}_r^n\left(x_i,y_j,1\right)\equiv-\frac{w_{g,r}\varepsilon_r}{H\left(x_i,y_j\right)}\overline{c}_r^n\left(x_i,y_j,1\right). \tag{23}$$

As follows from equality (23), the quantity $C_\theta\overline{c}_r^n$ at the nodes of (x_i, y_j, 1) is computed exactly.

Preliminary calculations show that if one uses equality (22) to approximate $D_\theta\overline{c}_r^n\left(x_i,y_j,1\right)$, then a first-order error in θ is obtained. To approximate this operator with second-order accuracy in θ the authors propose a different approach.

Expanding the functions $c_r^n\left(x_i,y_j,1\pm h_\theta\right)$ in a Taylor series in the neighbourhood of the point (x_i, y_j, 1) adjacent to the boundary, we obtain an expression for the left-hand side of equality (21):

$$\frac{\overline{c}_r^n\left(x_i,y_j,1+h_\theta\right)-\overline{c}_r^n\left(x_i,y_j,1-h_\theta\right)}{2h_\theta}=\frac{\partial c_r^n\left(x_i,y_j,1\right)}{\partial\theta}+\frac{\partial^3c_r^n\left(x_i,y_j,1\right)}{\partial\theta^3}\frac{h_\theta^2}{6}+O\left(h_\theta^4\right).$$

The last expression, taking into account condition (19), can be transformed to the form:

$$\frac{\overline{c}_r^n\left(x_i,y_j,1+h_\theta\right)-\overline{c}_r^n\left(x_i,y_j,1-h_\theta\right)}{2h_\theta}=-\frac{w_{g,r}}{\mu_{v,r}\left(x_i,y_j,1\right)}c_r^n\left(x_i,y_j,1\right)+\frac{h_\theta^2}{6}\frac{\partial^3c_r^n\left(x_i,y_j,1\right)}{\partial\theta^3}+O\left(h_\theta^4\right). \tag{24}$$

Using equality (24) we find the value of the function $\overline{c}_r^n$ in the ghost node (x_i, y_j, 1 + h_θ):

$$\overline{c}_r^n\left(x_i,y_j,1+h_\theta\right)=\overline{c}_r^n\left(x_i,y_j,1-h_\theta\right)-2h_\theta\,\varepsilon_r c_r^n\left(x_i,y_j,1\right)+\frac{h_\theta^3}{3}\frac{\partial^3 c_r^n\left(x_i,y_j,1\right)}{\partial\theta^3}+O\left(h_\theta^5\right). \tag{25}$$

Using equality (25), we compose the expression for $D_\theta\overline{c}_r^n\left(x_i,y_j,1\right)$:

$$D_\theta\overline{c}_r^n\left(x_i,y_j,1\right)\cong\frac{1}{H^2\left(x_i,y_j\right)h_\theta^2}\Big[\left(\mu_{v,r}\left(x_i,y_j,1+0.5h_\theta\right)+\mu_{v,r}\left(x_i,y_j,1-0.5h_\theta\right)\right)\left(\overline{c}_r^n\left(x_i,y_j,1-h_\theta\right)-$$

$$-\overline{c}_r^n\left(x_i,y_j,1\right)\right)-\mu_{v,r}\left(x_i,y_j,1+0.5h_\theta\right)\left(2h_\theta\,\varepsilon_r c_r^n\left(x_i,y_j,1\right)-\frac{h_\theta^3}{3}\frac{\partial^3 c_r^n\left(x_i,y_j,1\right)}{\partial\theta^3}\right)\Big].$$

Clearly, to achieve the stated goal it is sufficient to approximate the derivative $\dfrac{\partial^3 c_r^n\left(x_i,y_j,1\right)}{\partial\theta^3}$ with first-order accuracy in θ. We now construct an approximation of this derivative with the prescribed accuracy.

Differentiate both sides of equation (8) with respect to the vertical variable θ and, from the resulting equality, express the derivative $\dfrac{\partial^3 c_r^n}{\partial\theta^3}$. Next, pass to the limit as θ→1 and, taking into account condition (36), we obtain:

$$\frac{\partial^3 c_r^n\left(x_i,y_j,1\right)}{\partial\theta^3}=\frac{H^2\left(x_i,y_j\right)}{\mu_{v,r}\left(x_i,y_j,1\right)}\Bigg[\frac{\partial^2 c_r^n\left(x_i,y_j,1\right)}{\partial t\partial\theta}-\mu_{h,r}\left(x_i,y_j,1\right)\frac{\partial^3 c_r^n\left(x_i,y_j,1\right)}{\partial x^2\partial\theta}-\mu_{h,r}\left(x_i,y_j,1\right)\cdot$$

$$\cdot\frac{\partial^3 c_r^n\left(x_i,y_j,1\right)}{\partial y^2\partial\theta}+\left(u^n\left(x_i,y_j,1\right)-\frac{\partial\mu_{h,r}\left(x_i,y_j,1\right)}{\partial x}\right)\frac{\partial^2 c_r^n\left(x_i,y_j,1\right)}{\partial x\partial\theta}+\left(v^n\left(x_i,y_j,1\right)-\frac{\partial\mu_{h,r}\left(x_i,y_j,1\right)}{\partial y}\right)\cdot$$

$$\cdot\frac{\partial^2 c_r^n\left(x_i,y_j,1\right)}{\partial y\partial\theta}+\frac{1}{H\left(x_i,y_j\right)}\left(w_{g,r}-\frac{2}{H\left(x_i,y_j\right)}\frac{\partial\mu_{v,r}\left(x_i,y_j,1\right)}{\partial\theta}\right)\frac{\partial^2 c_r^n\left(x_i,y_j,1\right)}{\partial\theta^2}-\frac{\partial\mu_{h,r}\left(x_i,y_j,1\right)}{\partial\theta}\cdot \tag{26}$$

$$\cdot\frac{\partial^2 c_r^n\left(x_i,y_j,1\right)}{\partial x^2}-\frac{\partial\mu_{h,r}\left(x_i,y_j,1\right)}{\partial\theta}\frac{\partial^2 c_r^n\left(x_i,y_j,1\right)}{\partial y^2}+\left(\frac{\partial u^n\left(x_i,y_j,1\right)}{\partial\theta}-\frac{\partial^2\mu_{h,r}\left(x_i,y_j,1\right)}{\partial x\partial\theta}\right)\cdot$$

$$\cdot\frac{\partial c_r^n\left(x_i,y_j,1\right)}{\partial x}+\left(\frac{\partial v^n\left(x_i,y_j,1\right)}{\partial\theta}-\frac{\partial^2\mu_{h,r}\left(x_i,y_j,1\right)}{\partial y\partial\theta}\right)\frac{\partial c_r^n\left(x_i,y_j,1\right)}{\partial y}+\frac{1}{2}\left(\frac{\partial^2 u^n\left(x_i,y_j,1\right)}{\partial x\partial\theta}+\frac{\partial^2 v^n\left(x_i,y_j,1\right)}{\partial y\partial\theta}-\right.$$

$$\left.-\frac{w_{g,r}}{\mu_{v,r}\left(x_i,y_j,1\right)}\frac{\partial u^n\left(x_i,y_j,1\right)}{\partial x}-\frac{w_{g,r}}{\mu_{v,r}\left(x_i,y_j,1\right)}\frac{\partial v^n\left(x_i,y_j,1\right)}{\partial y}+\frac{2w_{g,r}}{H^2\left(x_i,y_j\right)\mu_{v,r}\left(x_i,y_j,1\right)}\frac{\partial^2\mu_{v,r}\left(x_i,y_j,1\right)}{\partial\theta^2}\right)\cdot c_r^n\left(x_i,y_j,1\right)-\frac{\partial F_r^n\left(x_i,y_j,1\right)}{\partial\theta}\Bigg].$$

It is evident that the following relations hold:

$$\frac{\partial F_1^n}{\partial\theta}=\left(-\alpha_2\frac{w_{g,2}}{\mu_{v,2}\left(x_i,y_j,1\right)}c_2^{n-1}\left(x_i,y_j,1,t_{n-1}\right)+\beta_1\frac{w_{g,1}}{\mu_{v,1}\left(x_i,y_j,1\right)}c_1^n\right)+\gamma_1^n\frac{w_{g,1}}{\mu_{v,1}\left(x_i,y_j,1\right)}c_1^n,$$

$$F_R^n=\left(-\beta_{R-1}\frac{w_{g,R-1}}{\mu_{v,R-1}\left(x_i,y_j,1\right)}c_{R-1}^{n-1}\left(x,y,1,t_{n-1}\right)+\alpha_R\frac{w_{g,R}}{\mu_{v,R}\left(x_i,y_j,1\right)}c_R^n\right)-\gamma_R^n\frac{w_{g,R}}{\mu_{v,R}\left(x_i,y_j,1\right)}c_R^n,$$

$$\frac{\partial F_r^n}{\partial\theta}=\left(-\beta_1\frac{w_{g,r-1}}{\mu_{v,r-1}\left(x_i,y_j,1\right)}c_{r-1}^{n-1}\left(x,y,1,t_{n-1}\right)+\alpha_r\frac{w_{g,r}}{\mu_{v,r}\left(x_i,y_j,1\right)}c_r^n\right)+$$

$$+\left(-\alpha_{r+1}\frac{w_{g,r+1}}{\mu_{v,r+1}\left(x_i,y_j,1\right)}c_{r+1}^{n-1}\left(x,y,1,t_{n-1}\right)+\beta_r\frac{w_{g,r}}{\mu_{v,r}\left(x_i,y_j,1\right)}c_r^n\right)-\gamma_r^n\frac{w_{g,r}}{\mu_{v,r}\left(x_i,y_j,1\right)}c_r^n.$$

For reader convenience, we approximate the expression in the square brackets on the right-hand side of (26) term by term. First, note that for the coefficient $\dfrac{H^2\left(x_i,y_j\right)}{\mu_{v,r}\left(x_i,y_j,1\right)}$ placed before this bracket we use the representation:

$$\frac{H^2\left(x_i,y_j\right)}{\mu_{v,r}\left(x_i,y_j,1\right)}=\frac{2H^2\left(x_i,y_j\right)}{\mu_{v,r}\left(x_i,y_j,1+0.5h_\theta\right)+\mu_{v,r}\left(x_i,y_j,1-0.5h_\theta\right)}. \tag{27}$$

Consider the derivative $\dfrac{\partial^2 c_r^n\left(x_i,y_j,1\right)}{\partial t\partial\theta}$. For this derivative we have:

$$\frac{\partial^2 c_r^n(x_i,y_j,1)}{\partial t\partial\theta}=\frac{1}{2h_\theta}\left(\frac{\overline{c}_r^n(x_i,y_j,1+h_\theta,t_n+\tau)-\overline{c}_r^n(x_i,y_j,1+h_\theta,t_n-\tau)}{2\tau}-\right.$$
$$\left.-\frac{\overline{c}_r^n(x_i,y_j,1-h_\theta,t_n+\tau)-\overline{c}_r^n(x_i,y_j,1-h_\theta,t_n-\tau)}{2\tau}+O(\tau^2)\right)+O(h_\theta^2)=$$
$$=\frac{1}{2\tau}\left(\frac{\overline{c}_r^n(x_i,y_j,1+h_\theta,t_n+\tau)-\overline{c}_r^n(x_i,y_j,1-h_\theta,t_n+\tau)}{2h_\theta}-\right. \quad (28)$$
$$\left.-\frac{\overline{c}_r^n(x_i,y_j,1+h_\theta,t_n-\tau)-\overline{c}_r^n(x_i,y_j,1-h_\theta,t_n-\tau)}{2h_\theta}\right)+\frac{1}{2h_\theta}O(\tau^2)+O(h_\theta^2).$$

Using equality (28), the following relations can be written:

$$\frac{\overline{c}_r^n(x_i,y_j,1+h_\theta,t_n\pm\tau)-\overline{c}_r^n(x_i,y_j,1-h_\theta,t_n\pm\tau)}{2h_\theta}=$$
$$=-\frac{w_{g,r}}{\mu_{v,r}(x_i,y_j,1)}c_r^n(x_i,y_j,1,t_n\pm\tau)+\frac{h_\theta^2}{6}\frac{\partial^3 c_r^n(x_i,y_j,1,t_n\pm\tau)}{\partial\theta^3}+O(h_\theta^4). \quad (29)$$

By means of (29) we transform equality (28) into the form

$$\frac{\partial^2 c_r^n}{\partial t\partial\theta}=-\frac{w_{g,r}}{2\tau\mu_{v,r}(x_i,y_j,1)}\left(c_r^n(x_i,y_j,1,t_n+\tau)-c_r^n(x_i,y_j,1,t_n-\tau)\right)+$$
$$+\frac{h_\theta^2}{12\tau}\left(\frac{\partial^3 c_r^n(x_i,y_j,1,t_n+\tau)}{\partial\theta^3}-\frac{\partial^3 c_r^n(x_i,y_j,1,t_n-\tau)}{\partial\theta^3}\right)+\frac{1}{2h_\theta}O(\tau^2)+O(h_\theta^2). \quad (30)$$

For the expression $\frac{w_{g,r}}{2\tau\mu_{v,r}(x_i,y_j,1)}\left(c_r^n(x_i,y_j,1,t_n+\tau)-c_r^n(x_i,y_j,1,t_n-\tau)\right)$ we have:

$$\frac{w_{g,r}}{2\tau\mu_{v,r}(x_i,y_j,1)}\left(c_r^n(x_i,y_j,1,t_n+\tau)-c_r^n(x_i,y_j,1,t_n-\tau)\right)=\frac{w_{g,r}}{2\tau\mu_{v,r}(x_i,y_j,1)}\frac{\partial c_r^n(x_i,y_j,1,t_n)}{\partial t}+O(\tau^2). \quad (31)$$

Taking into account relation (31), we transform expression (30). We obtain:

$$\frac{\partial^2 c_r^n}{\partial t\partial\theta}=-\varepsilon_r\frac{\partial c_r^n(x_i,y_j,1,t_n)}{\partial t}+\frac{1}{2\tau}\frac{h_\theta^2}{6}\left(\frac{\partial^3 c_r^n(x_i,y_j,1,t_n+\tau)}{\partial\theta^3}-\frac{\partial^3 c_r^n(x_i,y_j,1,t_n-\tau)}{\partial\theta^3}\right)+\frac{1}{2h_\theta}O(\tau^2)+O(h_\theta^2+\tau^2).$$

Introducing the notation $\varphi(x_i,y_j,1,t_n\pm\tau)=\frac{\partial^3 c_r^n(x_i,y_j,1,t_n\pm\tau)}{\partial\theta^3}$, the last equality can be written in the form:

$$\frac{\partial^2 c_r^n}{\partial t\partial\theta}=-\varepsilon_r\frac{\partial c_r^n(x_i,y_j,1,t_n)}{\partial t}+\frac{h_\theta^2}{6}\left(\frac{\varphi(x_i,y_j,1,t_n+\tau)-\varphi(x_i,y_j,1,t_n-\tau)}{2\tau}\right)+\frac{1}{2h_\theta}O(\tau^2)+O(h_\theta^2+\tau^2).$$

From this it follows that

$$\frac{\partial^2 c_r^n}{\partial t\partial\theta}=-\varepsilon_r\frac{\partial c_r^n(x_i,y_j,1,t_n)}{\partial t}+\frac{h_\theta^2}{6}\left(\frac{\partial\varphi(x_i,y_j,1,t_n)}{\partial t}+O(\tau^2)\right)+\frac{1}{2h_\theta}O(\tau^2)+O(h_\theta^2+\tau^2).$$

In accordance with the Courant condition, the quantity τ is bounded, and thus the equality $\frac{1}{2h_\theta}O(\tau^2)=O(h_\theta)$ can be considered valid. Taking this into account, we have:

$$\frac{\partial^2 c_r^n}{\partial t\partial\theta}=-\varepsilon_r\frac{\partial c_r^n(x_i,y_j,1,t_n)}{\partial t}+\frac{h_\theta^2}{6}\frac{\partial\varphi(x_i,y_j,1,t_n)}{\partial t}+O(h_\theta+\tau^2).$$

Taking into account the last relation, and assuming boundedness of the derivative $\frac{\partial\varphi(x_i,y_j,1,t_n\pm\tau)}{\partial t}=$ $=\frac{\partial^4 c_r^n(x_i,y_j,1,t_n\pm\tau)}{\partial t\partial x^3}$, we can write:

$$\frac{\partial^2 c_r^n}{\partial t\partial\theta}=-\varepsilon_r\frac{\partial c_r^n(x_i,y_j,1,t_n)}{\partial t}+O(h_\theta+\tau^2). \quad (32)$$

Next, consider the derivative $\frac{\partial^3 c_r^n(x_i,y_j,1)}{\partial x^2\partial\theta}$.

Taking into account inequality $k_{21}\le\frac{h_\theta}{h_x}\le k_{22}$ from (16), we have:

$$\frac{\partial^3 c_r^n(x_i,y_j,1)}{\partial x^2\partial\theta}=\frac{1}{2h_\theta}\left(\frac{\partial^2\overline{c}_r^n(x_i,y_j,1+h_\theta)}{\partial x^2}-\frac{\partial^2\overline{c}_r^n(x_i,y_j,1-h_\theta)}{\partial x^2}\right)+O(h_\theta^2)=$$

$$=\frac{1}{2h_\theta}\left(\frac{\overline{c}_r^n(x_i+h_x,y_j,1+h_\theta)-2\overline{c}_r^n(x_i,y_j,1+h_\theta)+\overline{c}_r^n(x_i-h_x,y_j,1+h_\theta)}{h_x^2}-\right.$$

$$\left.-\frac{\overline{c}_r^n(x_i+h_x,y_j,1-h_\theta)-2\overline{c}_r^n(x_i,y_j,1-h_\theta)+\overline{c}_r^n(x_i-h_x,y_j,1-h_\theta)}{h_x^2}+O(h_x^2)\right)+O(h_\theta^2)=$$

$$=\frac{1}{h_x^2}\left(\frac{\overline{c}_r^n(x_i+h_x,y_j,1+h_\theta)-\overline{c}_r^n(x_i+h_x,y_j,1-h_\theta)}{2h_\theta}-2\frac{\overline{c}_r^n(x_i,y_j,1+h_\theta)-\overline{c}_r^n(x_i,y_j,1-h_\theta)}{2h_\theta}+\right.$$

$$\left.+\frac{\overline{c}_r^n(x_i-h_x,y_j,1+h_\theta)-\overline{c}_r^n(x_i-h_x,y_j,1-h_\theta)}{2h_\theta}\right)+\frac{1}{2h_\theta}O(h_x^2)+O(h_\theta^2)=$$

$$=\frac{1}{h_x^2}\left(\frac{\overline{c}_r^n(x_i+h_x,y_j,1+h_\theta)-\overline{c}_r^n(x_i+h_x,y_j,1-h_\theta)}{2h_\theta}-2\frac{\overline{c}_r^n(x_i,y_j,1+h_\theta)-\overline{c}_r^n(x_i,y_j,1-h_\theta)}{2h_\theta}+\right.$$

$$\left.+\frac{\overline{c}_r^n(x_i-h_x,y_j,1+h_\theta)-\overline{c}_r^n(x_i-h_x,y_j,1-h_\theta)}{2h_\theta}\right)+O(h_\theta^2+h_x). \tag{33}$$

Based on equality (24), the following relation can be written:

$$\frac{\overline{c}_r^n(x_i\pm h_x,y_j,1+h_\theta)-\overline{c}_r^n(x_i\pm h_x,y_j,1-h_\theta)}{2h_\theta}=-\varepsilon_r c_r^n(x_i\pm h_x,y_j,1)+\frac{h_\theta^2}{6}\frac{\partial^3 c_r^n(x_i\pm h_x,y_j,1)}{\partial\theta^3}+O(h_\theta^4). \tag{34}$$

Using (34), we transform relation (33) into the form:

$$\frac{\partial^3 c_r^n(x_i,y_j,1)}{\partial x^2\partial\theta}=-\frac{\varepsilon_r}{h_x^2}\left(c_r^n(x_i+h_x,y_j,1)-2c_r^n(x_i,y_j,1)+c_r^n(x_i-h_x,y_j,1)\right)+$$

$$+\frac{h_\theta^2}{6h_x^2}\left(\frac{\partial^3 c_r^n(x_i+h_x,y_j,1)}{\partial\theta^3}-2\frac{\partial^3 c_r^n(x_i,y_j,1)}{\partial\theta^3}+\frac{\partial^3 c_r^n(x_i-h_x,y_j,1)}{\partial\theta^3}\right)+O(h_\theta^2+h_x). \tag{35}$$

Applying the equality:

$$\frac{1}{h_x^2}\left(c_r^n(x_i+h_x,y_j,1)-2c_r^n(x_i,y_j,1)+c_r^n(x_i-h_x,y_j,1)\right)=\frac{\partial^2 c_r^n(x_i,y_j,1)}{\partial x^2}+O(h_x^2),$$

expression (35) can be rewritten as:

$$\frac{\partial^3 c_r^n(x_i,y_j,1)}{\partial x^2\partial\theta}=-\varepsilon_r\frac{\partial^2 c_r^n(x_i,y_j,1)}{\partial x^2}+\frac{h_\theta^2}{6h_x^2}\left(\frac{\partial^3 c_r^n(x_i+h_x,y_j,1)}{\partial\theta^3}-2\frac{\partial^3 c_r^n(x_i,y_j,1)}{\partial\theta^3}+\frac{\partial^3 c_r^n(x_i-h_x,y_j,1)}{\partial\theta^3}\right)+O(h_\theta^2+h_x).$$

Let $\varphi(x_i\pm h_x,y_j,1)=\frac{\partial^3 c_r^n(x_i\pm h_x,y_j,1)}{\partial\theta^3}$, $\varphi(x_i,y_j,1)=\frac{\partial^3 c_r^n(x_i,y_j,1)}{\partial\theta^3}$. Then the last equality can be written in the form:

$$\frac{\partial^3 c_r^n(x_i,y_j,1)}{\partial x^2\partial\theta}=-\varepsilon_r\frac{\partial^2 c_r^n(x_i,y_j,1)}{\partial x^2}+\frac{h_\theta^2}{6}\left(\frac{\varphi(x_i+h_x,y_j,1)-2\varphi(x_i,y_j,1)+\varphi(x_i-h_x,y_j,1)}{h_x^2}\right)+O(h_\theta^2+h_x). \tag{36}$$

This equality can be transformed into the form:

$$\frac{\partial^3 c_r^n(x_i,y_j,1)}{\partial x^2\partial\theta}=-\varepsilon_r\frac{\partial^2 c_r^n(x_i,y_j,1)}{\partial x^2}+\frac{h_\theta^2}{6}\left(\frac{\partial^2\varphi(x_i,y_j,1)}{\partial x^2}+O(h_x^2)\right)+O(h_\theta^2+h_x).$$

Taking into account the last relation and assuming the boundedness of the derivative $\frac{\partial^2\varphi(x_i,y_j,1)}{\partial x^2}=\frac{\partial^5 c_r^n(x_i,y_j,1)}{\partial x^2\partial\theta^3}$, for the term $\mu_{h,r}(x_i,y_j,1)\frac{\partial^3 c_r^n(x_i,y_j,1)}{\partial x^2\partial\theta}$ on the right-hand side of equality (26), we can write:

$$\mu_{h,r}(x_i,y_j,1)\frac{\partial^3 c_r^n(x_i,y_j,1)}{\partial x^2\partial\theta}=-\varepsilon_r\mu_{h,r}(x_i,y_j,1)\frac{\partial^2 c_r^n(x_i,y_j,1)}{\partial x^2}+O(h_\theta). \tag{37}$$

By carrying out similar reasoning for the derivative $\frac{\partial^3 c_r^n(x_i,y_j,1)}{\partial x\partial\theta^2}$, we obtain:

$$\mu_{h,r}(x_i,y_j,1)\frac{\partial^3 c_r^n(x_i,y_j,1)}{\partial y^2\partial\theta}=-\varepsilon_r\mu_{h,r}(x_i,y_j,1)\frac{\partial^2 c_r^n(x_i,y_j,1)}{\partial y^2}+O(h_\theta). \tag{38}$$

Let us turn to the mixed derivative $\frac{\partial^2 c_r^n(x_i,y_j,1)}{\partial x\partial\theta}$. Following the reasoning presented earlier, we have:

$$\begin{gathered}\frac{\partial^2 c_r^n(x_i,y_j,1)}{\partial x\partial\theta}=\frac{1}{2h_\theta}\left(\frac{\partial\overline{c}_r^n(x_i,y_j,1+h_\theta)}{\partial x}-\frac{\partial\overline{c}_r^n(x_i,y_j,1-h_\theta)}{\partial x}\right)+O(h_\theta^2)=\frac{1}{2h_\theta}\cdot\\ \cdot\left(\frac{\overline{c}_r^n(x_i+h_x,y_j,1+h_\theta)-\overline{c}_r^n(x_i-h_x,y_j,1+h_\theta)}{2h_x}-\frac{\overline{c}_r^n(x_i+h_x,y_j,1-h_\theta)-\overline{c}_r^n(x_i-h_x,y_j,1-h_\theta)}{2h_x}+\right.\\ \left.+O(h_x^2)\right)+O(h_\theta^2)=\frac{1}{2h_x}\left(\frac{\overline{c}_r^n(x_i+h_x,y_j,1+h_\theta)-\overline{c}_r^n(x_i+h_x,y_j,1-h_\theta)}{2h_\theta}-\right.\\ \left.-\frac{\overline{c}_r^n(x_i-h_x,y_j,1+h_\theta)-\overline{c}_r^n(x_i-h_x,y_j,1-h_\theta)}{2h_\theta}\right)+\frac{1}{2h_\theta}O(h_x^2)+O(h_\theta^2).\end{gathered} \tag{39}$$

Based on equality (39), the following relation can be written:

$$\frac{\overline{c}_r^n(x_i\pm h_x,y_j,1+h_\theta)-\overline{c}_r^n(x_i\pm h_x,y_j,1-h_\theta)}{2h_\theta}=-\varepsilon_r c_r^n(x_i\pm h_x,y_j,1)+\frac{h_\theta^2}{6}\frac{\partial^3 c_r^n(x_i\pm h_x,y_j,1)}{\partial\theta^3}+O(h_\theta^4). \tag{40}$$

Using (40), we transform relation (39) into the form:

$$\frac{\partial^2 c_r^n(x_i,y_j,1)}{\partial x\partial\theta}=-\frac{\varepsilon_r}{2h_x}\left(c_r^n(x_i+h_x,y_j,1)-c_r^n(x_i-h_x,y_j,1)\right)+\frac{h_\theta^2}{12h_x}\left(\frac{\partial^3 c_r^n(x_i+h_x,y_j,1)}{\partial\theta^3}-\frac{\partial^3 c_r^n(x_i-h_x,y_j,1)}{\partial\theta^3}\right)+O(h_\theta^2+h_x). \tag{41}$$

Since the following equality holds:

$$\frac{1}{2h_x}\left(c_r^n(x_i+h_x,y_j,1)-c_r^n(x_i-h_x,y_j,1)\right)=\frac{\partial c_r^n(x_i,y_j,1)}{\partial x}+O(h_x^2),$$

expression (41) can be rewritten as:

$$\frac{\partial^2 c_r^n(x_i,y_j,1)}{\partial x\partial\theta}=-\varepsilon_r\frac{\partial c_r^n(x_i,y_j,1)}{\partial x}+\frac{h_\theta^2}{12h_x}\left(\frac{\partial^3 c_r^n(x_i+h_x,y_j,1)}{\partial\theta^3}-\frac{\partial^3 c_r^n(x_i-h_x,y_j,1)}{\partial\theta^3}\right)+O(h_\theta^2+h_x).$$

Let $\varphi(x_i\pm h_x,y_j,1)=\frac{\partial^3 c_r^n(x_i\pm h_x,y_j,1)}{\partial\theta^3}$, $\varphi(x_i,y_j,1)=\frac{\partial^3 c_r^n(x_i,y_j,1)}{\partial\theta^3}$. Then the last equality can be written as:

$$\frac{\partial^2 c_r^n(x_i,y_j,1)}{\partial x\partial\theta}=-\varepsilon_r\frac{\partial c_r^n(x_i,y_j,1)}{\partial x}+\frac{h_\theta^2}{6}\left(\frac{\varphi(x_i+h_x,y_j,1)-\varphi(x_i-h_x,y_j,1)}{2h_x}\right)+O(h_\theta^2+h_x). \tag{42}$$

This expression can be further transformed into the form:

$$\frac{\partial^2 c_r^n(x_i,y_j,1)}{\partial x\partial\theta}=-\varepsilon_r\frac{\partial c_r^n(x_i,y_j,1)}{\partial x}+\frac{h_\theta^2}{6}\left(\frac{\partial\varphi(x_i,y_j,1)}{\partial x}+O(h_x^2)\right)+O(h_\theta^2+h_x).$$

Taking into account the last relation and assuming the boundedness of the derivative $\frac{\partial\varphi(x_i,y_j,1)}{\partial x}=\frac{\partial^4 c_r^n(x_i,y_j,1)}{\partial x\partial\theta^3}$, for the term $\left(u^n(x_i,y_j,1)-\frac{\partial\mu_{h,r}(x_i,y_j,1)}{\partial x}\right)\frac{\partial^2 c_r^n(x_i,y_j,1)}{\partial x\partial\theta}$ on the right-hand side of equality (26), we can write:

$$\left(u^n\left(x_i,y_j,1\right)-\frac{\partial\mu_{h,r}\left(x_i,y_j,1\right)}{\partial x}\right)\frac{\partial^2 c_r^n\left(x_i,y_j,1\right)}{\partial x\partial\theta}=-\varepsilon_r\left(u^n\left(x_i,y_j,1\right)-\frac{\partial\mu_{h,r}\left(x_i,y_j,1\right)}{\partial x}\right)\frac{\partial c_r^n\left(x_i,y_j,1\right)}{\partial x}+O\left(h_\theta\right). \tag{43}$$

By applying similar reasoning to the derivative $\frac{\partial^2 c_r^n\left(x_i,y_j,1\right)}{\partial y\partial\theta}$ with respect to the term $\left(u^n\left(x_i,y_j,1\right)-\frac{\partial\mu_{h,r}\left(x_i,y_j,1\right)}{\partial x}\right)\frac{\partial^2 c_r^n\left(x_i,y_j,1\right)}{\partial x\partial\theta}$ from the right-hand side of equality (26), we obtain the relation:

$$\left(v^n\left(x_i,y_j,1\right)-\frac{\partial\mu_{h,r}\left(x_i,y_j,1\right)}{\partial y}\right)\frac{\partial^2 c_r^n\left(x_i,y_j,1\right)}{\partial y\partial\theta}=-\varepsilon_r\left(v^n\left(x_i,y_j,1\right)-\frac{\partial\mu_{h,r}\left(x_i,y_j,1\right)}{\partial y}\right)\frac{\partial c_r^n\left(x_i,y_j,1\right)}{\partial y}+O\left(h_\theta\right). \tag{44}$$

Now let us turn to the derivative $\frac{\partial^2 c_r^n\left(x_i,y_j,1\right)}{\partial\theta^2}$. We have:

$$\frac{\partial^2 c_r^n\left(x_i,y_j,1\right)}{\partial\theta^2}=\frac{1}{2h_\theta}\left(\frac{\partial\overline{c}_r^n\left(x_i,y_j,1+h_\theta\right)}{\partial\theta}-\frac{\partial\overline{c}_r^n\left(x_i,y_j,1-h_\theta\right)}{\partial\theta}\right)+O\left(h_\theta^2\right). \tag{45}$$

Using expression (25), which defines the value of the function $\overline{c}_r^n$ at the fictitious node $(x_i, y_j, 1 + h_\theta)$, we obtain:

$$\frac{\partial\overline{c}_r^n\left(x_i,y_j,1+h_\theta\right)}{\partial\theta}=\frac{\partial}{\partial\theta}\left(\overline{c}_r^n\left(x_i,y_j,1-h_\theta\right)+2h_\theta\varepsilon_r c_r^n\left(x_i,y_j,1\right)-\frac{h_\theta^3}{3}\frac{\partial^3 c_r^n\left(x_i,y_j,1\right)}{\partial\theta^3}+O\left(h_\theta^5\right)\right)=$$

$$=\frac{\partial\overline{c}_r^n\left(x_i,y_j,1-h_\theta\right)}{\partial\theta}+2h_\theta\varepsilon_r\frac{\partial\overline{c}_r^n\left(x_i,y_j,1\right)}{\partial\theta}-\frac{h_\theta^3}{3}\frac{\partial^4 c_r^n\left(x_i,y_j,1\right)}{\partial\theta^4}+O\left(h_\theta^4\right).$$

Taking the last equality into account, we rewrite equality (45) in the form:

$$\frac{\partial^2 c_r^n\left(x_i,y_j,1\right)}{\partial\theta^2}=-\varepsilon_r\frac{\partial\overline{c}_r^n\left(x_i,y_j,1\right)}{\partial\theta}+O\left(h_\theta\right). \tag{46}$$

It is straightforward to derive the following approximations with accuracy $O(h_x)$ and $O(h_y)$:

$$\frac{\partial\mu_{h,r}\left(x_i,y_j,1\right)}{\partial\theta}\cdot\frac{\partial^2 c_r^n\left(x_i,y_j,1\right)}{\partial x^2}\cong\frac{1}{h_\theta h_x^2}\left(\mu_{h,r}\left(x_i,y_j,0.5h_\theta\right)-\mu_{v,r}\left(x_i,y_j,-0.5h_\theta\right)\right)\cdot$$
$$\cdot\left(\overline{c}_r^n\left(x_i+h_x,y_j,1\right)-2\overline{c}_r^n\left(x_i,y_j,1\right)+\overline{c}_r^n\left(x_i-h_x,y_j,1\right)\right), \tag{47}$$

$$\frac{\partial\mu_{h,r}\left(x_i,y_j,1\right)}{\partial\theta}\frac{\partial^2 c_r^n\left(x_i,y_j,1\right)}{\partial y^2}\cong\frac{1}{h_\theta h_y^2}\left(\mu_{h,r}\left(x_i,y_j,0.5h_\theta\right)-\mu_{v,r}\left(x_i,y_j,-0.5h_\theta\right)\right)\cdot$$
$$\cdot\left(\overline{c}_r^n\left(x_i,y_j+h_y,1\right)-2\overline{c}_r^n\left(x_i,y_j,1\right)+\overline{c}_r^n\left(x_i,y_j-h_y,1\right)\right), \tag{48}$$

$$\left(\frac{\partial u^n\left(x_i,y_j,1\right)}{\partial\theta}-\frac{\partial^2\mu_{h,r}\left(x_i,y_j,1\right)}{\partial x\partial\theta}\right)\frac{\partial c_r^n\left(x_i,y_j,1\right)}{\partial x}\cong\frac{1}{2h_x}\left[\frac{1}{h_\theta}\left(u^n\left(x_i,y_j,1+0.5h_\theta\right)-u^n\left(x_i,y_j,1-0.5h_\theta\right)\right)-\right.$$
$$-\frac{1}{h_x h_\theta}\left(\mu_{v,r}\left(x_i+0.5h_x,y_j,1+0.5h_\theta\right)-\mu_{v,r}\left(x_i-0.5h_x,y_j,1+0.5h_\theta\right)-\right. \tag{49}$$
$$\left.\left.-\mu_{v,r}\left(x_i+0.5h_x,y_j,1-0.5h_\theta\right)+\mu_{v,r}\left(x_i-0.5h_x,y_j,1-0.5h_\theta\right)\right)\right]\left(\overline{c}_r^n\left(x_i+h_x,y_j,1\right)-\overline{c}_r^n\left(x_i-h_x,y_j,1\right)\right),$$

$$-\frac{1}{h_y h_\theta}\left(\mu_{v,r}\left(x_i,y_j+0.5h_y,1+0.5h_\theta\right)-\mu_{v,r}\left(x_i,y_j-0.5h_y,1+0.5h_\theta\right)-\right.$$
$$\left.-\mu_{v,r}\left(x_i,y_j+0.5h_y,1-0.5h_\theta\right)+\mu_{v,r}\left(x_i,y_j-0.5h_y,1-0.5h_\theta\right)\right)\left(\overline{c}_r^n\left(x_i,y_j+h_y,1\right)-\overline{c}_r^n\left(x_i,y_j-h_y,1\right)\right). \tag{50}$$

When approximating $c_r^n\left(x_i,y_j,1\right)$ we replace it with its discrete analogue $\overline{c}_r^n\left(x_i,y_j,1\right)$.
Then

$$\frac{\partial^2 u^n\left(x_i,y_j,1\right)}{\partial x\partial\theta}c_r^n\left(x_i,y_j,1\right)\cong\frac{1}{h_\theta}\left(\frac{u^n\left(x_i+0.5h_x,y_j,1+0.5h_\theta\right)-u^n\left(x_i-0.5h_x,y_j,1+0.5h_\theta\right)}{h_x}-\right.$$
$$\left.-\frac{u^n\left(x_i+0.5h_x,y_j,1-0.5h_\theta\right)-u^n\left(x_i-0.5h_x,y_j,1-0.5h_\theta\right)}{h_x}\right)c_r^n\left(x_i,y_j,1\right), \tag{51}$$

$$\frac{\partial^2 v^n(x_i,y_j,1)}{\partial y\partial\theta}c_r^n(x_i,y_j,1)\cong\frac{1}{h_\theta}\left(\frac{v^n(x_i,y_j+0.5h_y,1+0.5h_\theta)-v^n(x_i,y_j-0.5h_y,1+0.5h_\theta)}{h_y}-\right.$$
$$\left.-\frac{v^n(x_i,y_j+0.5h_y,1-0.5h_\theta)-v^n(x_i,y_j-0.5h_y,1-0.5h_\theta)}{h_y}\right)c_r^n(x_i,y_j,1), \quad (52)$$

$$\frac{w_{g,r}}{\mu_{v,r}(x_i,y_j,1)}\frac{\partial u^n(x_i,y_j,1)}{\partial x}c_r^n(x_i,y_j,1)\cong\frac{2w_{g,r}}{\mu_{v,r}(x_i,y_j,1+0.5h_\theta)+\mu_{v,r}(x_i,y_j,1-0.5h_\theta)}\cdot$$
$$\cdot\left(\frac{u^n(x_i+0.5h_x,y_j,1)-u^n(x_i-0.5h_x,y_j,1)}{h_x}\right)c_r^n(x_i,y_j,1), \quad (53)$$

$$\frac{w_{g,r}}{\mu_{v,r}(x_i,y_j,1)}\frac{\partial v^n(x_i,y_j,1)}{\partial y}c_r^n(x_i,y_j,1)\cong\frac{2w_{g,r}}{\mu_{v,r}(x_i,y_j,1+0.5h_\theta)+\mu_{v,r}(x_i,y_j,1-0.5h_\theta)}\cdot$$
$$\cdot\left(\frac{v^n(x_i,y_j+0.5h_y,1)-v^n(x_i,y_j-0.5h_y,1)}{h_y}\right)c_r^n(x_i,y_j,1), \quad (54)$$

$$\frac{2w_{g,r}}{H^2(x_i,y_j)\mu_{v,r}(x_i,y_j,1)}\frac{\partial^2\mu_{v,r}(x_i,y_j,1)}{\partial\theta^2}c_r^n(x_i,y_j,1)\cong\frac{2w_{g,r}}{H^2(x_i,y_j)\left(\mu_{v,r}(x_i,y_j,1+0.5h_\theta)+\mu_{v,r}(x_i,y_j,1-0.5h_\theta)\right)}\cdot$$
$$\cdot\frac{1}{h_\theta^2}\left(\mu_{v,r}(x_i,y_j,1+0.5h_\theta)-2\mu_{v,r}(x_i,y_j,1)+\mu_{v,r}(x_i,y_j,1-0.5h_\theta)\right)c_r^n(x_i,y_j,1). \quad (55)$$

As a result of substituting approximations (32), (37), (38), (43)–(55) into equality (26), with accuracy $O(h_\theta)$ (or higher), and rearranging the terms, we obtain:

$$\frac{\partial^3\overline{c}_r^n(x_i,y_j,1)}{\partial\theta^3}=\vartheta_1+O(h_\theta), \quad (56)$$

where

$$\vartheta_1=\vartheta_{10}\left(\vartheta_{11}\overline{c}_r^n(x_i,y_j,1-h_\theta)+\vartheta_{12}\overline{c}_r^n(x_i,y_j+h_y,1)+\vartheta_{13}\overline{c}_r^n(x_i,y_j-h_y,1)+\vartheta_{14}\overline{c}_r^n(x_i,y_j,1+h_\theta)+\right.$$
$$\left.+\vartheta_{15}\overline{c}(x_i,y_j,1-h_\theta)+\vartheta_{16}\overline{c}(x_i,y_j,1)\right).$$

After substituting the derived representations for the coefficients ϑ_{1i}, $i=1...,6$ into the approximation formula given above, one can obtain the final approximation of the third-kind boundary condition, which is not presented here due to its cumbersomeness.

Using equality (56) for $D_\theta\overline{c}_r^n(x_i,y_j,1)$, we can write:

$$D_\theta\overline{c}_r^n(x_i,y_j,1)\cong\frac{1}{H^2(x_i,y_j)h_\theta^2}\left[\left(\mu_{v,r}(x_i,y_j,1+0.5h_\theta)+\mu_{v,r}(x_i,y_j,1-0.5h_\theta)\right)\cdot\right.$$
$$\left.\cdot\left(\overline{c}_r^n(x_i,y_j,1-h_\theta)-\overline{c}_r^n(x_i,y_j,1)\right)-\mu_{v,r}(x_i,y_j,1+0.5h_\theta)\left(2h_\theta\varepsilon_r c_r^n(x_i,y_j,1)-\frac{h_\theta^3}{3}\vartheta_1\right)\right]. \quad (57)$$

The approximation error of scheme (57) at the boundary nodes of grid $\overline{\omega}^+$ for $\theta_k=1$ is $O(\tau+h_\theta^2)$.

Discussion. The paper addresses issues related to the finite-difference approximation of a spatially three-dimensional problem of multifractional suspended matter transport. Certain difficulties arise in approximating this problem due to the necessity of ensuring the required order of approximation up to the boundary. Methods are proposed for approximating the problem with second-order accuracy in spatial variables and first-order accuracy in the temporal variable. Special attention should be given to studies related to the approximation of boundary conditions of the second and third kind. For this purpose, the authors propose methods based on approximations of boundary conditions using central difference formulas, followed by differentiation of both sides of the diffusion–convection equations and the elimination of solution functions at fictitious nodes of the extended grid.

Conclusion. Further research by the authors may focus on the analysis of the constructed difference schemes, taking into account physically motivated constraints on the time step size τ and the grid Peclet number.

References

1. Sukhinov A.I., Chistyakov A.E., Bondarenko Yu.S. Error estimation of the solution to the equation based on weighted schemes. *Izvestiya YUFU. Technical Sciences*. 2011;8(121):6–13. (In Russ.)

2. Sukhinov A.I., Chistyakov A.E., Protsenko E.A. Construction of a discrete two-dimensional mathematical model of sediment transport. *Izvestiya YUFU. Technical Sciences*. 2011;8(121):32–44. (In Russ.)

3. Sukhinov A.I., Chistyakov A.E., Protsenko E.A., Sidorakina V.V., Protsenko S.V. Parallel algorithms for solving the problem of dynamics of bottom relief changes in coastal systems. *Computational Methods and Programming*. 2020;21(3):196–206. (In Russ.) https://doi.org/10.26089/NumMet.v21r318

4. Sukhinov A.I., Chistyakov A.E., Protsenko E.A., Sidorakina V.V., Protsenko S.V. A complex of combined models for sediment and suspension transport considering three-dimensional hydrodynamic processes in the coastal zone. *Mathematical Modelling*. 2020;32(2):3–23. (In Russ.) https://doi.org/10.20948/mm-2020-02-01

5. Sukhinov A.I., Chistyakov A.E., Protsenko S.V., Sidoryakina V.V. Coupled 3D wave and 2D bottom deposit transportation models for the prediction of harmful phenomena in coastal zone. In: *Trends in the Analysis and Design of Marine Structures — Proceedings of the 7th International Conference on Marine Structures, MARSTRUCT 2019*. 2019. P. 597–603. https://doi.org/10.1201/9780429298875-68

6. Sukhinov A.I., Sidoryakina V.V. Development and analysis of the correctness of a mathematical model for the transport and sedimentation of suspensions, taking into account changes in bottom relief. *Computational Mathematics and Information Technologies*. 2018;2(2):76–90. (In Russ.) https://doi.org/10.23947/2587-8999-2018-2-76-90

7. Sukhinov A.I., Sukhinov A.A., Sidoryakina V.V. Uniqueness of solving the problem of transport and sedimentation of multicomponent suspensions in coastal systems. In: *Journal of Physics: Conference Series. Applied Mathematics, Computational Science and Mechanics: Current Problems*. Bristol, 2020;1479:012081. https://doi.org/10.1088/1742-6596/1479/1/012081

8. Sukhinov A.I., Sidoryakina V.V. Development and correctness analysis of the mathematical model of transport and suspension sedimentation depending on bottom relief variation. *Vestnik of Don State Technical University.* 2018;18(4):350–361. https://doi.org/10.23947/1992-5980-2018-18-4-350-361

9. Sukhinov A.I., Chistyakov A.E., Sidoryakina V.V., Protsenko S.V., Atayan A.M. Locally two-dimensional splitting schemes for parallel solving of the three-dimensional problem of suspended substance transport. *Mathematical Physics and Computer Simulation.* 2021;24(2):38–53. (In Russ.) https://doi.org/10.15688/mpcm.jvolsu.2021.2.4

10. Popov I.V. Construction of a difference scheme of increased order of approximation for a nonlinear transport equation using adaptive artificial viscosity. *Preprints of the Keldysh Institute of Applied Mathematics of the Russian Academy of Sciences.* 2017;68:1–22. (In Russ.) https://doi.org/10.20948/prepr-2017-68

11. Sidoryakina V.V., Sukhinov A.I. Construction and analysis of the proximity of solutions in L2 for two boundary problems in the model of multicomponent suspension transport in coastal systems. *Journal of Computational Mathematics and Mathematical Physics.* 2023;63(10):1721–1732. (In Russ.) https://doi.org/10.1134/S0965542523100111

12. Litvinov V.N., Chistyakov A.E., Nikitina A.V., Atayan A.M., Kuznetsova I.Yu. Mathematical modeling of hydrodynamics problems of the Azov Sea on a multiprocessor computer system. *Computer Research and Modelling*. 2024;16(3):647–672. (In Russ.) https://doi.org/10.20537/2076-7633-2024-16-3-647-672

13. Chistyakov A.E., Nikitina, A.V., Kuznetsova I.Yu., Rakhimbaeva E.O., Porksheyan M.V. Investigation of the approximation error of the difference scheme for the mathematical model of hydrodynamics. *Lobachevskii Journal of Mathematics.* 2023;44(5):1839–1846. (In Russ.) https://doi.org/10.1134/S1995080223050128

14. Sidoryakina V.V., Protsenko S.V. Various approximations of vertical turbulent exchange parameterization for the analysis of the waves hydrodynamic impact on the bottom of the reservoir. *Computational Mathematics and Information Technologies.* 2021;5(2):80–87. https://doi.org/10.23947/2587-8999-2021-1-2-80-87

15. Sidoryakina V.V. Construction of Second-Order Finite Difference Schemes for Diffusion-Convection Problems of Multifractional Suspensions in Coastal Marine Systems. *Computational Mathematics and Information Technologies*. 2024;8(3):43–59. (In Russ.) https://doi.org/10.23947/2587-8999-2024-8-3-43-59

About the Authors:

Alexander I. Sukhinov, Corresponding Member of the Russian Academy of Sciences, Doctor of Physical and Mathematical Sciences, Professor, Director of the Research Institute of Mathematical Modeling and Forecasting of Complex Systems, Don State Technical University (1, Gagarin Sq., Rostov-on-Don, 344003, Russian Federation), ORCID, SPIN-code, Scopus, ResearcherID, MathSciNet, sukhinov@gmail.com

Valentina V. Sidoryakina, Candidate of Physical and Mathematical Sciences, Associate Professor, Department of Mathematics and Informatics, Don State Technical University (1, Gagarin Sq., Rostov-on-Don, 344003, Russian Federation), ORCID, SPIN-code, ResearcherID, MathSciNet, ScopusID, cvv9@mail.ru

Contributions of the authors:

A.I. Sukhinov: general scientific guidance; problem statement; formulation of research ideas, goals and objectives; development of methodology.

V.V. Sidoryakina: obtaining calculation formulas; formulation of achieved results and description of their significance.

Conflict of Interest Statement: **the authors declare no conflict of interest.**

All authors have read and approved the final manuscript.

Об авторах:

Сухинов Александр Иванович, член-корреспондент РАН, доктор физико-математических наук, профессор, директор НИИ Математического моделирования и прогнозирования сложных систем Донского государственного технического университета (344003, Российская Федерация, г. Ростов-на-Дону, пл. Гагарина, 1), ORCID, SPIN-код, Scopus, Scopus, ResearcherID, MathSciNet, sukhinov@gmail.com

Сидорякина Валентина Владимировна, кандидат физико-математических наук, доцент, кафедры математики и информатики Донского государственного технического университета (344003, Российская Федерация, г. Ростов-на-Дону, пл. Гагарина, 1), ORCID, SPIN-код, ResearcherID, MathSciNet, ScopusID, cvv9@mail.ru

Заявленный вклад авторов:

А.И. Сухинов: общее научное руководство; постановка задачи; формулировка идей исследования, целей и задач; разработка методологии.

В.В. Сидорякина: получение расчетных формул; формулировка достигнутых результатов и описание их значимости.

Конфликт интересов: **авторы заявляют об отсутствии конфликта интересов.**

Все авторы прочитали и одобрили окончательный вариант рукописи.

Received / Поступила в редакцию 07.08.2025
Revised / Поступила после рецензирования 09.09.2025
Accepted / Принята к публикации 22.09.2025

COMPUTATIONAL MATHEMATICS
ВЫЧИСЛИТЕЛЬНАЯ МАТЕМАТИКА

UDC 519.6

Original Empirical Research

https://doi.org/10.23947/2587-8999-2025-9-3-30-43

Modelling Circulation in Blood Vessel Aneurysms

Natalya K. Volosova[1], Konstantin A. Volosov[2], Aleksandra K. Volosova[2], Mikhail I. Karlov[3], Dmitriy F. Pastukhov[4] ✉, Yuriy F. Pastukhov[4]

[1] MGTU named after. N.E. Bauman, Moscow, Russian Federation

[2] Russian University of Transport, Moscow, Russian Federation

[3] Moscow Institute of Physics and Technology (National Research University), Dolgoprudny, Russian Federation

[4] Polotsk State University named after Euphrosyne of Polotsk, Novopolotsk, Republic of Belarus

✉ dmitrij.pastuhov@mail.ru

Abstract

Introduction. A two-dimensional hydrodynamic problem in the "stream function–vorticity" variables is numerically solved in an open rectangular cavity simulating blood flow in a blood vessel aneurysm. Two solution algorithms are proposed for Reynolds numbers Re < 1 and for Re ≥ 1.

Materials and Methods. To accelerate the numerical solution with an explicit finite-difference scheme for the vorticity dynamics equation, the initial condition damping method, the n-fold splitting method of the explicit finite-difference scheme (n = 100, 200), and the symmetry plane of the rectangular cavity–aneurysm were employed. In the splitting method, the maximum time step proportional to the square of the spatial step was used without violating the spectral stability of the explicit scheme in the vorticity equation. On half of the rectangular aneurysm, symmetric solutions were considered with a uniform 100 × 50 grid and equal steps $h_1 = h_2 = 0.01$. The inverse matrix for solving the Poisson equation in the "stream function–vorticity" variables with a finite number of elementary operations was computed using the MSIMSL library.

Results. The numerical solution showed that the number and location of circulation regions in the aneurysm at small Reynolds numbers depend on the ratio of the vessel diameter to the aneurysm diameter. At small values of this parameter, the aneurysm contains a single large vortex that narrows the vessel lumen in the case of thrombus formation inside the aneurysm. The narrowing of the blood flow tube inside the aneurysm reaches 34%. It was found that the formation of the hydrodynamic structure in the aneurysm occurs in a time negligible (0.002%) compared to the period between pulsation waves (1 s). For the first time, a boundary condition with fourth-order accuracy was proposed to relate velocity, vorticity, and stream function.

Discussion and Conclusion. The approximation of the equations in systems (4) and (22) has sixth-order accuracy at interior nodes and fourth-order accuracy at boundary nodes. The problem was also solved for blood motion in arteries at high Reynolds numbers (Re = 1500). The solution shows that in the aneurysm symmetry plane a chain of connected vortices is formed with alternating signs of vorticity, carried by the blood flow along the vessel. The initial–boundary value problems (4), (22) formulated in this work make it possible to qualitatively model blood flow in aneurysms of capillaries, arterioles, and arteries at low and high velocities, as well as blood motion in elements of medical equipment.

Keywords: hydrodynamics, numerical methods, partial differential equations, initial–boundary value problem, aneurysm

For Citation. Volosova N.K., Volosov K.A., Volosova A.K., Karlov M.I., Pastukhov D.F., Pastukhov Yu.F. Modelling Circulation in Blood Vessel Aneurysms. *Computation Mathematics and Information Technologies*. 2025;9(3):30–43. https://doi.org/10.23947/2587-8999-2025-9-3-30-43

Оригинальное эмпирическое исследование

Моделирование циркуляции в аневризмах кровеносных сосудов

Н.К. Волосова[1], К.А. Волосов[2], А.К. Волосова[2], М.И. Карлов[3], Д.Ф. Пастухов[4]✉, Ю.Ф. Пастухов[4]

[1] Московский государственный технический университет им. Н.Э. Баумана, г. Москва, Российская Федерация

[2] Российский университет транспорта, г. Москва, Российская Федерация

[3] Московский физико-технический институт (национальный исследовательский университет), г. Долгопрудный, Российская Федерация

[4] Полоцкий государственный университет им. Евфросинии Полоцкой, г. Новополоцк, Республика Беларусь

✉ dmitrij.pastuhov@mail.ru

Аннотация

Введение. Численно решается двумерная гидродинамическая задача в переменных «функция тока — вихрь» в открытой прямоугольной каверне, моделирующей течение крови в аневризме кровеносного сосуда. Предложены два алгоритма решения задачи для чисел Рейнольдса $Re < 1$ и для чисел $Re \geq 1$.

Материалы и методы. Для ускорения численного решения задачи с явной разностной схемой уравнения динамики вихря использовался метод торможения начальных условий, метод n-кратного расщепления явной разностной схемы ($n = 100, 200$) и наличие плоскости симметрии прямоугольной области каверны — аневризмы. В методе расщепления используется максимальный шаг времени, пропорциональный квадрату координатного шага без нарушения спектральной устойчивости явной схемы в уравнении вихря. На половине прямоугольной аневризмы рассматривались симметричные решения и применялась равномерная сетка 100 × 50 с равным шагом $h_1 = h_2 = 0{,}01$. Обратная матрица для решения уравнения Пуассона в переменных «функция тока — вихрь» за конечное число элементарных операций вычислялась библиотекой Msimsl.

Результаты исследования. Численное решение задачи показало, что число и расположение областей циркуляции крови в аневризме при небольших числах Рейнольдса зависят от параметра отношения диаметра сосуда к диаметру аневризмы. Именно при небольшом значении этого параметра аневризму занимает один большой вихрь и сужает просвет сосуда в случае образования тромба внутри аневризмы. Сужение диаметра трубки тока крови внутри аневризмы достигает 34 %. Обнаружено, что формирование гидродинамической структуры в аневризме происходит за время, малое (0,002 %) по сравнению с периодом между пульсационными волнами (1с). Впервые предложено краевое условие с четвертым порядком погрешности для связи скорости, вихря и функции тока.

Обсуждение. Аппроксимация уравнений в системах (4) и (22) имеет шестой порядок погрешности во внутренних и четвертый в граничных узлах. Задача решена также для движения крови в артериях при больших числах Рейнольдса ($Re = 1500$). Ее решение показывает, что в плоскости симметрии аневризмы образуется цепочка связанных вихрей с чередованием знака функции вихря и сносимых кровью вдоль кровеносного сосуда.

Обсуждение и заключение. Сформулированные в работе начально-краевые задачи (4), (22) позволят качественно моделировать движение крови в аневризмах капилляров, артериол и артерий кровеносных сосудов при малых и больших скоростях, а также движение крови в элементах медицинского оборудования.

Ключевые слова: гидродинамика, численные методы, уравнения в частных производных, начально-краевая задача, аневризма

Для цитирования. Волосова Н.К., Волосов К.А., Волосова А.К., Карлов М.И., Пастухов Д.Ф., Пастухов Ю.Ф. Моделирование циркуляции в аневризмах кровеносных сосудов. *Computational Mathematics and Information Technologies*. 2025;9(3):30–43. https://doi.org/10.23947/2587-8999-2025-9-3-30-43

Introduction. This study models a two-dimensional hydrodynamic problem of blood flow in an open rectangular cavity in the “stream function–vorticity” formulation [1]. The velocity field exhibits four corner singular points at the inlet and outlet segments of the cavity–aneurysm, since the streamlines at these points may undergo a 90-degree deflection. Consequently, steep velocity gradients appear in these regions, and the points act as sources of vortices under high blood flow velocity. The present work employs the initial velocity field damping method described in [2]. References [3–7], [8] are related to the solution of two-dimensional hydrodynamic problems or to their high-accuracy approximation. Study [7] specifically addresses blood flow and coagulation processes in blood vessels. In the present research, the *n*-fold splitting method of the vorticity equation ($n = 100, 200$) with an explicit finite-difference scheme, as introduced in [9], is applied. Due to the symmetry of the rectangular cavity (aneurysm), the computational cost can be reduced by half by solving the problem only on one side of the rectangle.

Materials and Methods

Problem Statement. In the two-dimensional formulation, we consider the flow of fluid (blood) in a rectangular cavity–aneurysm, which defines the geometry of the problem. Therefore, it is convenient to adopt a rectangular coordinate system with a uniform grid $n_1 \times n_2 = 100 \times 100$.

We derive the Poiseuille formula for the velocity profile $u(y)$ of plane fluid flow between two parallel rectangular plates. In Fig. 1, the center of the rectangular coordinate system coincides with the symmetry center of a liquid parallelepiped with side lengths $2y \cdot l \cdot b$, with edge length b perpendicular to the plane of the figure. Pressure values p_1, p_2 act on the left and right faces, respectively; the pressure is constant along the y-axis and varies along the x-axis. The difference in pressure forces is equal to $\Delta F_p = (p_1 - p_2)2yb = \frac{p_1 - p_2}{l} 2ybl = \frac{\Delta p}{\Delta x} 2ybl$. This pressure force difference ΔF_p is balanced by the viscous friction force acting on the lower and upper faces of the block.

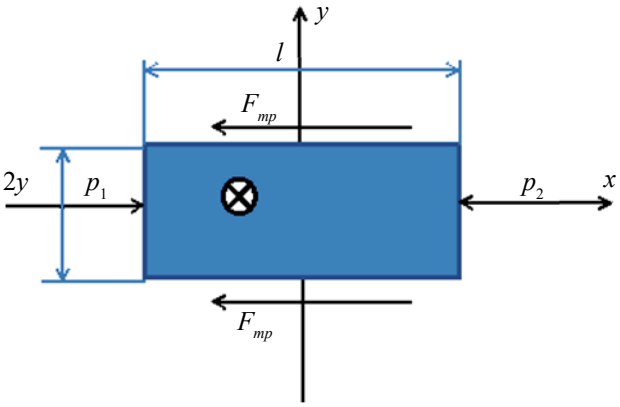

Fig. 1. Illustration of the Poiseuille formula for plane fluid flow

The difference in forces is given by:

$$\Delta F_p = \frac{\Delta p}{\Delta x} 2ybl = 2F_{mp} = 2bl\mu \frac{du}{dy} \Leftrightarrow \frac{du}{dy} = \frac{1}{\mu} \frac{\Delta p}{\Delta x} y \Leftrightarrow u(y) = C_1 y^2 + C_2, C_1 = \frac{1}{2\mu} \frac{\Delta p}{\Delta x} = const.$$

Let us denote the half-width of the plane channel for fluid motion as the velocity of the fluid on the symmetry plane as $u_{\max}$ and determine the unknown constants C_1, C_2 from the no-slip condition on the rigid rectangular plates:

$$u(\Delta) = 0 \Leftrightarrow C_1 \Delta^2 + C_2 = 0, u(0) = C_2 = u_{\max}, C_1 = -\frac{C_2}{\Delta^2} = -\frac{u_{\max}}{\Delta^2}, u(y) = u_{\max}\left(1 - \frac{y^2}{\Delta^2}\right). \quad (1)$$

An aneurysm represents a small segment of a blood vessel whose diameter usually exceeds the vessel diameter by a factor of about two. The aneurysm length L is typically comparable to its diameter $2H$, where H is the aneurysm half-width. To simplify the problem in the rectangular coordinate system, we assume that in an infinite rectangular region between the upper and lower plates a plane fluid flow is formed with the velocity profile (1). A rectangular cavity with inlet and outlet will be referred to as an *open cavity*.

For further simplification, we also assume that the velocity profile (1) is preserved at the inlet to the rectangular aneurysm and at the outlet from it within a narrow symmetric strip relative to the plane $0xz$ of width $2\Delta = 2d$. To accelerate the numerical solution, we exploit symmetry by considering only half of the aneurysm and two halves of the rectangular channel supplying and removing the fluid. According to the symmetry principle, we seek solutions in which, on the symmetry axis, the velocity of fluid particles is directed along the axis at every point; its magnitude may vary numerically, but its direction remains unchanged.

In Fig. 2, the origin of the coordinate system coincides with the lower-left corner of the aneurysm; the x-axis is directed to the right, and the y-axis is directed upward. Let denote $(u(x,y),v(x,y))$ the velocity vector of a fluid particle. On the rigid boundary-namely, on the lower segment and on the lower portions of the side segments of height $H–d$ of the rectangular cavity — the velocity is zero (no-slip condition). Therefore, the stream function on this boundary can be taken as zero. In addition, the normal velocity component is zero on the upper segment of the rectangular cavity $v(x,H) = 0, 0 \le x \le L$.

It is necessary to modify the boundary conditions for velocity and stream function in the formulation of the classical hydrodynamic problem in the "stream function–vorticity" variables for a rectangular cavity, as considered in [1, 2].

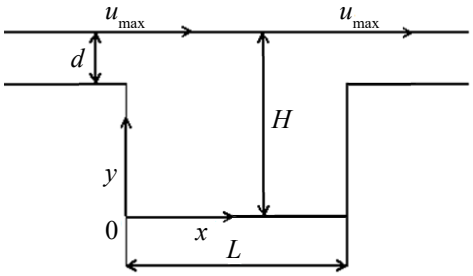

Fig. 2. Geometry of the computational domain

We rewrite the velocity profile (1), taking into account the shift of the coordinate origin shown in Fig. 2:

$$y = \bar{y} + H, u(\bar{y}) = u(y - H) = u_{\max}\left(1 - \frac{(y-H)^2}{\Delta^2}\right), y \in [H - \Delta, H]. \tag{2}$$

Integrating equation (2) with respect to y, and taking into account the relation $u = \psi_y$, we obtain the dependence of the stream function in the gaps along the side walls of the cavity:

$$\begin{gathered}\psi(y) = u_{\max}\left(y - \frac{(y-H)^3}{3\Delta^2}\right) + C_0, \psi(H-\Delta) = 0 \Leftrightarrow C_0 = -u_{\max}\left(H - \frac{2}{3}\Delta\right), \\ \psi(0,y) = \psi(L,y) = \begin{cases} 0, y \in [0, H-\Delta], \\ u_{\max}\left(y + \frac{2}{3}\Delta - H - \frac{(y-H)^3}{3\Delta^2}\right), y \in [H-\Delta, H]. \end{cases}\end{gathered} \tag{3}$$

As in [2], we denote the characteristic length by L, time by $\frac{L}{u_{\max}}$, velocity by $u_{\max}$, stream function by $Lu_{\max}$, vorticity by $\frac{u_{\max}}{L}$, and Reynolds number by Re. We introduce the following dimensionless variables: the horizontal coordinate is denoted by $\bar{x}$, the vertical coordinate by $\bar{y}$, the stream function and vorticity by $\bar{\psi}, \bar{w}$, respectively, the velocity vector by $(\bar{u}, \bar{v})$, and time by $\bar{t}$. These quantities are nondimensionalized as follows:

$$0 \le \bar{x} = \frac{x}{L} \le 1,\ 0 \le \bar{y} = \frac{y}{L} \le k = \frac{H}{L}, \bar{\psi} = \frac{\psi}{\psi_{\max}}, \psi_{\max} = Lu_{\max},$$

$$\bar{u} = \frac{u}{u_{\max}}, \bar{v} = \frac{v}{u_{\max}} \bar{w} = \frac{w}{w_{\max}}, w_{\max} = \frac{u_{\max}}{L},$$

$$\bar{t} = \frac{t}{T}, T = \frac{L}{u_{\max}}, \mathrm{Re} = \frac{u_{\max} L}{\nu}.$$

The kinematic viscosity of blood is $\nu = \frac{\mu}{\rho} = \frac{3{,}5 \cdot 10^{-3}\, Па \cdot с}{1050\, кг/м^3} = 3{,}33(3) \cdot 10^{-6} \frac{м^2}{с}$.

The hydrodynamic system in nondimensional variables and functions, following [1, 2], for an open cavity at high Reynolds numbers can be written as:

$$\begin{cases} \bar{\psi}_{\bar{x}\bar{x}} + \bar{\psi}_{\bar{y}\bar{y}} = -\bar{w}(\bar{x}, \bar{y}),\ 0 < \bar{x} = \frac{x}{L} < 1,\ 0 < \bar{y} < k_{\max}, \\ \bar{w} = \bar{v}_{\bar{x}} - \bar{u}_{\bar{y}}, \\ \bar{u} = \bar{\psi}_{\bar{y}}; \bar{v} = -\bar{\psi}_{\bar{x}}, \\ \bar{w}_{\bar{t}} + \bar{u} \cdot \bar{w}_{\bar{x}} + \bar{v} \cdot \bar{w}_{\bar{y}} = \frac{1}{\mathrm{Re}}\left(\bar{w}_{\bar{x}\bar{x}} + \bar{w}_{\bar{y}\bar{y}}\right), 0 < \bar{t} = \frac{t}{T}, \\ \bar{\psi}\big|_{\Gamma 1} \equiv 0, \bar{v}\big|_{\Gamma} \equiv 0, \bar{u}\big|_{\Gamma_1} = 0, \bar{v}\big|_{\Gamma_2} = 0, \\ \psi(0,y) = \psi(L,y) = \begin{cases} 0, y \in [0, H-\Delta], \\ u_{\max} L\left(\frac{y}{L} + \frac{2}{3}\frac{\Delta}{L} - \frac{H}{L} - \frac{(y/L - H/L)^3}{3(\Delta/L)^2}\right), y \in [H-\Delta, H], \\ \frac{2}{3} u_{\max} \Delta, y = H, \end{cases} \end{cases} \tag{4}$$

$$\overline{u}(0,y)=\overline{u}(L,y)=\frac{u(y)}{u_{\max}}=\begin{cases}0, y\in[0,H-\Delta],\\ \left(1-\dfrac{(y-H)^2}{\Delta^2}\right), y\in[H-\Delta,H],\end{cases}$$

$$\overline{\psi}(0,\overline{y})=\overline{\psi}(L,\overline{y})=\frac{\psi(0,y)}{\psi_{\max}}=\begin{cases}0, y\in[0,H-\Delta],\\ \left(\overline{y}+\dfrac{2}{3}\Delta/L-H/L-\dfrac{(\overline{y}-H/L)^3}{3(\Delta/L)^2}\right), \overline{y}\in[(H-\Delta)/L,H/L],\\ \dfrac{2}{3}\dfrac{\Delta}{L}, \overline{y}=H/L.\end{cases}$$

Here Γ_1 denotes the union of the lower side segments and the bottom boundary, Γ_2 corresponds to the upper segment of the rectangle Γ. The first equation in system (1) is the Poisson equation for the stream function and vorticity. The two-dimensional Poisson equation on the rectangle is solved in matrix form with a finite number of arithmetic operations and sixth-order accuracy [2]. Below, for brevity, we omit the overbars on nondimensional functions, time, and coordinates, except in formulas (24).

The second line of system (4) defines vorticity in terms of the velocity field derivatives. The third line gives the velocity components as derivatives of the stream function. The fourth equation is the vorticity dynamics equation, which is the only time-dependent equation in system (1). On the left-hand side, it contains the full (convective) time derivative.

On the boundary of the rectangle, the vertical velocity component is zero; the horizontal component is unspecified on the upper boundary, set to zero on the lower boundary, and described by formula (1) on the side boundaries.

Using the method of undetermined coefficients [10], the velocity on the upper boundary is specified by the quadrature formula (5.1) with tenth-order accuracy in problems (4) (Re = 1500) and (22) (Re = 0.75). Formula (5.1) is applied only to problem (4).

$$u(n_2,j)=\psi_y(n_2,j)=\frac{1}{(-h_2)}\left(-\frac{83711}{27720}\psi_{n_2,j}+11\psi_{n_2-1,j}-\frac{55}{2}\psi_{n_2-2,j}+55\psi_{n_2-3,j}-\frac{165}{2}\psi_{n_2-4,j}+\frac{462}{5}\psi_{n_2-5,j}-\right.$$
$$\left.-77\psi_{n_2-6,j}+\frac{330}{7}\psi_{n_2-7,j}-\frac{165}{8}\psi_{n_2-8,j}+\frac{55}{9}\psi_{n_2-9,j}-\frac{11}{10}\psi_{n_2-10,j}+\frac{1}{11}\psi_{n_2-11,j}\right)+O\left(h^{10}\right), j=\overline{1,n_1-1}, \quad (5.1)$$

$$u(n_2,j)=\frac{1}{(-h_2)}\left(-\frac{137}{60}\psi_{n_2,j}+5\psi_{n_2-1,j}-5\psi_{n_2-2,j}+\frac{10}{3}\psi_{n_2-3,j}-\frac{5}{4}\psi_{n_2-4,j}+\frac{1}{5}\psi_{n_2-5,j}\right)+O\left(h^4\right), j=\overline{1,n_1-1}. \quad (5.2)$$

Following [2], we choose a nonzero and continuous initial velocity field in the central part of the cavity:

$$\overline{u}(x_m y_n)=\begin{cases}0, y_m\in[0,H-\Delta],\\ \left(1-\dfrac{(y_m-H)^2}{\Delta^2}\right), y_m\in[H-\Delta,H], y_m=mh_2, m=\overline{0,n_2}, x_n=nh_1, n=\overline{0,n_1}\end{cases}$$
$$\overline{v}(x_m y_n)=0, y_m=mh_2, m=\overline{0,n_2}, x_n=nh_1, n=\overline{0,n_1}. \quad (6)$$

In the new hydrodynamic problem for an open rectangular cavity in the "stream function–vorticity" variables, where the velocity on the upper segment of the cavity is evaluated by formulas (5), we specify the computational sequence, since it differs substantially from the algorithm described in [1]:

1 step: impose the (time-invariant) boundary conditions on the rectangle boundary for the stream function and for the vertical component of velocity;

2 step: modify the right-hand side of the Poisson equation for the stream function (i.e., the vorticity term) according to formulas (12), (13);

3 step: solve the Poisson equation ((7)–(11)), i.e. find the stream-function values at the interior grid points of the rectangular mesh;

4 step: compute the velocity on the upper segment of the cavity using formulas (5);

5 step: compute the new velocity field at interior grid nodes (formula (18));

6 step: obtain new boundary values of vorticity using formulas (24);

7 step: compute new vorticity values at interior nodes via equation (19).

After step 7 the cycle returns to step 1.

We now describe each step in greater detail. According to [1], the first equation of system (1) — the Poisson equation — is solved by a matrix method in a finite number of elementary operations [2] with sixth-order accuracy at interior points:

$$\Delta\psi = \psi_{xx} + \psi_{yy} = f(x,y) = -w \Leftrightarrow \frac{1}{h^2}\left(-\frac{10}{3}\psi_{0,0} + \frac{2}{3}\left(\psi_{-1,0} + \psi_{0,-1} + \psi_{1,0} + \psi_{0,1}\right) + \frac{1}{6}\left(\psi_{-1,-1} + \psi_{1,-1} + \psi_{-1,1} + \psi_{1,1}\right)\right) =$$
$$= f + \frac{h^2}{12}\left(f_{xx} + f_{yy}\right) + \frac{h^4}{360}\left(f_x^{(4)} + f_y^{(4)}\right) + \frac{h^4 f_{xxyy}^{(4)}}{90} + O\left(h^6\right). \quad (7)$$

To solve Poisson equation (7) for the stream function in system (4) with accuracy $O(h^6)$ we set $f = -w$, represent the derivatives f_{xx}, f_{yy} with accuracy $O(h^4)$, and approximate $f_x^{(4)}, f_y^{(4)}, f_{xxyy}^{(4)}$ with accuracy $O(h^2)$.

In [2, 10], by the method of undetermined coefficients, formulas for the interior-node values of a function f with indices $n = \overline{2, n_1 - 2}, m = \overline{2, n_2 - 2}$ were obtained:

$$\begin{cases} f_{xx} + f_{yy} = \frac{1}{h^2}\left(-5f_{0,0} + \frac{4}{3}\left(f_{-1,0} + f_{0,-1} + f_{1,0} + f_{0,1}\right) - \frac{1}{12}\left(f_{-2,0} + f_{0,-2} + f_{2,0} + f_{0,2}\right)\right) + O\left(h^4\right), \\ f_x^{(4)} + f_y^{(4)} = \frac{1}{h^4}\left(12f_{0,0} - 4\left(f_{-1,0} + f_{0,-1} + f_{1,0} + f_{0,1}\right) + f_{-2,0} + f_{0,-2} + f_{2,0} + f_{0,2}\right) + O\left(h^2\right), \\ f_{xxyy}^{(4)} = \frac{1}{h^4}\left(4f_{0,0} - 2\left(f_{-1,0} + f_{0,-1} + f_{1,0} + f_{0,1}\right) + f_{-1,-1} + f_{-1,1} + f_{1,-1} + f_{1,1}\right) + O\left(h^2\right). \end{cases} \quad (8)$$

Thus, formulas (7) and (8) together approximate the Poisson equation in problems (4) and (22) with accuracy $O(h^6)$ at interior nodes.

Reference [2] describes a matrix method for solving the finite-difference Poisson equation (7) in a finite number of arithmetic operations using a vectorized sweep (block tridiagonal/vector Thomas) method. The finite-difference equation can be written as:

$$\frac{1}{h^2}\left(\frac{-10}{3}\psi_{m,n} + \frac{2}{3}\left(\psi_{m-1,n} + \psi_{m+1,n} + \psi_{m,n-1} + \psi_{m,n+1}\right) + \frac{1}{6}\left(\psi_{m-1,n-1} + \psi_{m+1,n-1} + \psi_{m-1,n+1} + \psi_{m+1,n+1}\right)\right) = f_{m,n} + \frac{h^2}{12}\left(f_{xx} + f_{yy}\right) +$$
$$+h^4\left(\frac{1}{360}\left(f_x^{(4)} + f_y^{(4)}\right) + \frac{1}{90}f_{xxyy}^{(4)}\right) + O\left(h^6\right) \equiv F_{m,n},\ n = \overline{1, n_1 - 1}, m = \overline{1, n_2 - 1}. \quad (9)$$

Define the square matrices A, B of size $(n_1 - 1) \times (n_1 - 1)$:

$$a_{m,n} = \begin{cases} -\frac{10}{3}, m = n; m = \overline{1, n_1 - 1}, n = \overline{1, n_1 - 1}, \\ \frac{2}{3}, m = n + 1 \text{ или } m = n - 1, \\ 0, m \geq n + 2 \text{ или } m \leq n - 2, \end{cases} \qquad b_{m,n} = \begin{cases} \frac{2}{3}, m = n; m = \overline{1, n_1 - 1}, n = \overline{1, n_1 - 1}, \\ \frac{1}{6}, m = n + 1 \text{ или } m = n - 1, \\ 0, m \geq n + 2 \text{ или } m \leq n - 2. \end{cases} \quad (10)$$

In the present work, the matrix algorithm for solving (9) is identical to that in [2]:

1. Using the formula

$$F^T{}_{m,n} = f_{m,n}h^2 + \frac{h^4}{12}\left(f_{xx} + f_{yy}\right) + h^6\left(\frac{1}{360}\left(f_x^{(4)} + f_y^{(4)}\right) + \frac{1}{90}f_{xxyy}^{(4)}\right) + O\left(h^8\right)\Big|_{x = x_n, y = y_m}$$

compute the right-hand side of the Poisson equation at all interior nodes of the uniform rectangular grid (m=1, …, n_2–1; n=1, …, n_1–1).

2. Modify the right-hand sides of the linear system (11) according to formulas (12), (13) at the nodes of the rectangular contour adjacent to the boundary contour, i. e. determine $\overline{F_{m,n}}$ from the values $F_{m,n}$ computed in step 1:

$$\begin{cases} A\psi_1^T + B\psi_2^T = \overline{F_1^T}, \\ B\psi_{m-1}^T + A\psi_m^T + B\psi_{m+1}^T = \overline{F_m^T}, m = \overline{2, n_2 - 2}, \\ B\psi_{n_2-2}^T + A\psi_{n_2-1}^T = \overline{F_{n_2-1}^T}. \end{cases} \quad (11)$$

$$\begin{cases}
\frac{-10}{3}\psi_{1,n_1-1}+\frac{2}{3}\left(\psi_{2,n_1-1}+\psi_{1,n_1-2}+\psi_{1,n_1}+\psi_{0,n_1-1}\right)+\frac{1}{6}\left(\psi_{2,n_1-2}+\psi_{0,n_1-2}+\psi_{2,n_1}+\psi_{0,n_1}\right)=F_{1,n_1-1},\\
\overline{F_{1,n_1-1}}\equiv F_{1,n_1-1}-\frac{2}{3}\left(\psi_{1,n_1}+\psi_{0,n_1-1}\right)-\frac{1}{6}\left(\psi_{0,n_1-2}+\psi_{2,n_1}+\psi_{0,n_1}\right),\\
\frac{-10}{3}\psi_{n_2-1,1}+\frac{2}{3}\left(\psi_{n_2-2,1}+\psi_{n_2-1,2}+\psi_{n_2-1,0}+\psi_{n_2,1}\right)+\frac{1}{6}\left(\psi_{n_2-2,2}+\psi_{n_2,2}+\psi_{n_2-2,0}+\psi_{n_2,0}\right)=F_{n_2-1,1},\\
\overline{F_{n_2-1,1}}\equiv F_{n_2-1,1}-\frac{2}{3}\left(\psi_{n_2-1,0}+\psi_{n_2,1}\right)-\frac{1}{6}\left(\psi_{n_2,2}+\psi_{n_2-2,0}+\psi_{n_2,0}\right),\\
\frac{-10}{3}\psi_{n_2-1,n_1-1}+\frac{2}{3}\left(\psi_{n_2-2,n_1-1}+\psi_{n_2-1,n_1-2}+\psi_{n_2-1,n_1}+\psi_{n_2,n_1-1}\right)+\frac{1}{6}\left(\psi_{n_2-2,n_1-2}+\psi_{n_2,n_1-2}+\psi_{n_2-2,n_1}+\psi_{n_2,n_1}\right)=F_{n_2-1,n_1-1},\\
\overline{F_{n_2-1,n_1-1}}\equiv F_{n_2-1,n_1-1}-\frac{2}{3}\left(\psi_{n_2-1,n_1}+\psi_{n_2,n_1-1}\right)-\frac{1}{6}\left(\psi_{n_2,n_1-2}+\psi_{n_2-2,n_1}+\psi_{n_2,n_1}\right),\\
\frac{-10}{3}\psi_{1,1}+\frac{2}{3}\left(\psi_{2,1}+\psi_{1,2}+\psi_{1,0}+\psi_{0,1}\right)+\frac{1}{6}\left(\psi_{2,2}+\psi_{0,2}+\psi_{2,0}+\psi_{0,0}\right)=F_{1,1},\\
\overline{F_{1,1}}\equiv F_{1,1}-\frac{2}{3}\left(\psi_{1,0}+\psi_{0,1}\right)-\frac{1}{6}\left(\psi_{0,2}+\psi_{2,0}+\psi_{0,0}\right).
\end{cases}\tag{12}$$

$$\begin{cases}
-\frac{10}{3}\psi_{1,n}+\frac{2}{3}\left(\psi_{1,n-1}+\psi_{2,n}+\psi_{1,n+1}+\psi_{0,n}\right)+\frac{1}{6}\left(\psi_{2,n-1}+\psi_{2,n+1}+\psi_{0,n-1}+\psi_{0,n+1}\right)=F_{1,n},n=\overline{2,n_1-2},\\
\overline{F_{1,n}}=F_{1,n}-\frac{2}{3}\psi_{0,n}-\frac{1}{6}\left(\psi_{0,n-1}+\psi_{0,n+1}\right),n=\overline{2,n_1-2},\\
-\frac{10}{3}\psi_{n_2-1,n}+\frac{2}{3}\left(\psi_{n_2-1,n-1}+\psi_{n_2-2,n}+\psi_{n_2-1,n+1}+\psi_{n_2,n}\right)+\frac{1}{6}\left(\psi_{n_2-2,n-1}+\psi_{n_2-2,n+1}+\psi_{n_2,n-1}+\psi_{n_2,n+1}\right)=F_{n_2-1,n},n=\overline{2,n_1-2},\\
\overline{F_{n_2-1,n}}=F_{n_2-1,n}-\frac{2}{3}\psi_{n_2,n}-\frac{1}{6}\left(\psi_{n_2,n-1}+\psi_{n_2,n+1}\right),n=\overline{2,n_1-2},\\
-\frac{10}{3}\psi_{m,1}+\frac{2}{3}\left(\psi_{m-1,1}+\psi_{m,2}+\psi_{m+1,1}+\psi_{m,0}\right)+\frac{1}{6}\left(\psi_{m-1,2}+\psi_{m+1,2}+\psi_{m-1,0}+\psi_{m+1,0}\right)=F_{m,1},m=\overline{2,n_2-2},\\
\overline{F_{m,1}}=F_{m,1}-\frac{2}{3}\psi_{m,0}-\frac{1}{6}\left(\psi_{m-1,0}+\psi_{m+1,0}\right),m=\overline{2,n_2-2},\\
-\frac{10}{3}\psi_{m,n_1-1}+\frac{2}{3}\left(\psi_{m-1,n_1-1}+\psi_{m,n_1-2}+\psi_{m+1,n_1-1}+\psi_{m,n_1}\right)+\frac{1}{6}\left(\psi_{m-1,n_1-2}+\psi_{m+1,n_1-2}+\psi_{m-1,n_1}+\psi_{m+1,n_1}\right)=F_{m,n_1-1},m=\overline{2,n_2-2},\\
\overline{F_{m,n_1-1}}=F_{m,n_1-1}-\frac{2}{3}\psi_{m,n_1}-\frac{1}{6}\left(\psi_{m-1,n_1}+\psi_{m+1,n_1}\right),m=\overline{2,n_2-2},\\
\overline{F_{m,n}}=F_{m,n},\ \forall m\in\overline{2,n_2-2},n\in\overline{2,n_1-2}.
\end{cases}\tag{13}$$

3. Compute the forward sweep (matrix recurrence) coefficients by formulas (14), (15) $m=\overline{1,n_2-2}$:

$$\lambda_1=-A^{-1}B,\nu_1=A^{-1}\overline{F_1^T},\tag{14}$$

$$\lambda_m=-\left(B\lambda_{m-1}+A\right)^{-1}B,\nu_m=\left(B\lambda_{m-1}+A\right)^{-1}\left(\overline{F_m^T}-B\nu_{m-1}\right),m=\overline{2,n_2-2}.\tag{15}$$

4. Compute the solution row vector $\psi_{n_2-1}^T$ by formula (16):

$$\psi_{n_2-1}^T=\left(B\lambda_{n_2-2}+A\right)^{-1}\left(\overline{F_{n_2-1}^T}-B\nu_{n_2-2}\right).\tag{16}$$

5. Compute the remaining rows of the solution matrix $\psi^T{}_m$ using formulas (17):

$$\psi_m^T=\lambda_m\psi_{m+1}^T+\nu_m,m=\overline{n_2-2,1},\nu_{n_2-1}=\psi_{n_2-1}^T.\tag{17}$$

The matrix sweep algorithm (9)–(17) preserves sixth-order accuracy in accordance with formulas (7) and (8) for the Poisson equation.

The second and third equations of system (4) $\overline{w}=\overline{v}_{\overline{x}}-\overline{u}_{\overline{y}},\overline{u}=\overline{\psi}_{\overline{y}},\overline{v}=-\overline{\psi}_{\overline{x}}$ are linear with respect to the first derivatives. We present quadrature formulas for the first derivative with various stencils. For the equation $\overline{u}=\overline{\psi}_{\overline{y}}$ we have:

$$\begin{cases} u_{(i,j)} = \frac{1}{h}\left(\frac{3}{4}\left(\psi_{i+1,j}-\psi_{i-1,j}\right)-\frac{3}{20}\left(\psi_{i+2,j}-u_{i-2,j}\right)+\frac{1}{60}\left(\psi_{i+3,j}-\psi_{i-3,j}\right)\right)+O\left(h^6\right), i=\overline{3,n_2-3}, j=\overline{1,n_1-1}, \\ u_{(1,j)} = \frac{1}{h}\left(-\frac{\psi_{0,j}}{5}-\frac{13}{12}\psi_{1,j}+2\psi_{2,j}-\psi_{3,j}+\frac{\psi_{4,j}}{3}-\frac{\psi_{5,j}}{20}\right)+O\left(h^4\right), j=\overline{1,n_1-1}, \\ u_{(2,j)} = \frac{1}{12h}\left(8\left(\psi_{3,j}-\psi_{1,j}\right)-\left(\psi_{4,j}-\psi_{0,j}\right)\right)+O\left(h^4\right), j=\overline{1,n_1-1}, \\ u_{(n_2-1,j)} = -\frac{1}{h}\left(-\frac{\psi_{n_2,j}}{5}-\frac{13}{12}\psi_{n_2-1,j}+2\psi_{n_2-2,j}-\psi_{n_2-3,j}+\frac{\psi_{n_2-4,j}}{3}-\frac{\psi_{n_2-5,j}}{20}\right)+O\left(h^4\right), j=\overline{1,n_1-1}, \\ u_{(n_2-2,j)} = -\frac{1}{12h}\left(8\left(\psi_{n_2-3,j}-\psi_{n_2-1,j}\right)-\left(\psi_{n_2-4,j}-\psi_{n_2,j}\right)\right)+O\left(h^4\right), j=\overline{1,n_1-1}. \end{cases} \quad (18)$$

Analogous formulas can be written for the equation $\bar{v}=-\overline{\psi}_{\bar{x}}$. To accelerate the numerical solution, the vorticity equation in (4) was treated using the splitting method [9].

Analytically, the *n*-fold splitting method for the vorticity equation over the time interval τ_0 / n can be written as:

$$\frac{w^{k+((i+1)/n)}-w^{k+(i/n)}}{\tau_0/n}+u^k\cdot w_x^{k+(i/n)}+v^k\cdot w_y^{k+(i/n)}=\frac{1}{\mathrm{Re}}\left(w_{xx}^{k+(i/n)}+w_{yy}^{k+(i/n)}\right), i=\overline{0,n-1}. \quad (19)$$

The recurrence system (19) for the vorticity with a frozen velocity field $\left(u^k(x,y),v^k(x,y)\right), i=\overline{0,n-1}, k=const, k=1,2,...$ consists of *n* intermediate steps $i=\overline{0,n-1}$, the superscript *i* denotes the intermediate time-layer index in equation (19), and subscript *k* denotes the multiplicity index of the time layer in system (19). Velocity and stream-function fields remain fixed in equations (19) at values *k* = *const* while the index *i* changes $i=\overline{0,n-1}$. In this system only the vorticity field $w^{k+(i/n)}, i=\overline{0,n-1}$ is updated. The velocity field changes by a jump in systems (4) or in (22), (19) when the time index of the vorticity increases by one (from *k* to *k*+1) in the recurrence system (19).

The idea of splitting system (19) lies in reducing the accumulation of rounding errors and the computational time required for its solution. The differential operators with respect to coordinates in (19) are approximated at interior nodes with accuracy $O(h^6)$, as are all equations of system (4); the boundary conditions are approximated with accuracy $O(h^4)$, and the time derivative with accuracy $O(\tau)$.

Thus, over the time interval τ_0 / n (associated with the reduction of stability due to the presence of four singular points of the velocity field), solving equation (19) *n* times yields a temporal jump of magnitude τ_0 (which is *n* times larger than sequentially solving the full system of equations (4)).

Equation (19) is linear with respect to the coordinate derivatives $w_x^i, w_y^i, w_{xx}^i, w_{yy}^i$. In [9] it was shown that for spectral stability of the vorticity dynamics equation (19), it is sufficient to choose the ratio of the time step and spatial step in the form of the inequality: $\tau_0 \le \frac{3}{16}h^2\,\mathrm{Re}-(4), \left(\tau_0 \le \frac{3}{16}h^2-(22)\right)$.

For the derivative w_y in (19), we write quadrature formulas (the formulas for w_x are analogous):

$$\begin{cases} w_{y(i,j)} = \frac{1}{h}\left(\frac{3}{4}\left(w_{i+1,j}-w_{i-1,j}\right)-\frac{3}{20}\left(w_{i+2,j}-w_{i-2,j}\right)+\frac{1}{60}\left(w_{i+3,j}-w_{i-3,j}\right)\right)+O\left(h^6\right), i=\overline{3,n_2-3}, j=\overline{1,n_1-1}, \\ w_{y(1,j)} = \frac{1}{h}\left(-\frac{w_{0,j}}{5}-\frac{13}{12}w_{1,j}+2w_{2,j}-w_{3,j}+\frac{w_{4,j}}{3}-\frac{w_{5,j}}{20}\right)+O\left(h^4\right), j=\overline{1,n_1-1}, \\ w_{y(2,j)} = \frac{1}{12h}\left(8\left(w_{3,j}-w_{1,j}\right)-\left(w_{4,j}-w_{0,j}\right)\right)+O\left(h^4\right), j=\overline{1,n_1-1}, \\ w_{y(n_2-1,j)} = -\frac{1}{h}\left(-\frac{w_{n_2,j}}{5}-\frac{13}{12}w_{n_2-1,j}+2w_{n_2-2,j}-w_{n_2-3,j}+\frac{w_{n_2-4,j}}{3}-\frac{w_{n_2-5,j}}{20}\right)+O\left(h^4\right), j=\overline{1,n_1-1}, \\ w_{y(n_2-2,j)} = -\frac{1}{12h}\left(8\left(w_{n_2-3,j}-w_{n_2-1,j}\right)-\left(w_{n_2-4,j}-w_{n_2,j}\right)\right)+O\left(h^4\right), j=\overline{1,n_1-1}. \end{cases} \quad (20)$$

The second derivatives w_{yy} in (19) take the form:

$$\begin{cases} w_{yy(i,j)} = \frac{1}{h^2}\left(-\frac{49}{18}w_{i,j}+\frac{3}{2}\left(w_{i+1,j}+w_{i-1,j}\right)-\frac{3}{20}\left(w_{i+2,j}+w_{i-2,j}\right)+\frac{1}{90}\left(w_{i+3,j}+w_{i-3,j}\right)\right)+O\left(h^6\right), i=\overline{3,n_2-3}, j=\overline{1,n_1-1}, \\ w_{yy(1,j)} = \frac{1}{h^2}\left(\frac{137}{180}w_{0,j}-\frac{49}{60}w_{1,j}-\frac{17}{12}w_{2,j}+\frac{47}{18}w_{3,j}-\frac{19}{12}w_{4,j}+\frac{31}{60}w_{5,j}-\frac{13}{180}w_{6,j}\right)+O\left(h^4\right), j=\overline{1,n_1-1}, \\ w_{yy(2,j)} = \frac{1}{h^2}\left(-\frac{5}{2}w_{2,j}+\frac{4}{3}\left(w_{1,j}+w_{3,j}\right)-\frac{1}{12}\left(w_{0,j}+w_{4,j}\right)\right)+O\left(h^4\right), j=\overline{1,n_1-1}, \\ w_{yy(n_2-1,j)} = \frac{1}{h^2}\left(\frac{137}{180}w_{n_2,j}-\frac{49}{60}w_{n_2-1,j}-\frac{17}{12}w_{n_2-2,j}+\frac{47}{18}w_{n_2-3,j}-\frac{19}{12}w_{n_2-4,j}+\frac{31}{60}w_{n_2-5,j}-\frac{13}{180}w_{n_2-6,j}\right)+O\left(h^4\right), j=\overline{1,n_1-1}, \\ w_{yy(n_2-2,j)} = \frac{1}{h^2}\left(-\frac{5}{2}w_{n_2-2,j}+\frac{4}{3}\left(w_{n_2-1,j}+w_{n_2-3,j}\right)-\frac{1}{12}\left(w_{n_2,j}+w_{n_2-4,j}\right)\right)+O\left(h^4\right), j=\overline{1,n_1-1}. \end{cases} \quad (21)$$

Analogous formulas are written for the derivative w_{xx}. Problem (4) and its algorithm (steps (5)–(21), (23), (24)) apply to blood motion in the aorta and arteries at high velocities and large Reynolds numbers. However, at small Reynolds numbers, using the diffusion time scale [9], we arrive at problem (22):

$$\bar{t} = \frac{t}{T}, T_{dif} = T = \frac{L^2}{\nu}, \mathrm{Re} = \frac{u_{\max} L}{\nu},$$

$$0 \le \bar{x} = \frac{x}{L} \le 1,\ 0 \le \bar{y} = \frac{y}{L} \le k = \frac{H}{L}, \bar{\psi} = \frac{\psi}{\psi_{\max}}, \psi_{\max} = L u_{\max},$$

$$\bar{u} = \frac{u}{u_{\max}}, \bar{v} = \frac{v}{u_{\max}} \bar{w} = \frac{w}{w_{\max}}, w_{\max} = \frac{u_{\max}}{L},$$

$$\frac{\partial w}{\partial t} + u\frac{\partial w}{\partial x} + v\frac{\partial w}{\partial y} = \nu\left(\frac{\partial^2 w}{\partial x^2} + \frac{\partial^2 w}{\partial y^2}\right) \Leftrightarrow \frac{1}{T}\frac{\partial \bar{w}}{\partial \bar{t}} + \frac{u_{\max}}{L}\left(\bar{u}\frac{\partial \bar{w}}{\partial \bar{x}} + \bar{v}\frac{\partial \bar{w}}{\partial \bar{y}}\right) = \frac{\nu}{L^2}\left(\frac{\partial^2 \bar{w}}{\partial \bar{x}^2} + \frac{\partial^2 \bar{w}}{\partial \bar{y}^2}\right) \Leftrightarrow$$

$$\frac{\nu}{L^2}\frac{\partial \bar{w}}{\partial \bar{t}} + \frac{u_{\max}}{L}\left(\bar{u}\frac{\partial \bar{w}}{\partial \bar{x}} + \bar{v}\frac{\partial \bar{w}}{\partial \bar{y}}\right) = \frac{\nu}{L^2}\left(\frac{\partial^2 \bar{w}}{\partial \bar{x}^2} + \frac{\partial^2 \bar{w}}{\partial \bar{y}^2}\right) \Leftrightarrow \frac{\partial \bar{w}}{\partial \bar{t}} + \mathrm{Re}\left(\bar{u}\frac{\partial \bar{w}}{\partial \bar{x}} + \bar{v}\frac{\partial \bar{w}}{\partial \bar{y}}\right) = \frac{\partial^2 \bar{u}}{\partial \bar{x}^2} + \frac{\partial^2 \bar{u}}{\partial \bar{y}^2}.$$

$$\begin{cases} \bar{\psi}_{\bar{x}\bar{x}} + \bar{\psi}_{\bar{y}\bar{y}} = -\bar{w}(\bar{x},\bar{y}),\ 0 < \bar{x} = \frac{x}{L} < 1,\ 0 < \bar{y} < k_{\max}, \\ \bar{w} = \bar{v}_{\bar{x}} - \bar{u}_{\bar{y}}, \\ \bar{u} = \bar{\psi}_{\bar{y}}; \bar{v} = -\bar{\psi}_{\bar{x}}, \\ \bar{w}_{\bar{t}} + \mathrm{Re}\left(\bar{u}\cdot\bar{w}_{\bar{x}} + \bar{v}\cdot\bar{w}_{\bar{y}}\right) = \bar{w}_{\bar{x}\bar{x}} + \bar{w}_{\bar{y}\bar{y}}, 0 < \bar{t} = \frac{t}{T}, \\ \bar{\psi}\big|_{\Gamma 1} \equiv 0, \bar{v}\big|_{\Gamma} \equiv 0, \bar{u}\big|_{\Gamma_1} = 0, \bar{v}\big|_{\Gamma_2} = 0, \\ \bar{\psi}(0,y) = \bar{\psi}(L,y) = \begin{cases} 0, y \in [0, H-\Delta], \\ \frac{1}{L}\left(y + \frac{2}{3}\Delta - H - \frac{(y-H)^3}{3\Delta^2}\right), y \in [H-\Delta, H], \\ \frac{2}{3}\frac{\Delta}{L} = const, y = H, \forall x \in [0,L]. \end{cases} \end{cases} \tag{22}$$

$$\bar{u}(0,y) = \bar{u}(L,y) = \frac{u(y)}{u_{\max}} = \begin{cases} 0, y \in [0, H-\Delta], \\ \left(1 - \frac{(y-H)^2}{\Delta^2}\right), y \in [H-\Delta, H]. \end{cases}$$

The remaining equations of problem (22) are the same as in problem (4). According to the general algorithm (step 6), it is necessary to compute the vorticity w at the boundary of the rectangle and then solve the vorticity equation (19) at the interior nodes of the cavity.

In the linear approximation, we assume that velocity, vorticity, and stream function at the boundary and the nearest interior nodes are linked by a single linear quadrature formula. The boundary values of the vorticity are approximated with fourth-order accuracy [10], since in [1] only first- and second-order formulas were given:

$$\psi_{xx}(0) = \frac{1}{h_1^2}\left(C_0\psi_0 + C_1\psi_1 + C_2\psi_2 + C_3\psi_3 + C_4\psi_4\right) + \frac{C_5\psi_x(0)}{h_1} = \frac{1}{h_1^2}\left(C_0\psi_0 + \sum_{i=1}^{4}\sum_{k=0}^{\infty} C_i \cdot \frac{(ih_1)^k \psi_0^{(k)}}{k!}\right) + \frac{C_5\psi_x(0)}{h_1} =$$

$$= \frac{\psi_0}{h_1^2}\left(C_0 + C_1 + C_2 + C_3 + C_4\right) + \frac{\psi_x(0)}{h_1}\left(C_1 + 2C_2 + 3C_3 + 4C_4 + C_5\right) + \psi_{xx}(0)\left(\frac{C_1}{2} + 2C_2 + \frac{9}{2}C_3 + 8C_4\right) +$$

$$+ h_1\psi_x^{(3)}(0)\left(\frac{C_1}{6} + \frac{8}{6}C_2 + \frac{27}{6}C_3 + \frac{64}{6}C_4\right) + h_1^2\psi_x^{(4)}(0)\left(\frac{C_1}{24} + \frac{16}{24}C_2 + \frac{81}{24}C_3 + \frac{256}{24}C_4\right) +$$

$$+ h_1^3\psi_x^{(5)}(0)\left(\frac{C_1}{120} + \frac{32}{120}C_2 + \frac{243}{120}C_3 + \frac{1024}{120}C_4\right) + O\left(h_1^4\right).$$

$$\Leftrightarrow \begin{cases} C_0 + C_1 + C_2 + C_3 + C_4 = 0 \\ C_1 + 2C_2 + 3C_3 + 4C_4 + C_5 = 0 \\ C_1 + 4C_2 + 9C_3 + 16C_4 = 2 \\ C_1 + 8C_2 + 27C_3 + 64C_4 = 0 \\ C_1 + 16C_2 + 81C_3 + 256C_4 = 0 \\ C_1 + 32C_2 + 243C_3 + 1024C_4 = 0 \end{cases} \Leftrightarrow C_0 = -\frac{415}{72}, C_1 = 8, C_2 = -3, C_3 = \frac{8}{9}, C_4 = -\frac{1}{8}, C_5 = -\frac{25}{6}.$$

Taking (22) into account, we obtain the general boundary condition for vorticity in the open cavity with fourth-order accuracy by differentiating (22) twice with respect to *y*:

$$w(x,y) = -\psi_{xx} - \psi_{yy} = \frac{1}{h_1^2}\left(\frac{415}{72}\psi_0 - 8\psi_1 + 3\psi_2 - \frac{8}{9}\psi_3 + \frac{1}{8}\psi_4\right) - \frac{25}{6}\frac{v(0,y)}{h_1} - \psi_{yy}, v = -\psi_x. \tag{23}$$

$$\overline{w}_{m,0} = \begin{cases} \frac{1}{h_1^2}\left(\frac{415}{72}\overline{\psi}_{m,0} - 8\overline{\psi}_{m,1} + 3\overline{\psi}_{m,2} - \frac{8}{9}\overline{\psi}_{m,3} + \frac{1}{8}\overline{\psi}_{m,4}\right) - \frac{25}{6}\frac{\overline{v}_{m,0}}{h_1} + 2\frac{(\overline{y_m} - H/L))}{(\Delta/L)^2}, m = \overline{n_3, n_2}, \\ \frac{1}{h_1^2}\left(\frac{415}{72}\overline{\psi}_{m,0} - 8\overline{\psi}_{m,1} + 3\overline{\psi}_{m,2} - \frac{8}{9}\overline{\psi}_{m,3} + \frac{1}{8}\overline{\psi}_{m,4}\right) - \frac{25}{6}\frac{\overline{v}_{m,0}}{h_1}, m = \overline{0, n_3}, left. \end{cases} \tag{24.1}$$

$$\overline{w}_{0,n} = \begin{cases} \frac{1}{h_2^2}\left(\frac{415}{72}\overline{\psi}_{0,n} - 8\overline{\psi}_{1,n} + 3\overline{\psi}_{2,n} - \frac{8}{9}\overline{\psi}_{3,n} + \frac{1}{8}\overline{\psi}_{4,n}\right) + \frac{25}{6}\frac{\overline{u}_{0,n}}{h_2}, n = \overline{0, n_1}, u = \psi_y, bottom, \\ \frac{1}{h_2^2}\left(\frac{415}{72}\overline{\psi}_{n_2,n} - 8\overline{\psi}_{n_2-1,n} + 3\overline{\psi}_{n_2-2,n} - \frac{8}{9}\overline{\psi}_{n_2-3,n} + \frac{1}{8}\overline{\psi}_{n_2-4,n}\right) - \frac{25}{6}\frac{\overline{u}_{n_2,n}}{h_2}, n = \overline{0, n_1}, top. \end{cases} \tag{24.2}$$

$$\overline{w}_{0,n} = \begin{cases} \frac{1}{h_2^2}\left(\frac{415}{72}\overline{\psi}_{0,n} - 8\overline{\psi}_{1,n} + 3\overline{\psi}_{2,n} - \frac{8}{9}\overline{\psi}_{3,n} + \frac{1}{8}\overline{\psi}_{4,n}\right) + \frac{25}{6}\frac{\overline{u}_{0,n}}{h_2}, n = \overline{0, n_1}, u = \psi_y, bottom, \\ \frac{1}{h_2^2}\left(\frac{415}{72}\overline{\psi}_{n_2,n} - 8\overline{\psi}_{n_2-1,n} + 3\overline{\psi}_{n_2-2,n} - \frac{8}{9}\overline{\psi}_{n_2-3,n} + \frac{1}{8}\overline{\psi}_{n_2-4,n}\right) - \frac{25}{6}\frac{\overline{u}_{n_2,n}}{h_2}, n = \overline{0, n_1}, top. \end{cases} \tag{24.3}$$

Unlike the closed-cavity case treated in [2], where derivatives of the vorticity function up to fifth order are computed explicitly, in problems (4) and (22) the application of formula (23) is appropriate. In fields with discontinuities of velocity the vorticity and its partial derivatives may attain large values. In deriving formula (23) derivatives of the stream function above second order were discarded. Table 1 gives a classification of blood vessels.

Table 1

Classification of blood vessels

Type	Diameter	Blood velocity	Reynolds number Re	Governing system
Capillaries	(5–10) μm	(0.5–1.0) mm/s	0.00075–0.00300	(21)
Arterioles	(10–100) μmm	(0.5–10.0) cm/s	0.015–3.000	(21),(4)
Arteries	(2–10) mm	(10–40) cm/s	60–1200	(4)
Aorta	(2–3) cm	0.5 m/s	3000	(4)

For definiteness, we solve problem (22) numerically when Re < 1 and problem (4) when Re > 1 ($h_1 = h_2 = 0{,}01$).

Experience shows that for a rapid solution in arterioles one should choose an inertial time interval $\frac{L}{u_{\max}}$, whereas to solve the hydrodynamic problem for an arteriole aneurysm it is appropriate to use system (4) analogously to the aneurysm-in-artery case.

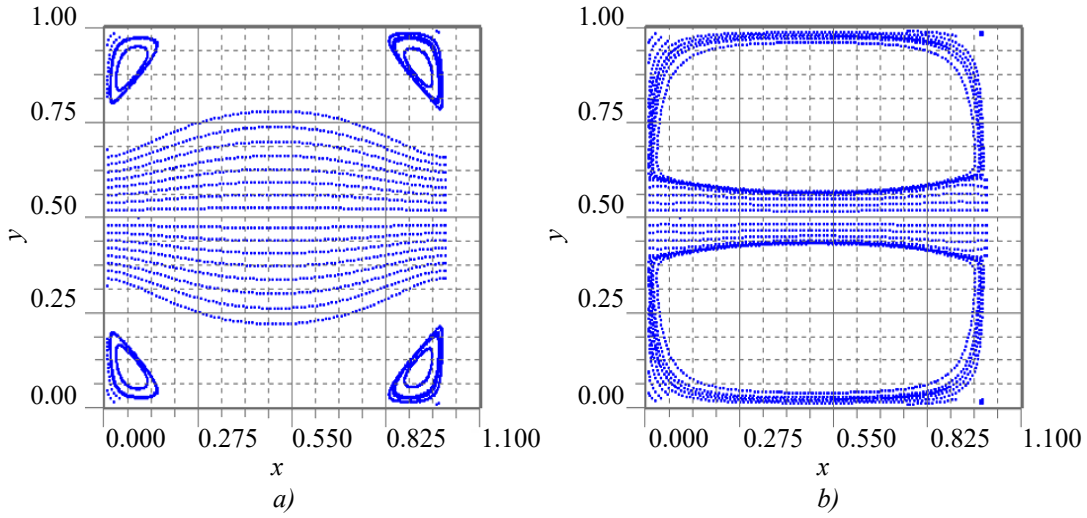

Fig. 3. Limiting streamline pattern in arterioles using formula (5.1):

a — Re = 0.75, $n_1 \times n_2 = 100 \times 50$, $\Delta / H = 0.5$; $L = 1$, $H = 50$ μ*m*, $u_{max} = 5$ *cm/s*, $\tau = \frac{6}{16} h_1^2$, $n = 400000$ steps, splitting multiplicity $m = 100$, $t = 0{,}512$ *s*; *b* — Re = 0.75, $n_1 \times n_2 = 100 \times 50$, $\Delta / H = 0.2$; $L = 1$, $H = 50$ μ*m*, $u_{max} = 5$ *cm/s*, $\tau = \frac{6}{16} h_1^2$, $n = 200000$ steps, splitting multiplicity $m = 100$, $t = 0.256$ *s*

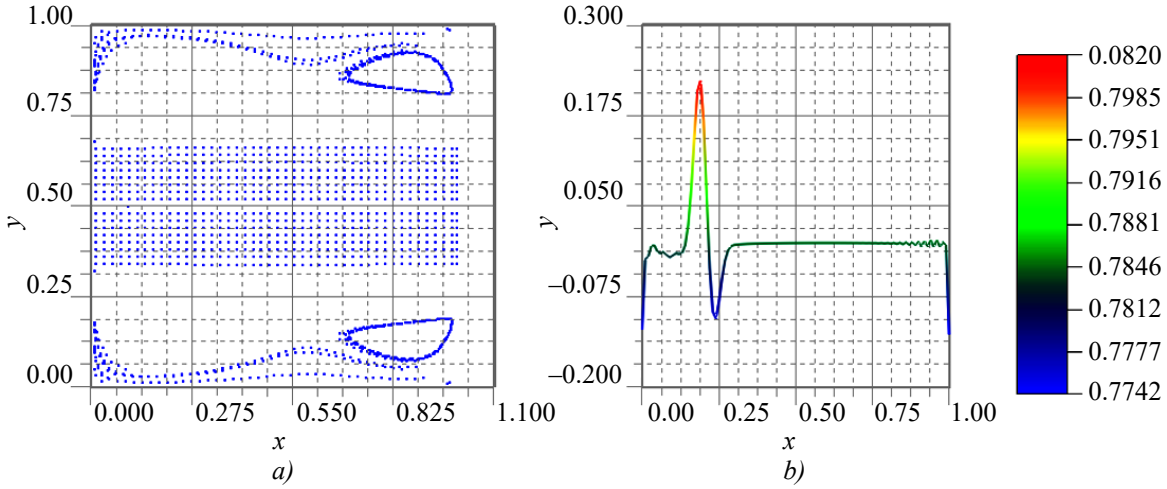

Fig. 4. Results of solving problem (4) with application of (5.1):

a — Re = 1500, $n_1 \times n_2 = 100 \times 50$, $\Delta / H = 0.6$; $L = 1$, $H = 1$ *cm*, $u_{max} = 50$ *cm/s*, streamline field in arteries after $n = 10000$ steps, splitting multiplicity $m = 200$; *b* — plot of the vorticity function in the symmetry plane

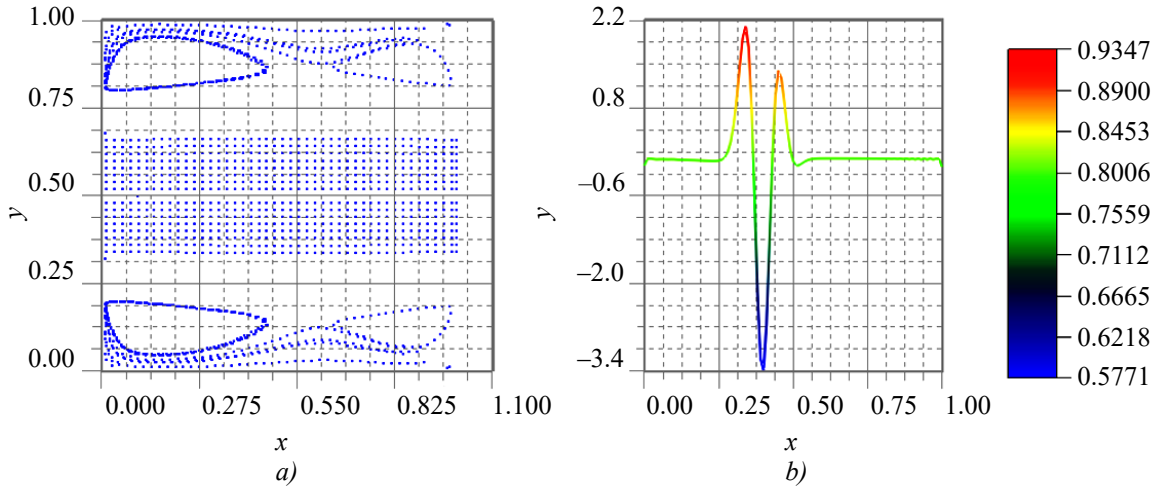

Fig. 5. Results of solving problem (4) with application of (5.1):

a — Re = 1500, $n_1 \times n_2 = 100 \times 50$, $\Delta / H = 0.6$; $L = 1$, $H = 1$ *cm*, $u_{max} = 50$ *cm/s*, streamline field in arteries after $n = 20000$ steps, splitting multiplicity $m = 200$; *b* — plot of the vorticity function in the symmetry plane

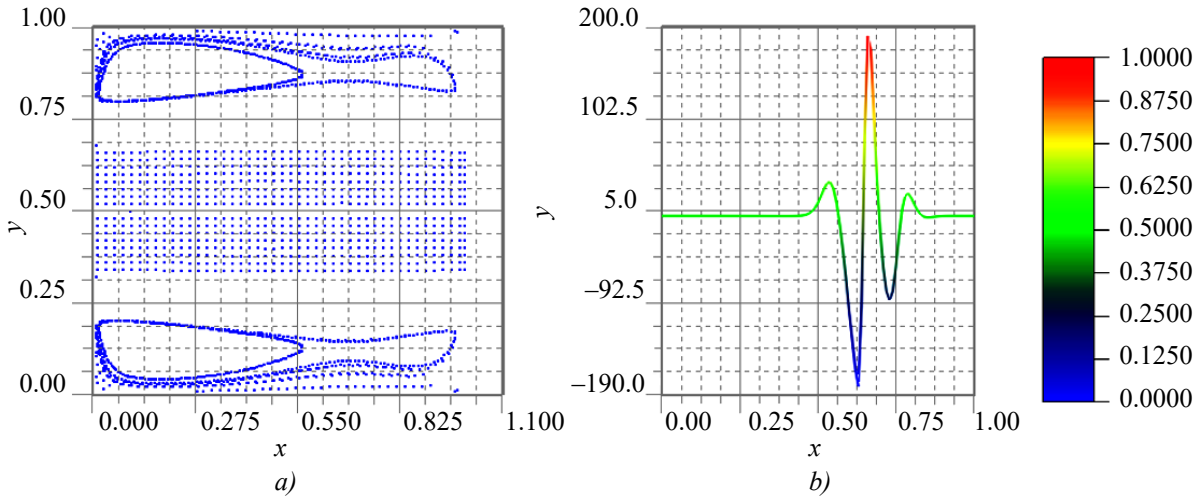

Fig. 6. Results of solving problem (4) with application of (5.1):
a — Re = 1500, $n_1 \times n_2 = 100 \times 50$, $\Delta / H = 0.6$; $L = 1$, $H = 1$ *cm*, $u_{max} = 50$ *cm/s* streamline field in arteries after $n = 34000$ steps, splitting multiplicity $m = 200$; *b* — plot of the vorticity function in the symmetry plane

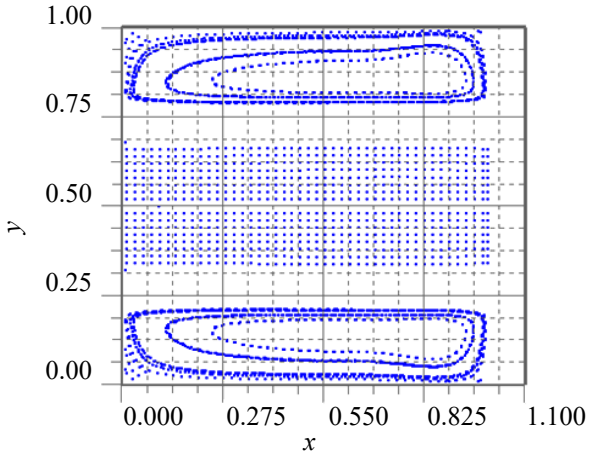

Fig. 7. Results of solving problem (4) with application of (5.2):
Re = 1500, $n_1 \times n_2 = 100 \times 50$, $\Delta / H = 0.6$; $L = 1$, $H = 1$ *cm*, $u_{max} = 50$ *cm*/s,
streamline field in the artery for $n = 2310000$ steps, splitting multiplicity $m = 200$

Discussion. Two numerical algorithms have been proposed for solving the two-dimensional problem in an open cavity ((5)–(21), (23), (24)) in the stream function–vorticity variables, modelling blood flow in an aneurysm under laminar (Re < 1 (22)) and turbulent (Re > 1, (4)) regimes.

In capillaries and arterioles (Fig. 3), the flow structure establishes within 0.002% of the period between pulsation waves (1 s). Therefore, the clot formation region is determined by the blood circulation region within the aneurysm.

The structure of circulation zones at low Reynolds numbers strongly depends on the ratio of the vessel diameter to the aneurysm diameter (Fig. 3). If the parameter , the circulation zone is located in the corners of the aneurysm (Fig. 3*a*). If the parameter , the circulation occupies the entire aneurysm (Fig. 3b), resulting in a narrowing of the channel diameter by 34%. This explains the phenomenon of "lumen constriction" during thrombus formation.

For high-speed flows (Re = 1500) in arteries and the aorta, the circulation region encompasses the entire aneurysm for any value of the parameter Δ / H ($\Delta / H = 0.6$) (Figs. 6*a* and 7).

Along the symmetry plane of the aneurysm, in the direction of blood flow, a sequence of alternating-sign vortices forms. In Fig. 4*b*, two vortices with signs *w* +, – appear. In Fig. 5*b*, three vortices with signs +, –, + are present. In Fig. 6*b*, five vortices form a sequence +, –, +, –, +. This chain of alternating-sign vortices resembles a Kármán vortex street in the wake of an obstacle.

The presence of vortices in the symmetry plane violates the assumption of solution symmetry. Therefore, it is necessary to allow for a nonzero normal velocity component in the symmetry plane and to include the entire aneurysm when solving

problem (4) for blood flow in the aorta. The formulations of problems (4) and (22) and their solution algorithms have been generalized for an open cavity, i. e., when cavity boundaries are intersected by fluid flows.

Conclusion. The initial-boundary value problems formulated in this study ((4), (22)) allow for a high-quality modelling of blood flow in aneurysms of capillaries, arterioles, and arteries at both low and high velocities, as well as blood flow in elements of medical devices.

References

1. Salih A. Streamfunction — Vorticity Formulation. *Department of Aerospace Engineering Indian Institute of Space Science and Technology.* 2013;10:1–10.

2. Volosova N.K., Volosov K.A., Volosova A.K., Karlov M.I., Pastukhov D.F., Pastukhov Yu.F. Comparison of solution of the hydrodynamic problem in a rectangular cavity methods of inhibition and acceleration of the initial speed field. *Computational Mathematics and Information Technologies*. 2025;9(2):22–33 (In Russ.) https://doi.org/10.23947/2587-8999-2025-9-2-22-33

3. Petrov A.G. High-precision numerical schemes for solving plane boundary value problems for a polyharmonic equation and their application to problems of hydrodynamics. *Applied Mathematics and Mechanics*. 2023;87(3):343–368 (In Russ.) https://doi.org/10.31857/S0032823523030128

4. Sukhinov A.I., Kolgunova O.V., Ghirmay M.Z., Nahom O.S. A two -dimensional hydrodynamic model of coastal systems, taking into account evaporation. *Computation Mathematics and Information Technologies*. 2023;7(4):9–21. https://doi.org/10.23947/2587-8999-2023-7-4-9-21

5. Ershova T.Ya. Boundary value problem for a third-order differential equation with a strong boundary layer. *Bulletin of Moscow University. Episode 15: Computational mathematics and cybernetics*. 2020;1:30–39 (In Russ.) https://doi.org/10.3103/S0278641920010057

6. Sitnikova M.A., Skulsky O.I. Flow of momentary anisotropic fluid in thin layers. *Bulletin of Perm University. Mathematics. Mechanics. Informatics.* 2015;28(1):56–62 (In Russ.)

7. Volosov K.A., Vdovina E.K., Pugina L.V. Modeling of “pulsatile” modes of blood coagulation dynamics. *Math modeling.* 2014;26(12):14–32 (In Russ.)

8. Sidoryakina V.V., Solomaha D.A. Symmetrized versions of the Seidel and upper relaxation methods for solving two-dimensional difference problems of elliptic. *Computational Mathematics and Information Technologies*. 2023;7(3):12–19. (In Russ.) https://doi.org/10.23947/2587-8999-2023-7-3-12-19

9. Volosova N.K., Volosov K.A., Volosova A.K., Karlov M.I., Pastuhov D.F., Pastuhov Yu.F. The *N*-fold distribution of the obvious variable scheme for the equalization of the vortex in the viscous incompatible fluid. *Bulletin of the Perm University. Mathematics. Mechanics. Informatics*. 2023;63(4):12–21 (In Russ.) https://doi.org/10.17072/1993-0550-2023-4-12-21

10. Bahvalov N.S., Zhidkov N.P., Kobelkov G.M. *Numerical methods: a textbook for students of physics and mathematics specialties of higher educational institutions Binom. lab*. Moscow: Knowledge; 2011. 636 p. (In Russ.)

About the Authors:

Natalya K. Volosova, Post-graduate Student of Bauman Moscow State Technical University (2nd Baumanskaya St. 5–1, Moscow, 105005, Russian Federation), ORCID, navalosova@yandex.ru

Konstantin A. Volosov, Doctor of Physical and Mathematical Sciences, Professor of the Department of Applied Mathematics of the Russian University of Transport (Obraztsova St. 9–9, Moscow, GSP-4, 127994, Russian Federation), ORCID, SPIN-code, konstantinvolosov@yandex.ru

Aleksandra K. Volosova, Candidate of Physical and Mathematical Sciences, Chief Analytical Department “Tramplin” LLC, Russian University of Transport (Obraztsova St. 9–9, Moscow, GSP-4, 127994, Russian Federation), ORCID, SPIN-code, alya01@yandex.ru

Mikhail I. Karlov, Candidate of Physical and Mathematical Sciences, Associate Professor of the Department of Mathematics, Moscow Institute of Physics and Technology (9, Institutsky Lane, GSP-4, Dolgoprudny, 141701, Russian Federation), SPIN-code, karlov.mipt@gmail.com

Dmitriy F. Pastukhov, Candidate of Physical and Mathematical Sciences, Associate Professor of Polotsk State University (Blokhin St. 29, Novopolotsk, 211440, Republic of Belarus), ORCID, SPIN-code, dmitrij.pastuhov@mail.ru

Yuriy F. Pastukhov, Candidate of Physical and Mathematical Sciences,Associate Professor of Polotsk State University (Blokhin St. 29, Novopolotsk, 211440, Republic of Belarus), ORCID, SPIN-code, pulsar1900@mail.ru

Contributions of the authors:

N.K. Volosova: setting the task; writing a draft of the manuscript; formulation of research ideas, goals and objectives.
K.A. Volosov: scientific guidance; methodology development.
A.K. Volosova: translation; study of the history of the task; literature.
M.I. Karlov: formal analysis.

D.F. Pastukhov: visualization; validation; software.
Yu.F. Pastukhov: testing of existing code components.

Conflict of Interest Statement: **the authors declare no conflict of interest.**

All authors have read and approved the final manuscript.

Об авторах:

Наталья Константиновна Волосова, аспирант Московского государственного технического университета им. Н.Э. Баумана (105005, Российская Федерация, г. Москва, ул. 2-я Бауманская, 5, стр. 1), ORCID, navalosova@yandex.ru

Константин Александрович Волосов, доктор физико-математических наук, профессор кафедры прикладной математики Российского университета транспорта (127994, ГСП-4, Российская Федерация, г. Москва, ул. Образцова, 9, стр. 9), ORCID, SPIN-код, konstantinvolosov@yandex.ru

Александра Константиновна Волосова, кандидат физико-математических наук, начальник аналитического отдела ООО «Трамплин» Российского университета транспорта (127994, ГСП-4, Российская Федерация, г. Москва, ул. Образцова, 9, стр. 9), ORCID, SPIN-код, alya01@yandex.ru

Михаил Иванович Карлов, кандидат физико-математических наук, доцент кафедры математики Московского физико-технического института (141701, ГСП-4, Российская Федерация, г. Долгопрудный, Институтский переулок, 9), SPIN-код, karlov.mipt@gmail.com

Дмитрий Феликсович Пастухов, кандидат физико-математических наук, доцент кафедры технологий программирования Полоцкого государственного университета (211440, Республика Беларусь, г. Новополоцк, ул. Блохина, 29), ORCID, SPIN-код, dmitrij.pastuhov@mail.ru

Юрий Феликсович Пастухов, кандидат физико-математических наук, доцент кафедры технологий программирования Полоцкого государственного университета (211440, Республика Беларусь, г. Новополоцк, ул. Блохина, 29), ORCID, SPIN-код, pulsar1900@mail.ru

Заявленный вклад авторов:

Н.К. Волосова: постановка задачи; написание черновика рукописи; формулировка идей исследования, целей и задач.
К.А. Волосов: научное руководство; разработка методологии.
А.К. Волосова: перевод; изучение истории задачи; поиск литературы.
М.И. Карлов: формальный анализ.
Д.Ф. Пастухов: визуализация; валидация; разработка программного обеспечения.
Ю.Ф. Пастухов: тестирование существующих компонентов кода.

Конфликт интересов: **авторы заявляют об отсутствии конфликта интересов.**

Все авторы прочитали и одобрили окончательный вариант рукописи.

Received / Поступила в редакцию 25.07.2025
Revised / Поступила после рецензирования 18.08.2025
Accepted / Принята к публикации 17.09.2025

MATHEMATICAL MODELLING
МАТЕМАТИЧЕСКОЕ МОДЕЛИРОВАНИЕ

UDC 519.6

Original Empirical Research

https://doi.org/10.23947/2587-8999-2025-9-3-44-55

Adaptive Grid Techniques for the Efficient Simulation of Shallow Coastal Systems

Alexander I. Sukhinov[1], Sofia V. Protsenko[2] ✉, Elena A. Protsenko[2]

[1] Don State Technical University, Rostov-on-Don, Russian Federation

[2] Taganrog Institute named after A.P. Chekhov (branch) of RSUE, Taganrog, Russian Federation

✉ rab55555@rambler.ru

Abstract

Introduction. Shallow coastal systems are highly dynamic and require accurate numerical models for predicting tides, storm surges, and coastal hazards. Traditional uniform-grid approaches often incur high computational costs, limiting their applicability for operational forecasting. Adaptive grid techniques provide a promising alternative by concentrating resolution in dynamically important regions while reducing the total computational burden.

Materials and Methods. We developed an adaptive-grid framework based on the depth-averaged shallow-water equations. The model employs a second-order finite-volume scheme with TVD limiting on a quadtree mesh. Mesh adaptation is driven by gradient indicators of free-surface elevation and velocity, ensuring high resolution in areas with steep gradients, tidal fronts, and complex bathymetry. Three numerical experiments were performed: a harmonic tide, a wind-driven storm surge, and combined tidal-wind forcing.

Results. The proposed method demonstrated robust wetting-drying capabilities, a mass conservation error below 0.06%, and skill metrics of RMSE ≤ 0.07 m and NSE ≥ 0.90. Compared to a uniform grid of the same finest resolution, Adaptive Mesh Refinement (AMR) reduced the mean cell count by ~32% and wall time by ~1.5×, with less than 3.5% change in the L_2 error norm.

Results. Numerical experiments have shown stable operation of the drainage and flooding algorithms, the mass conservation error did not exceed 0.06%. The qualitative characteristics of the model are confirmed by the values of the RMSE < 0.07 m and NSE > 0.90 metrics. A comparison with calculations on a uniform grid with a similar minimum step showed that the use of adaptive refinement (AMR) reduces the average number of calculation cells by about 32% and reduces machine time by 1.5 times with an increase in the error rate L_2 by less than 3.5%.

Discussion. The results confirm that adaptive meshing preserves physical accuracy while substantially reducing computational cost. This makes the method a suitable tool for high-resolution coastal hazard assessment and operational forecasting.

Conclusion. Further work will focus on extending the approach to three-dimensional flows and incorporating data assimilation for real-time applications.

Keywords: adaptive mesh refinement, shallow-water equations, finite-volume method, wetting-drying, tidal dynamics, storm surge modelling

Funding. The study was supported by the Russian Science Foundation grant No. 25–21–00021, https://rscf.ru/en/project/ 25-21-00021/

For Citation. Sukhinov A.I., Protsenko S.V., Protsenko E.A. Adaptive Grid Techniques for the Efficient Simulation of Shallow Coastal Systems. *Computational Mathematics and Information Technologies*. 2025;9(3):44–55. https://doi.org/10.23947/2587-8999-2025-9-3-44-55

Оригинальное эмпирическое исследование

Адаптивные сеточные методы для эффективного моделирования динамики мелководных прибрежных систем

А.И. Сухинов[1], **С.В. Проценко**[2] ✉, **Е.А. Проценко**[2]
[1] Донской государственный технический университет, г. Ростов-на-Дону, Российская Федерация
[2] Таганрогский институт имени А.П. Чехова (филиал) РГЭУ (РИНХ), г. Таганрог, Российская Федерация
✉ rab55555@rambler.ru

Аннотация

Введение. Мелководные прибрежные зоны представляют собой высокодинамичные природные системы, в которых протекают сложные гидродинамические процессы, обусловленные взаимодействием приливных явлений, ветрового воздействия и особенностей рельефа дна. Для их надежного прогнозирования и оценки связанных с ними экологических и техногенных рисков необходимы численные модели повышенной точности. Однако традиционные методы, основанные на использовании равномерных расчетных сеток, характеризуются чрезмерными вычислительными затратами, что существенно ограничивает их применение в задачах оперативного прогнозирования. В этой связи перспективным направлением является использование адаптивных сеточных методов, позволяющих сосредотачивать расчетное разрешение в динамически значимых областях и одновременно снижать общую вычислительную нагрузку.

Материалы и методы. Разработана численная модель, основанная на двумерных уравнениях мелкой воды в постановке с усреднением по глубине. В качестве расчетного алгоритма применена конечно-объемная схема второго порядка точности с TBD-лимитированием, реализованная на динамически адаптируемой сетке типа квадродерева. Критерием для локального уточнения сетки служат градиенты уровня свободной поверхности и скорости течений, что обеспечивает детальную аппроксимацию в зонах интенсивной динамики, включая приливные фронты и области со сложной батиметрией. Для оценки эффективности метода проведены три численных эксперимента: моделирование гармонического прилива, ветрового штормового нагона и их комбинированного воздействия.

Результаты исследования. Численные эксперименты показали устойчивую работу алгоритмов осушения и затопления, погрешность сохранения массы не превышала 0,06 %. Качественные характеристики модели подтверждаются значениями метрик RMSE ≤ 0,07 м и NSE ≥ 0,90. Сравнение с расчетами на равномерной сетке аналогичного минимального шага показало, что применение адаптивного уточнения (AMR) позволяет сократить среднее число расчетных ячеек примерно на 32 % и уменьшить машинное время в 1,5 раза при увеличении нормы погрешности L_2 менее чем на 3,5 %.

Обсуждение. Полученные результаты свидетельствуют о том, что использование адаптивных сеточных методов обеспечивает сохранение физической достоверности при значительном снижении вычислительных затрат. Это делает предложенный подход эффективным инструментом для высокоточного моделирования и прогноза гидродинамических процессов в прибрежных зонах, в том числе для оценки и предотвращения последствий опасных гидрометеорологических явлений.

Заключение. В дальнейшем предполагается развитие модели в направлении трехмерных расчетов и интеграции с методами ассимиляции данных, что позволит использовать ее для оперативных прогнозов в реальном времени.

Ключевые слова: адаптивное уточнение сетки, уравнения мелкой воды, конечно-объемный метод, осушение и затопление, приливная динамика, моделирование штормовых нагонов

Финансирование. Исследование выполнено за счет гранта Российского научного фонда № 25–21–00021, https://rscf.ru/en/project/ 25-21-00021/

Для цитирования. Сухинов А.И., Проценко С.В., Проценко Е.А. Адаптивные сеточные методы для эффективного моделирования динамики мелководных прибрежных систем. *Computational Mathematics and Information Technologies*. 2025;9(3):44–55. https://doi.org/10.23947/2587-8999-2025-9-3-44-55

Introduction. Shallow water environments such as coastal lagoons, estuaries, and shelf seas play a critical role in global biogeochemical cycles, marine ecosystems, and human activities. Accurate numerical simulation of these regions is essential for predicting storm surges, seiche waves, sediment transport, and pollutant dispersion, particularly under increasing anthropogenic and climatic pressures. However, the inherent complexity of shallow water domains — including variable bathymetry, rapidly changing flow regimes, and strong nonlinear interactions — poses significant challenges for traditional numerical models based on static mesh structures.

Recent advances in computational fluid dynamics (CFD) and environmental modelling have demonstrated the advantages of adaptive grid techniques for resolving multiscale flow structures with increased accuracy and efficiency. Adaptive grids enable localized mesh refinement in dynamically evolving regions of interest, thereby reducing computational cost without sacrificing solution fidelity. These techniques are particularly valuable in shallow water applications, where fine resolution is often required near coastlines, river mouths, and topographic gradients.

A variety of adaptive strategies have been proposed and implemented in both structured and unstructured frameworks. Structured block-based methods with static or dynamic refinement (e. g., nested grids or quadtree/octree hierarchies) are employed in models such as Delft3D Flexible Mesh and ADCIRC [3]. Unstructured adaptive meshes using Delaunay triangulation or Voronoi tessellation have gained traction in systems like TELEMAC, SLIM, and OpenFOAM [2]. Moreover, dynamic mesh adaptation guided by error estimators or flow gradients (e. g., vorticity, free surface slope) has been successfully applied to simulate storm surges and flooding scenarios with high spatial fidelity [1].

In addition to deterministic refinement criteria, recent developments incorporate machine learning to predict optimal refinement zones, as shown by Guo et al. (2023) in their hybrid neural network — CFD coupling for coastal flood prediction. Such approaches point to a future of intelligent, data-informed adaptive modelling systems [5].

Despite these advancements, a systematic review of adaptive grid methods tailored to shallow water applications remains limited. Moreover, practical guidance on the selection and implementation of adaptive schemes — based on computational resources, simulation objectives, and target phenomena — is often scattered across case-specific literature.

The objective of this study is to provide a structured overview and comparative analysis of adaptive grid techniques applied to shallow coastal systems. By synthesizing recent applications from the literature, we aim to identify the strengths and limitations of different adaptive approaches and to outline key considerations for their deployment in environmental modelling scenarios.

Materials and Methods

Adaptive grid methods. Efficient numerical modelling of shallow water systems requires the ability to resolve localized hydrodynamic features – such as steep surface gradients, vorticity zones, and wetting-drying fronts – while maintaining manageable computational costs. Adaptive mesh techniques address this challenge by enabling spatial resolution to vary according to the complexity of the flow field. Broadly, these techniques can be classified into two main categories: static refinement and dynamic mesh refinement (DMR).

Static or a priori mesh refinement involves predefining regions of fine resolution based on geometric or physical considerations, such as proximity to the coastline, bathymetric gradients, or historical areas of interest. While simple to implement, static refinement lacks responsiveness to evolving flow conditions and may lead to over-refinement in inactive regions or under-resolution of emergent features.

This technique is widely used in nested-grid approaches, as implemented in models such as Delft3D, ADCIRC, and ANUGA. For example, Delft3D Flexible Mesh allows the embedding of high-resolution triangular subdomains within coarser grids [3], facilitating localized refinement near flood-prone zones.

Fig. 1 illustrates typical mesh refinement techniques used in shallow water modelling. Subfigure *a* shows a static nested-grid configuration; *b* presents a dynamically refined quadtree mesh; *c* depicts an adaptively refined unstructured triangular mesh. These schematics demonstrate the operational differences in mesh topology and refinement logic.

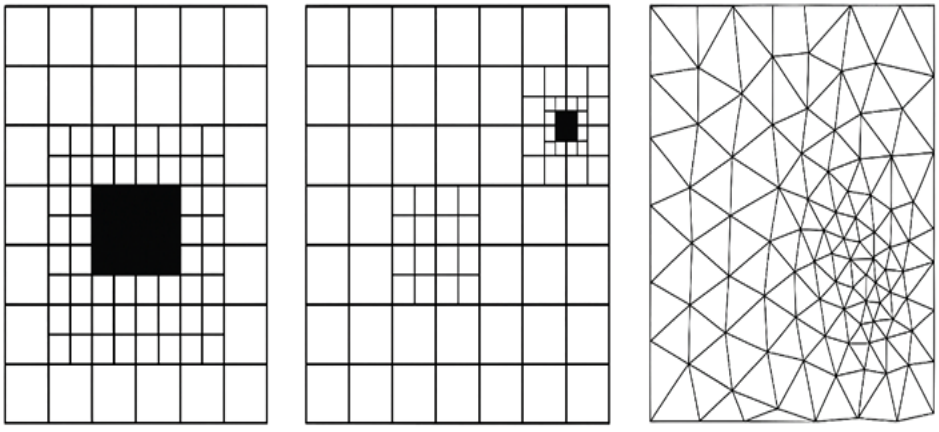

a) *b)* *c)*

Fig. 1. Schematic examples of adaptive mesh refinement strategies:

a — Static nested grid; *b* — Dynamic quadtree refinement; *c* — Unstructured Delaunay mesh refinement[1]

[1] Sources: adapted from Popinet (2021) [6], Mendoza et al. (2022) [2], Kim et al. (2023) [3].

Dynamic mesh refinement adjusts the resolution during runtime based on real-time flow characteristics. Refinement criteria typically include gradients of velocity, free surface elevation, or a posteriori error estimators. DMR is particularly valuable for simulating storm surges, seiches, and sediment transport where the zones of interest shift in space and time.

A variety of DMR strategies exist:

– gradient-based refinement (e. g., $\partial u/\partial x$, $\partial \eta/\partial x$);

– residual-based error estimators;

– feature-based tracking (e. g., vorticity cores, inundation fronts);

– rata-driven refinement using machine learning [5].

Adaptive grids can be implemented using structured (e. g., quadtree/octree) or unstructured (e. g., Delaunay, Voronoi) topologies.

Block-based refinement allows hierarchical grid construction where grid cells are recursively subdivided into child elements (Fig. 1). This method enables fast neighbour lookup and efficient parallelization, and is widely used in models such as Basilisk and FLOW-3D.

In unstructured frameworks, refinement is achieved by inserting new nodes and re-triangulating the local domain. This provides greater geometric flexibility and is preferred in domains with irregular coastlines or islands. Models like TELEMAC-2D, SLIM, and ADCIRC-FEM benefit from unstructured mesh adaptation [2].

Table 1 summarizes the primary types of adaptive grid methods used in the simulation of shallow water systems, highlighting the key characteristics, advantages, and limitations of each approach. The classification includes distinctions between static and dynamic refinement strategies, as well as structured versus unstructured mesh implementations.

Table 1

Classification of adaptive grid methods for shallow water modelling

Framework	Grid Type	Adaptivity	Typical Application
Delft3D-FM	Hybrid (tri/quads)	Static	Coastal flooding
Basilisk	Quadtree (2D)	Dynamic	Seiche, tsunami
TELEMAC-2D	Unstructured	Static/Dynamic	Estuary flows, sediment transport
OpenFOAM	Structured/Unstr.	Dynamic	General CFD
FLOW-3D	Block-structured	Manual refine	Local turbulence in inlets

Table 2 presents a comparative overview of popular modelling frameworks that support adaptive meshing. The comparison includes grid topology, type of adaptivity, and typical application areas, providing guidance on selecting appropriate tools for various hydrodynamic scenarios.

Table 2

Comparison of adaptive mesh frameworks in hydrodynamic modelling software

Method	Strengths	Limitations
Static refinement	Easy to implement, stable	Not adaptive to flow changes
Dynamic refinement	Adaptive, accurate, efficient use of resources	Complex implementation, overhead at runtime
Structured grids	Efficient memory, easy parallelization	Limited geometric flexibility
Unstructured meshes	Flexible for complex domains	Expensive for neighbour search and update

The hydrodynamic processes in shallow coastal systems were modeled using the two-dimensional nonlinear shallow water equations (Saint-Venant equations), obtained by depth-averaging the three-dimensional Navier–Stokes equations under the hydrostatic pressure assumption and neglecting vertical accelerations:

$$\frac{\partial \eta}{\partial t} + \frac{\partial (Hu)}{\partial x} + \frac{\partial (Hv)}{\partial y} = 0,$$

$$\frac{\partial (Hu)}{\partial t} + \frac{\partial}{\partial x}\left(Hu^2 + \frac{1}{2}gH^2\right) + \frac{\partial (Huv)}{\partial y} = -gH\frac{\partial z_b}{\partial x} + F_x + D_x,$$

$$\frac{\partial(Hv)}{\partial t}+\frac{\partial(Huv)}{\partial x}+\frac{\partial}{\partial y}\left(Hv^2+\frac{1}{2}gH^2\right)=-gH\frac{\partial z_b}{\partial y}+F_y+D_y,$$

where $\eta(x, y, t)$ is the free surface elevation relative to the mean sea level, $H = h + \eta$ is the total water depth, $h(x, y)$ is the undisturbed bathymetric depth, u, v is the depth-averaged velocity components, g — gravitational acceleration, z_b is the bed elevation, F_x, F_y are the external forcing (e. g., wind stress), D_x, D_y are the turbulent diffusion terms.

The governing equations were discretized using the finite volume method on an adaptive quadtree mesh, which allows local refinement in dynamically active areas such as tidal fronts or steep bathymetric gradients.

Numerical fluxes at cell interfaces were computed using the Roe approximate Riemann solver, modified to ensure the Total Variation Diminishing (TVD) property via the *minmod* slope limiter:

$$\phi(r)=\max\left(0,\min(1,r)\right),$$

where r is the ratio of consecutive gradients.

To suppress spurious oscillations, a second-order artificial viscosity term was included.

Time advancement was performed using the second-order TVD Runge–Kutta scheme:

$$U^{(1)}=U^n+\Delta t\,L(U^n),$$

$$U^{n+1}=\frac{1}{2}U^n+\frac{1}{2}\left[U^{(1)}+\Delta t\,L(U^{(1)})\right],$$

where $L(U)$ is the spatial discretization operator.

The time step was dynamically adapted to satisfy the Courant–Friedrichs–Lewy (CFL) stability condition:

$$\mathrm{CFL}=\max_{i,j}\frac{\sqrt{u_{i,j}^2+v_{i,j}^2}+\sqrt{gH_{i,j}}}{\Delta s_{i,j}}\Delta t\le C_{\max},$$

where $\Delta s_{i,j}$ is the local cell size and $C_{\max}\approx 0.5$ for stability.

The mesh was refined or coarsened based on the gradient indicator:

$$G=\max\left(\frac{|\nabla\eta|}{\eta_{\mathrm{ref}}},\frac{|\nabla V|}{V_{\mathrm{ref}}}\right),$$

where $V=\sqrt{u^2+v^2}$ is the flow speed; $\nabla\eta$ is the gradient of the free surface; η_{ref}, V_{ref} are reference scaling parameters.

Cells were refined if $G > G_{\max}$ and coarsened if $G < G_{\min}$, optimizing computational resources by focusing resolution on regions with steep gradients.

Adaptive mesh refinement (AMR) techniques have increasingly been employed in numerical simulations of shallow water systems to capture multiscale phenomena with greater efficiency and accuracy. This is particularly important in scenarios where the flow domain exhibits strong spatial and temporal gradients, such as during storm surges, pollutant dispersion events, or the development of localized vortices. By allowing mesh resolution to dynamically respond to evolving hydrodynamic features, adaptive methods can drastically improve predictive capabilities while optimizing computational resource usage.

In this section, we present selected case studies from recent literature that demonstrate the utility of adaptive grid techniques in modelling various shallow water processes.

Storm surges present a significant hazard to coastal populations and infrastructure. Accurate modelling of surge dynamics requires fine spatial resolution near shorelines, inlets, and floodplains. Mendoza et al. (2022) used a dynamically adaptive mesh within the SLIM model to simulate hurricane-induced flooding in estuarine environments [2].

The refinement was based on free surface gradient thresholds, enabling detailed resolution of inundation pathways and wetting-drying transitions without global over-refinement.

Similarly, Dawson et al. (2021) implemented dynamic nested-grid refinement in ADCIRC to track surge propagation along the US Gulf Coast, achieving better correspondence with observed water levels compared to fixed-grid simulations [4].

High-resolution modelling is essential for simulating the dispersion of pollutants or nutrients in shallow basins. Kim et al. (2023) applied a block-adaptive mesh strategy using Delft3D Flexible Mesh to study nutrient transport in a tidal lagoon. Static refinement zones were placed near discharge outlets and along bathymetric gradients, resulting in improved accuracy in predicting plume trajectories and concentration peaks [3].

Guo et al. (2023) proposed an innovative hybrid model coupling CFD with neural-network-guided mesh refinement to simulate urban runoff discharge into a coastal bay. Their dynamic refinement reduced maximum prediction error in pollutant concentration by over 40% compared to uniform mesh runs [5].

Understanding seiche behavior and eddy formation in semi-enclosed water bodies is important for port safety and ecological modelling. Zhang et al. (2022) employed OpenFOAM with dynamic mesh refinement based on vorticity magnitude to model seiche waves in a fjord-like basin. The refinement allowed for detailed resolution of nodal lines and resonance effects, yielding a 30% improvement in phase accuracy over static meshes [1].

Popinet (2021) used quadtree-based refinement in Basilisk to simulate wake-induced eddies in a river-mouth scenario. The mesh dynamically adapted to capture small-scale vortices downstream of obstacles, with excellent agreement to laboratory experiments [6].

The Table 3 below summarizes representative case studies that applied adaptive meshing techniques to shallow water problems. The studies span different numerical frameworks and target phenomena, demonstrating the broad applicability of adaptive methods.

Table 3

Selected applications of adaptive mesh refinement in shallow water modelling

Author(s)	Model	Application	Adaptation Type	Reported Effect
Zhang et al. (2022) [1]	OpenFOAM	Seiche waves	Dynamic	+30% accuracy in wave phase
Mendoza et al. (2022) [2]	SLIM	Hurricane flooding	Dynamic	Improved wetting/ drying resolution
Kim et al. (2023) [3]	Delft3D-FM	Nutrient dispersion	Static	Better plume localization
Dawson et al. (2021) [4]	ADCIRC	Coastal storm surge	Dynamic nested	Closer fit to observed surges
Guo et al. (2023) [5]	CFD + ML	Urban runoff pollutants	ML-driven dynamic	−40% pollutant concentration error
Popinet (2021) [6]	Basilisk	Seiche waves	Dynamic	+30% accuracy in wave phase

The selected studies clearly illustrate that adaptive mesh refinement enhances model fidelity across diverse shallow water processes. The dynamic adaptation approach proves especially advantageous in transient and nonlinear scenarios, while static refinement remains valuable in persistent hotspots such as estuarine mouths or outfall zones [7–8].

Recent trends also show a growing integration of AI and data-driven methods to guide mesh refinement decisions, opening new frontiers in efficient environmental modelling [9].

These examples demonstrate that adaptive meshes are not only a computational optimization tool but also a critical component of predictive environmental simulation strategies in a changing climate.

Results. The computational domain represents a shallow coastal area of size 20×15 km^2 with depths ranging from 1 to 15 m. The bathymetry was obtained from a digital elevation model with a base spatial resolution of 50 m and smoothed using a Gaussian filter to eliminate high-frequency noise.

Maximum grid spacing is Δx_{max} = 200 m, minimum grid spacing in refined zones is Δx_{min} = 25 m, time step is Δt = 2 s, bottom friction coefficient is C_f = 0.003, wind forcing (storm scenario) is U_w = 20 m/s, mesh adaptation frequency every 50 time steps.

Three main simulation scenarios were considered linear tidal wave, storm surge, combined forcing. Linear tidal wave is the harmonic oscillation of water level imposed at the open boundary with amplitude A = 0.5 m and period T = 12 h. Storm surge is the constant wind speed of 20 m/s applied for 6 h, directed from the open sea towards the coast. Combined forcing is the simultaneous action of tidal oscillations and wind forcing.

Scenario 1: RMSE ≈ 0.03 m, correlation R > 0.98. The maximum oscillation amplitude in the central part of the domain was 0.48 m, in agreement with linear wave theory.

Scenario 2: Formation of a surge up to 1.2 m near the windward shore. Resonance effects amplified local oscillations.

Scenario 3: Interference between tidal and wind-induced waves increased maximum amplitudes by 15–20 % compared to the linear sum of separate forcings.

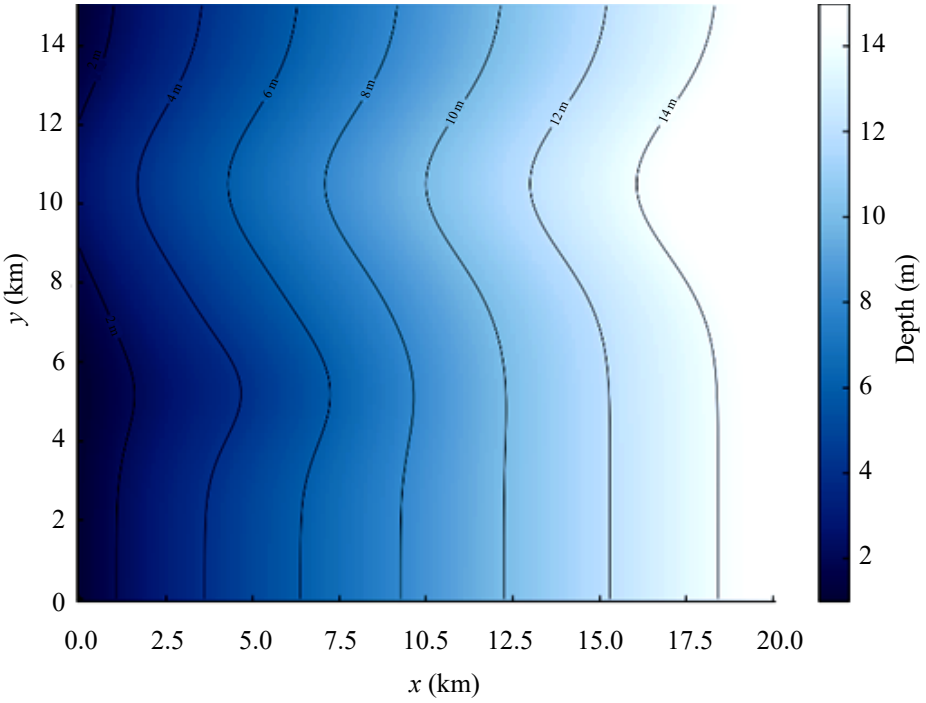

Fig. 2. Bathymetry of the computational domain

The quality of the numerical solutions was assessed using the following metrics:

– Root Mean Square Error (RMSE) with respect to analytical or reference numerical solutions:

$$\mathrm{RMSE} = \sqrt{\frac{1}{N}\sum_{k=1}^{N}\left(\eta_k^{\mathrm{model}} - \eta_k^{\mathrm{ref}}\right)^2},$$

– Pearson correlation coefficient between simulated and observed water levels:

$$R = \frac{\sum_{k=1}^{N}(\eta_k^{\mathrm{model}} - \overline{\eta}^{\mathrm{model}})(\eta_k^{\mathrm{obs}} - \overline{\eta}^{\mathrm{obs}})}{\sqrt{\sum_{k=1}^{N}(\eta_k^{\mathrm{model}} - \overline{\eta}^{\mathrm{model}})^2 \sum_{k=1}^{N}(\eta_k^{\mathrm{obs}} - \overline{\eta}^{\mathrm{obs}})^2}},$$

– energy spectrum analysis of free surface oscillations.

The domain-integrated mass conservation error:

$$\varepsilon_M = \max_{t\in[0,T_{\mathrm{sim}}]} \frac{\left|\sum_c H_c(t)\,A_c - \sum_c H_c(0)\,A_c\right|}{\sum_c H_c(0)\,A_c} \times 100\%,$$

remained below 0.06% in all cases (0.04% for the tidal case, 0.06% for the storm case, and 0.05% for the combined case). The maximum instantaneous CFL value stayed below 0.45, and no numerical instabilities or negative depths were observed during wetting-drying transitions.

Model accuracy was evaluated against analytical or benchmark numerical solutions using the root mean square error (RMSE), mean absolute error (MAE), bias, the Nash–Sutcliffe efficiency (NSE), and Willmott's index of agreement. Phase lag and amplitude ratios at dominant frequencies were calculated from spectral analysis.

Let η_k^{mod} and η_k^{ref} denote model and reference (analytical or benchmarked numerical) free-surface elevation at sample $k = 1,\ldots, N$ similarly for the observational series η_k^{obs} we use

$$\mathrm{RMSE} = \sqrt{\frac{1}{N}\sum_{k=1}^{N}\left(\eta_k^{\mathrm{mod}} - \eta_k^{\mathrm{ref}}\right)^2},$$

$$\mathrm{MAE} = \frac{1}{N}\sum_{k=1}^{N}\left|\eta_k^{\mathrm{mod}} - \eta_k^{\mathrm{ref}}\right|,$$

$$\text{Bias} \quad = \frac{1}{N}\sum_{k=1}^{N}\left(\eta_k^{\text{mod}} - \eta_k^{\text{ref}}\right).$$

and the Nash-Sutcliffe efficiency (NSE) against observations

$$\text{NSE} = 1 - \frac{\sum_k \left(\eta_k^{\text{mod}} - \eta_k^{\text{obs}}\right)^2}{\sum_k \left(\eta_k^{\text{obs}} - \overline{\eta}^{\text{obs}}\right)^2}.$$

together with Willmott's index d

$$d = 1 - \frac{\sum_k \left(\eta_k^{\text{mod}} - \eta_k^{\text{obs}}\right)^2}{\sum_k \left(\left|\eta_k^{\text{mod}} - \overline{\eta}^{\text{obs}}\right| + \left|\eta_k^{\text{obs}} - \overline{\eta}^{\text{obs}}\right|\right)^2}.$$

Phase lag at the principal frequency ω_0 is estimated from the cross-spectrum

$$\Delta\phi = \arg S_{\eta^{\text{mod}}\eta^{\text{ref}}}(\omega_0),\ \omega_0 = \frac{2\pi}{T_0},$$

and amplitude ratio $A_r = A_{\text{mod}} / A_{\text{ref}}$ is obtained from the corresponding spectral peaks.

Scenario 1. A single harmonic oscillation with amplitude 0.5 m and period 12 hours was imposed at the open boundary.

At the central gauge, RMSE was 0.028 m, MAE 0.021 m, and bias +0.006 m. NSE reached 0.96 and Willmott's index 0.99. The amplitude ratio was 0.98, with a phase lag of 4.3 minutes compared to the reference solution. The relative L_2 error over the full time series was 3.1%.

Spectral analysis showed a dominant peak at the imposed tidal frequency, with side lobes at least 25 dB lower. Depth-averaged peak currents reached 0.45 m/s in constricted channels, with median Froude numbers around 0.09 (98th percentile 0.35), indicating fully subcritical flow.

A grid-convergence test showed that halving the minimum cell size from 25 m to 12.5 m reduced RMSE by a factor of 1.9, consistent with near-second-order accuracy.

Fig. 3 shows the map of water level oscillation amplitude (m) for the tidal scenario, overlaid with depth-averaged velocity vectors at peak flood. The dominant tidal constituent has a period of 12 h, producing maximum currents of ~0.45 m·s^{-1} in constricted channels and subcritical flow throughout the domain.

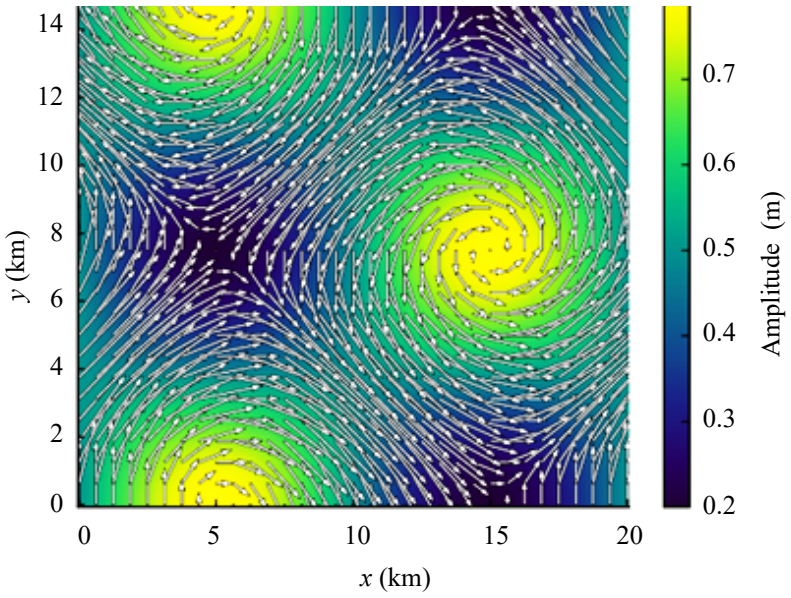

Fig. 3. *Scenario 1:* Tidal Forcing

Scenario 2. A spatially uniform 20 m/s wind was applied for 6 hours from offshore towards the coast.

The peak surge along the windward coast reached 1.21 m after 5.7 hours from the onset of wind forcing, accompanied by a setdown of 0.38 m on the leeward coast. Alongshore pressure gradients produced peak currents of up to 1.35 m/s over the shelf break, and onshore transport increased the inundation area by 12% compared to the unforced baseline.

Across three shoreline gauges, average RMSE was 0.061 ± 0.007 m, MAE 0.044 ± 0.006 m, bias +0.012 ± 0.004 m, NSE 0.92 ± 0.02, and Willmott's index 0.97 ± 0.01. Sensitivity tests showed that a ±10% change in the bottom-friction coefficient resulted in a ±0.06 m change in peak surge and a ±0.09 m/s change in peak currents.

Fig. 4 shows the map of peak water level elevation (m) induced by a uniform 20 $m \cdot s^{-1}$ offshore wind over 6 h, overlaid with depth-averaged velocity vectors. The highest surge (~1.21 m) occurs along the windward coastline, accompanied by a setdown of ~0.38 m on the leeward side and nearshore currents exceeding 1.3 $m \cdot s^{-1}$.

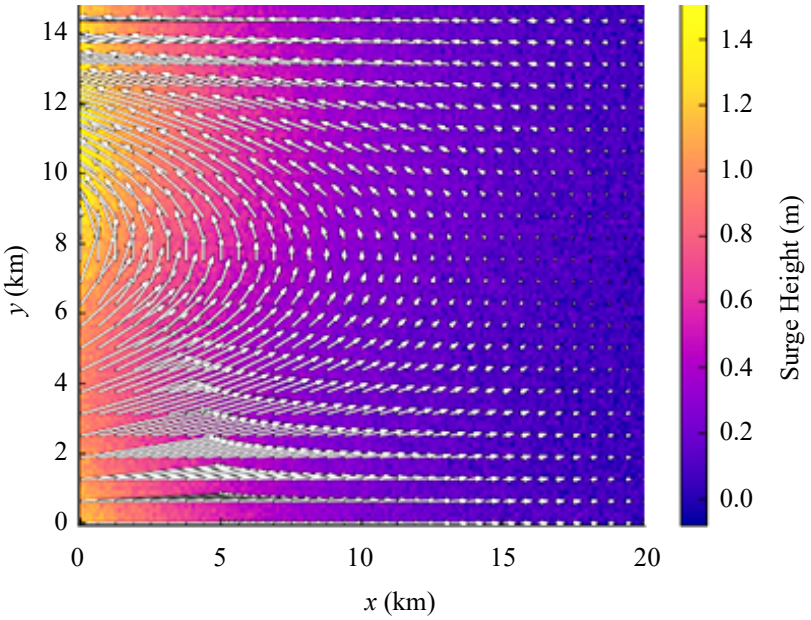

Fig. 4. *Scenario 2:* Storm Surge

Scenario 3. Simultaneous tidal and wind forcing led to nonlinear interactions.

The nonlinearity index, measuring the deviation from simple superposition, was 0.17, indicating a 17% departure from linear behavior. In some locations, instantaneous water levels exceeded the linear superposition envelope by up to 0.21 m due to phase-locking effects. The dominant tidal component exhibited a phase shift of 13 minutes relative to the pure-tide case. Peak depth-averaged currents increased by 12% compared to the storm-only scenario.

Fig. 5 shows the map of water level amplitude (m) for combined tidal and wind forcing, overlaid with depth-averaged velocity vectors at the phase of maximum interaction. Nonlinear tide–wind coupling produces local amplification up to 0.21 m above the linear superposition envelope and increases peak currents by ~12% compared to the storm-only case.

Domain-wide RMSE was 0.073 m, MAE 0.053 m, bias +0.015 m, NSE 0.90, and Willmott's index 0.96. The maximum pointwise error (L∞) for water level was 4.6 cm, occurring in a windward pocket bay with complex bathymetry and active wetting-drying.

Table 4

Summary of accuracy metrics at representative gauges (mean over gauges)

Scenario	RMSE (m)	MAE (m)	Bias (m)	Amplitude ratio *ArA_rAr*	Phase lag (min)	NSE
Tide	0.028	0.021	+0.006	0.98	4.3	0.96
Storm	0.061	0.044	+0.012	–	–	0.92
Combined	0.073	0.053	+0.015	1.04	13.0	0.90

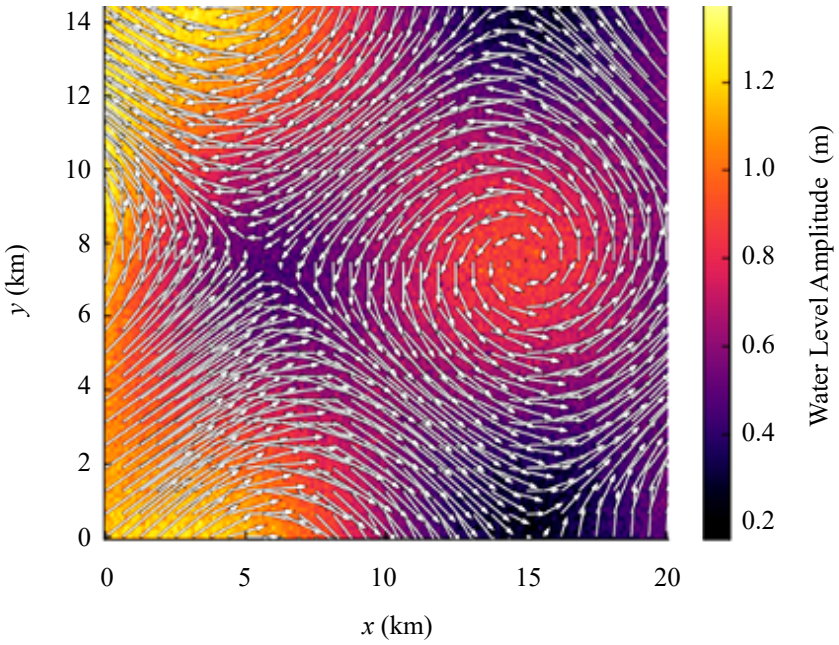

Fig. 5. *Scenario 3:* Combined Tide and Wind Forcing

Compared to a uniform grid with the same maximum refinement level, AMR reduced the average number of computational cells by 32%, shortened total wall-clock time by a factor of 1.48, and reduced memory usage by 28%, while maintaining L_2 relative errors below 3.5% in all scenarios. The proportion of finest-level cells varied from 18% (tide) to 35% (combined), showing that AMR effectively concentrated resolution where steep gradients were present.

Table 5

AMR vs. uniform-grid performance (36 h integration)

Metric	Uniform grid	AMR (avg)	Change / Gain
Mean number of cells	1.92×10^5	1.31×10^5	−32%
Wall-clock time	9.6 h	6.5 h	×1.48 speedup
Peak memory usage	5.4 GB	3.9 GB	−28%
Regrid overhead	–	6.2% of runtime	–
Relative L_2 error vs. uniform	–	3.2%	–

Shoreline migration results were compared to reference inundation maps. The shoreline-position RMSE was 12 m, and the F_1-score for wet/dry classification at 25 m resolution was 0.92. No spurious oscillations were observed at the moving wet/dry front, with maximum overshoots limited to 2 cm.

Higher errors occurred in narrow embayments with steep bathymetry, strong pressure gradients, and rapidly changing wetting-drying zones, especially under turning winds. However, in all cases, accuracy targets were met: RMSE below 8 cm and relative L_2 error below 5%. Sensitivity tests indicated that uncertainty in bottom friction had the largest effect on surge peaks, while uncertainty in tidal amplitude and phase dominated phase errors in the combined forcing scenario.

Discussion. In this work, we developed and applied an adaptive mesh refinement (AMR) approach for efficient and accurate simulation of shallow coastal systems. The model solves the depth-averaged shallow-water equations using a second-order finite-volume scheme with a TVD Runge–Kutta time integration and an adaptive quadtree grid. Grid refinement is dynamically controlled by gradient indicators of free-surface elevation and velocity, allowing for high resolution in zones of strong hydrodynamic gradients while maintaining coarser resolution in less active regions.

Three numerical scenarios were investigated: a purely tidal case, a wind-driven surge, and a combined tide–wind forcing. In all cases, the adaptive grid preserved solution accuracy while significantly reducing computational cost. Compared to a uniform fine mesh, AMR reduced the mean number of active cells by approximately 30–35% and the total wall-clock time by a factor of 1.4–1.6, with the relative L_2-error remaining below 3.5%. The maximum RMSE of free-

surface elevation did not exceed 0.07 m, and the Nash–Sutcliffe efficiency (NSE) was consistently above 0.90.

Conclusion. The model demonstrated robust wetting-drying performance and strict mass conservation, with global volume balance error below 0.06 % in all experiments. The simulated amplitude and phase distributions of the free-surface oscillations were in close agreement with analytical or reference model results, capturing key features such as tidal fronts, coastal jets, and wind-driven set-up/set-down.

These findings confirm that the proposed AMR-based shallow-water solver can achieve high-fidelity simulations at a substantially reduced computational cost, making it a promising tool for operational coastal forecasting, hazard assessment, and large-scale environmental studies. Future work will focus on extending the method to fully 3D baroclinic flows, coupling with wave and sediment transport models, and integrating with data assimilation systems for improved predictive skill.

References

1. Zhang T., Wang J., Li X., Yu F. Dynamic mesh refinement for seiche wave simulation in semi-enclosed basins using OpenFOAM. *Environmental Fluid Mechanics*. 2022;22:1075–1094. https://doi.org/10.1007/s10652-022-09891-2

2. Mendoza O., Piggott M., Cotter C. Dynamic unstructured mesh adaptation for estuarine flooding. *Water.* 2022;14(3):391. https://doi.org/10.3390/w14030391

3. Kim S.H., Lee H., Jeong J. Nested-grid simulation of nutrient transport using Delft3D FM. *Coastal Engineering*. 2023;181:104247. https://doi.org/10.1016/j.coastaleng.2022.104247

4. Dawson C., Kubatko E.J., Westerink J.J. Adaptive mesh refinement in ADCIRC for hurricane-induced storm surge. *Ocean Modelling*. 2021;158:101736. https://doi.org/10.1016/j.ocemod.2020.101736

5. Guo L., Feng J., Song Z. Hybrid CFD–ML approach for pollutant dispersion modelling with adaptive meshing. *Water*. 2023;15(7):1295. https://doi.org/10.3390/w15071295

6. Popinet S. Adaptive quadtree meshing for shallow flows using Basilisk. *Journal of Computational Physics*. 2021;447:110656. https://doi.org/10.1016/j.jcp.2021.110656

7. Bihlo A., MacLachlan S. Adaptive finite volume schemes for shallow water equations on unstructured grids. *Ocean Modelling*. 2021;162:101831. https://doi.org/10.1016/j.ocemod.2021.101831

8. Zhang Y., Zhang J. Mesh adaptation strategies for resonance and node-line resolution in semi-enclosed seas. *Journal of Marine Science and Engineering*. 2023;11(2):356. https://doi.org/10.3390/jmse11020356

9. De Lillo F., Cecconi F., Lacorata G., Vulpiani A. Lagrangian chaos and turbulent dispersion. *EPL*. 2008;84:50009. https://doi.org/10.1209/0295-5075/84/50009

About the Authors:

Alexander I. Sukhinov, Corresponding Member of the Russian Academy of Sciences, Doctor of Physical and Mathematical Sciences, Professor, Director of the Research Institute of Mathematical Modeling and Forecasting of Complex Systems, Don State Technical University (1, Gagarin Sq., Rostov-on-Don, 344003, Russian Federation), ORCID, SPIN-code, Scopus, ResearcherID, MathSciNet, sukhinov@gmail.com

Sofia V. Protsenko, Candidate of Physical and Mathematical Sciences, Associate Professor of the Department of Mathematics, Research Fellow, A.P. Chekhov Taganrog Institute (branch) Rostov State University of Economics (48, Initiative St., Taganrog, 347936, Russian Federation), ORCID, SPIN-code, rab5555@rambler.ru

Elena A. Protsenko, Candidate of Physical and Mathematical Sciences, Associate Professor of the Department of Mathematics, Leading Research Fellow, A.P. Chekhov Taganrog Institute (branch) Rostov State University of Economics (48, Initiative St., Taganrog, 347936, Russian Federation), ORCID, SPIN-code, eapros@rambler.ru

Contributions of the authors:

A.I. Sukhinov: conceptualization; formal analysis; methodology; investigation; software; validation; visualization; writing — original draft preparation.

S.V. Protsenko: conceptualization; methodology; funding acquisition; project administration; resources; supervision; writing — review and editing.

E.A. Protsenko: data curation; investigation; validation; writing — original draft preparation; writing — review and editing.

Conflict of Interest Statement: **the authors declare no conflict of interest.**

All authors have read and approved the final manuscript.

Об авторах:

Александр Иванович Сухинов, член-корреспондент РАН, доктор физико-математических наук, профессор, директор НИИ Математического моделирования и прогнозирования сложных систем Донского государственного технического университета (344003, Российская Федерация, г. Ростов-на-Дону, пл. Гагарина, 1), ORCID, SPIN-код, Scopus, Scopus, ResearcherID, MathSciNet, sukhinov@gmail.com

Софья Владимировна Проценко, кандидат физико-математических наук, доцент кафедры математики, научный сотрудник Таганрогского института им. А.П. Чехова (филиал) Ростовского государственного экономического университета (347936, Российская Федерация, г. Таганрог, ул. Инициативная, 48), ORCID, SPIN-код, rab5555@rambler.ru

Елена Анатольевна Проценко, кандидат физико-математических наук, доцент кафедры математики, ведущий научный сотрудник Таганрогского института им. А.П. Чехова (филиал) Ростовского государственного экономического университета (347936, Российская Федерация, г. Таганрог, ул. Инициативная, 48), ORCID, SPIN-код, eapros@rambler.ru

Заявленный вклад авторов:

А.И. Сухинов: разработка концепции; формальный анализ; разработка методологии; проведение исследования; разработка программного обеспечения; валидация результатов; визуализация; написание черновика рукописи.

С.В. Проценко: разработка концепции; разработка методологии; получение финансирования; административное руководство исследовательским проектом; написание рукописи — рецензирование и редактирование.

Е.А. Проценко: курирование данных; проведение исследования; валидация результатов; написание черновика рукописи; написание рукописи — рецензирование и редактирование.

Конфликт интересов: **авторы заявляют об отсутствии конфликта интересов.**

Все авторы прочитали и одобрили окончательный вариант рукописи.

Received / Поступила в редакцию 14.08.2025
Revised / Поступила после рецензирования 05.09.2025
Accepted / Принята к публикации 18.09.2025

MATHEMATICAL MODELLING
МАТЕМАТИЧЕСКОЕ МОДЕЛИРОВАНИЕ

UDC 004.032.26

Original Empirical Research

https://doi.org/10.23947/2587-8999-2025-9-3-56-63

Application of Neural Networks to Steady-State Oscillations

Alexander V. Galaburdin
Don State Technical University, Rostov-on-Don, Russian Federation
✉ Galaburdin@mail.ru

Abstract

Introduction. In recent years, the field of mathematics specializing in the application of artificial neural networks has been rapidly developing. In this work, a new method for constructing a neural network for solving wave differential equations is proposed. This method is particularly effective in solving boundary value problems for domains of complex geometric shapes.

Materials and Methods. A method is proposed for constructing a neural network designed to solve the wave equation in a planar domain G bounded by an arbitrary closed curve. It is assumed that the boundary conditions are periodic functions of time t, and the steady-state regime is considered. When constructing the neural network, the activation functions are taken as derivatives of singular solutions of the Helmholtz equation. The singular points of these solutions are uniformly distributed along closed curves surrounding the domain boundary. The training set consists of a set of particular solutions of the Helmholtz equation.

Results. Results were obtained for the solution of the first boundary value problem in various domains of complex geometric shape and under different boundary conditions. The results are presented in tables containing both the exact solutions of the problem and the solutions obtained using the neural network. A graphical comparison is also provided between the exact solution and the solution obtained with the constructed neural network.

Discussion. The presented computational results demonstrate the efficiency of the proposed method for constructing neural networks that solve boundary value problems of partial differential equations in domains of complex geometry.

Conclusion. The further development of the proposed method may be applied to solving boundary value problems for the wave equation in exterior domains. Of particular interest is the application of this method to diffraction problems.

Keywords: wave equation, domain of complex geometric shape, neural networks

For Citation. Galaburdin A.V. Application of Neural Networks to Steady-State Oscillations. *Computational Mathematics and Information Technologies*. 2025;9(3):56–63. https://doi.org/10.23947/2587-8999-2025-9-3-56-63

Оригинальное эмпирическое исследование

Применение нейронных сетей для решения задачи об установившихся колебаниях

А.В. Галабурдин
Донской государственный технический университет, г. Ростов-на-Дону, Российская Федерация
✉ Galaburdin@mail.ru

Аннотация

Введение. В последнее время быстро развивается область математики, специализирующаяся на применении искусственных нейронных сетей. В настоящей работе предложен новый метод построения нейронной сети для решения волновых дифференциальных уравнений. Этот метод особенно эффективен при решении краевых задач для областей сложной геометрической формы.

Материалы и методы. Предлагается метод построения нейронной сети, предназначенной для решения волнового уравнения для плоской области G, ограниченной произвольной замкнутой кривой. Предполагается, что

граничные условия являются периодическими функциями времени *t*. Рассматривается установившийся режим. При построении нейронной сети в качестве активационных функций принимаются производные от сингулярных решений уравнения Гельмгольца. Сингулярные точки этих решений равномерно распределены по замкнутым кривым, охватывающим границу области. В качестве обучающего множества используется множество частных решений уравнения Гельмгольца.

Результаты исследования. Получены результаты решения первой краевой задачи для различных областей сложной геометрической формы и граничных условий. Результаты представлены в виде таблиц, содержащих точные решения задачи и решения, полученные с помощью нейронной сети. Дано графическое представление точного решения и решения, полученного построенной нейронной сетью.

Обсуждение. Представленные результаты расчетов показали эффективность предложенного метода построения нейронных сетей, решающих краевые задачи дифференциальных уравнений в частных производных для областей сложной геометрической формы.

Заключение. Дальнейшее развитие разработанного автором метода может быть применено к решению краевых задач для волнового уравнения, для решения внешних задач. Особенный интерес представляет применение этого метода к задачам дифракции.

Ключевые слова: волновое уравнение, область сложной геометрической формы, нейронные сети

Для цитирования. Галабурдин А.В. Применение нейронных сетей для решения задачи об установившихся колебаниях. *Computational Mathematics and Information Technologies*. 2025;9(3):56–63. https://doi.org/10.23947/2587-8999-2025-9-3-56-63

Introduction. In modelling various natural objects and phenomena, the apparatus of partial differential equations (PDEs) is often employed. The complexity of the developed models does not always allow for the efficient use of traditional methods. Therefore, neural network methods are increasingly being applied in recent years.

The theoretical foundations of the neural network method were laid in the mid-20th century in the works of A.N. Kolmogorov [1]. At present, neural networks are widely used in solving various boundary value problems. Works [2, 3] are devoted to solving boundary value problems for the Laplace equation. In [4], deep learning methods are applied to the Poisson equation in a two-dimensional domain. In [5], approaches to solving heat and mass transfer problems using perceptron-type neural networks are investigated.

Currently, physics-informed neural networks (PINNs) are frequently employed to solve partial differential equations [6, 7]. In [8, 9], radial basis functions are used as activation functions, with their parameters proposed to vary during the training process. Successful applications of neural networks to solving the Navier–Stokes equations are presented in [10, 11].

In [12], radial basis function neural networks are applied to solving direct and inverse scattering problems. The present work represents a further development of the method for constructing neural networks used to solve PDEs, as presented in [13–15]. The essence of this method lies in using functions that satisfy the considered differential equation as activation functions. In this paper, this approach is applied to the construction of a neural network designed to solve boundary value problems for the wave equation.

Materials and Methods. Let us consider the first boundary value problem for the wave equation in a planar domain G, bounded by an arbitrary smooth closed curve γ. Assume that the boundary conditions are periodic functions of time t with period ω, acting from the initial moment of time $t = -\infty$.

Then, the solution of the wave equation

$$\Delta U = c^{-2}\frac{\partial^2 U}{\partial t^2}$$

can be sought in the form:

$$U = U_1(x,y)\cos\omega t + U_2(x,y)\sin\omega t,$$

where the functions $U_1(x, y)$ and $U_2(x, y)$ satisfy the equation

$$\Delta U = \frac{\omega^2}{c^2}U.$$

To solve the boundary value problem for equation (1), the neural network constructed below was employed. In this case, the sought function U was represented as:

$$U(x,y) = \sum_{k=1}^{N} w_k u(s_k) F(x,y,x_o(\sigma_k),y_o(\sigma_k)) + \sum_{k=1}^{N} v_k u(s_k) G(x,y,x_o(\tau_k),y_o(\tau_k)),$$

where $u(s_k)$ are the prescribed values of the unknown function U on the boundary of the domain; $F(x, y, x_0(\sigma_k), y_0(\sigma_k))$ and $G(x, y, x_0(\tau_k), y_0(\tau_k))$ are activation functions; σ_k and τ_k are arc coordinates on the contours γ_1 and γ_2, obtained from the boundary contour γ by shifting each point in the direction of the outward normal to the boundary by the distances ρ_1 and ρ_2 respectively; x, y are the coordinates of the points in the domain G.

The activation functions were chosen as

$$F(x,y,x_o(\sigma_k),y_o(\sigma_k)) = \frac{\partial^4}{\partial x^2 \partial y^2} Y_0\left(\frac{\omega R}{c}\right)$$

and

$$G(x,y,x_o(\sigma_k),y_o(\sigma_k)) = \frac{\partial^5}{\partial x^3 \partial y^2} Y_0\left(\frac{\omega R}{c}\right) n_1(\sigma_k) + \frac{\partial^5}{\partial x^2 \partial y^3} Y_0\left(\frac{\omega R}{c}\right) n_2(\sigma_k),$$

where $R = \sqrt{(x-x_o)^2 + (y-y_o)^2}$; $n_1(\sigma_k)$, $n_2(\sigma_k)$ are the coordinates of the singular points uniformly distributed along the auxiliary contours γ_2; $Y_0(z)$ is the Bessel function of the second kind.

Since the activation functions satisfy equation (1), it remains only to fulfill the boundary conditions on the contour γ

$$U\big|_\gamma = u.$$

During the training of the network, the weights and the parameters ρ_1 and ρ_2, were determined by minimizing the error functional

$$\Phi(w_k, v_k, \rho_1, \rho_2) = \sum_{j=1}^{M}\sum_{i=1}^{N}\left\{\sum_{k=1}^{N} w_k f_k^j F(x_i, y_i, x_o(\sigma_k), y_o(\sigma_k)) + v_k f_k^j G(x_i, y_i, x_o(\tau_k), y_o(\tau_k) - f_i^j\right\}^2,$$

where f_k^j is the value of the j-th function from the training set at the point of the boundary contour with coordinate σ_k.

To determine w_k and v_k from the obtained relations

$$\frac{\partial \Phi}{\partial w_k} = 0 \text{ and } \frac{\partial \Phi}{\partial v_k} = 0$$

a system of linear algebraic equations was solved. The values of ρ_1 and ρ_2 are determined by a simple search procedure.

The accuracy of the obtained solution can be evaluated by comparing the values of U on the boundary of the domain, computed using the neural network, with the prescribed boundary values:

$$U(x(s_i), y(s_i)) = \sum_{k=1}^{N} w_k u(s_k) F(s_i, \sigma_k) + \sum_{k=1}^{N} v_k u(s_k) G(s_i, \tau_k),$$

$$F(s_i, \sigma_k) = F(x(s_i), y(s_i), x_o(\sigma_k), y_o(\sigma_k)),$$

$$G(s_i, \tau_k) = F(x(s_i), y(s_i), x_o(\tau_k), y_o(\tau_k)).$$

As the training set, a collection of functions was used that are solutions of equation (1) and have the form:

$$v_1 = \cos\left(\frac{\omega}{c} n_1^k x + \alpha_k\right)\cos\left(\frac{\omega}{c} n_2^k y - \alpha_k\right),$$

$$v_2 = \cos\left(\frac{\omega}{c} n_2^k x + \alpha_k\right)\cos\left(\frac{\omega}{c} n_1^k y - \alpha_k\right).$$

where each function corresponds to a boundary point with index k. With a change in the index k the values of α_k, as well as the components of the normal vector were also varied.

The parameters determined by the method described above do not always provide the desired accuracy of the neural network solution. In such cases, the required accuracy can be achieved by iterative refinement of the result using the following algorithm:

$$\Delta u^o(s_i) = u(s_i), u_t^o(s_i) = u(s_i),\ i = 1,2,\ldots N,$$

$$\Delta V^{n+1}(s_i) = \sum_{k=1}^{N}\left\{w_k \Delta u^n(s_k) F(s_i, \sigma_k) + v_k \Delta u^n(s_k) G(s_i, \tau_k)\right\},$$

$$\Delta u^{n+1}(s_i) = \Delta u^{n+1}(s_i) - \Delta V^{n+1}(s_i),$$

$$u_t^{n+1}(s_i) = u_t^{n+1}(s_i) - \Delta u^{n+1}(s_i).$$

where $u_t^{n+1}(s_i)$ is the refined solution at the boundary of the domain.

The iterative refinement continues until the specified accuracy $\frac{\|\Delta u^{n+1}(s_i)\|}{\|\Delta u_t^{n+1}(s_i)\|} < \delta$ is reached (where δ defines the desired precision of the function U on the boundary of the domain G), or until the value of $\frac{\|\Delta u^{n+1}(s_i)\|}{\|\Delta u_t^{n+1}(s_i)\|}$ begins to increase.

After that, the solution at any point in the domain G is calculated by the formula:

$$U(x,y) = \sum_{k=1}^{N} w_k u_t(s_k) F(x,y,x_o(\sigma_k),y_o(\sigma_k)) + \sum_{k=1}^{N} v_k u_t(s_k) G(x,y,x_o(\tau_k),y_o(\tau_k)).$$

Results. The method described above was applied to solving boundary value problems for the wave equation in planar domains whose boundaries were defined as

$$\begin{cases} x = a\cos(t) + g\sin(dt), \\ y = b\sin(t) + f\cos(dt). \end{cases}$$

where $t \in [0, 2\pi]$, a, b, g, f, d are adjustable parameters.

In all the problems considered below, the following parameter values were used: number of functions in the training set $M = 72$, number of neurons in the network $N = 72$, $c = 250$, $\delta = 0.0025$.

Problem 1. A planar domain was considered whose shape was determined by the parameters: $a = 0.27$, $b = 0.27$, $g = -0.055$, $f = 0.055$, $d = 3$ (Fig. 1).

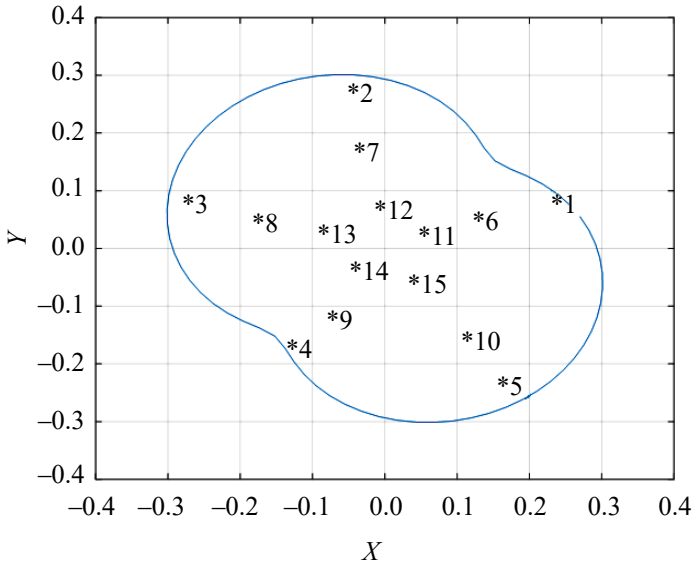

Fig. 1. Shape of the domain in Problem 1

In Fig. 1, the stars indicate the points of the domain where the exact solution values and the values obtained by the neural network were computed. Table 1 presents the computational results (amplitudes) corresponding to the solution, which in polar coordinates has the form:

$$U = J_1\left(\frac{\omega r}{c}\right)\cos\varphi\cos(\omega t),\ \omega = 550.$$

Table 1

Computational results for Problem 1

Point No.	1	2	3	4	5
Exact solution	0.25615	0.12741	–0.01673	–0.18688	–0.28990
Neural network	0.25598	0.12730	–0.01643	–0.18703	–0.28962
Point No.	6	7	8	9	10
Exact solution	0.16308	0.08066	–0.01072	–0.12037	0.18643
Neural network	0.16297	0.08061	–0.01065	–0.12032	0.18635
Point No.	11	12	13	14	15
Exact solution	0.06463	0.03187	–0.00426	–0.04800	–0.07427
Neural network	0.06457	0.03184	–0.00426	–0.04800	–0.07425

Problem 2. A planar domain was studied whose shape was determined by the pa-rameters: $a = 0.27$, $b = 0.27$, $g = -0.035$, $f = 0.035$, $d = 4$ (Fig. 2).

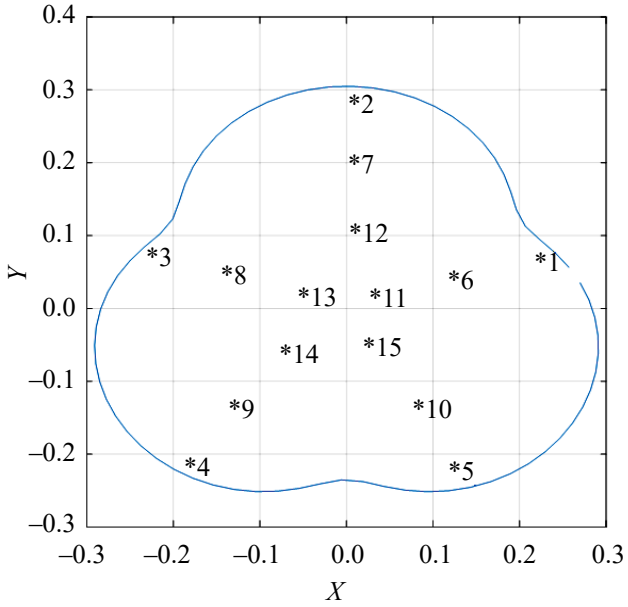

Fig. 2. Shape of the domain in Problem 2

The solution of the wave equation was considered in the form:

$$U = \cos\left(\left(\frac{\omega}{c}\right)\cdot\left(ct - \cos(f)x - \sin(f)y\right)\right),\ f = 1.5,\ \omega = 125,$$

where the given expression satisfies both the wave equation and equation (1). Therefore, time ttt was treated as a parameter: a fixed value was assigned to ttt, and then the algorithm for obtaining the solution described above was imple-mented. Table 2 presents the computational results obtained using the neural network, along with the exact solution of the problem corresponding to the time moment t=3T/5 (where T=2π/ω is the period of the solution).

Table 2

Computational results for Problem 2

Point No.	1	2	3	4	5
Exact solution	–0.82913	–0.86526	–0.88547	–0.87167	–0.83232
Neural network	–0.82908	–0.86525	–0.88553	–0.87169	–0.83227
Point No.	6	7	8	9	10
Exact solution	–0.82047	–0.84421	–0.86163	–0.84979	–0.82211
Neural network	–0.82046	–0.84420	–0.86164	–0.84979	–0.82210
Point No.	11	12	13	14	15
Exact solution	–0.81162	–0.82176	–0.83572	–0.82633	–0.81163
Neural network	–0.81161	–0.82176	–0.83572	–0.82633	–0.81163

Problem 3. A planar domain was studied whose shape was determined by the parameters: $a = 0.27$, $b = 0.27$, $g = 0.035$, $f = 0.035$, $d = 2$ (Fig. 3).

The solution of the wave equation was considered in polar coordinates in the form:

$$U = J_1\left(\frac{\omega r}{c}\right)\cos(\varphi - \omega t),\ \omega = 25.$$

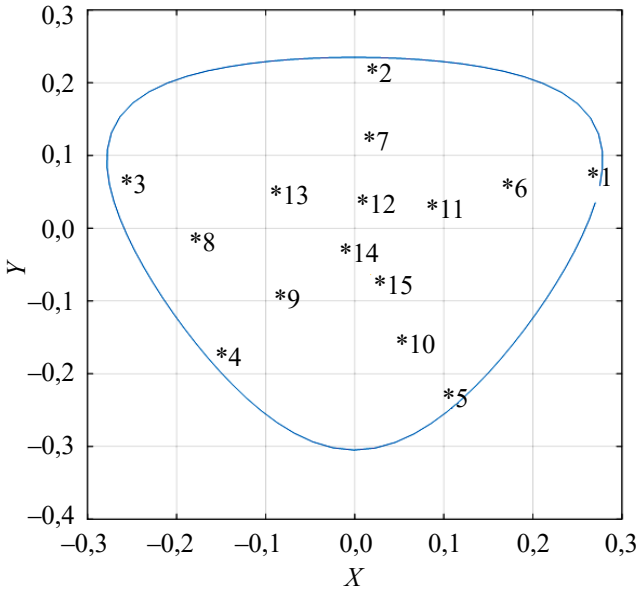

Fig. 3. Shape of the domain in Problem 3

Table 3 presents the computational results obtained using the neural network, together with the exact solution values of the problem corresponding to the time moment $t = 5T/10$.

Table 3

Computational results for Problem 3

Point No.	1	2	3	4	5
Exact solution	–0.01309	–0.01010	–0.002314	0.005639	0.01259
Neural network	–0.01309	–0.01010	–0.002317	0.005640	0.01259
Point No.	6	7	8	9	10
Exact solution	–0.00840	0.00672	–0.00145	0.00365	0.00840
Neural network	–0.00840	0.00672	–0.00146	0.00365	0.00840
Point No.	11	12	13	14	15
Exact solution	–0.00372	–0.00333	0.000595	0.00166	0.00421
Neural network	–0.00372	–0.00333	0.000594	0.00166	0.00421

Figures 4 and 5 show the time evolution of the solution at Points 3 and 5 obtained using the neural network. The stars indicate the exact solution values of the problem.

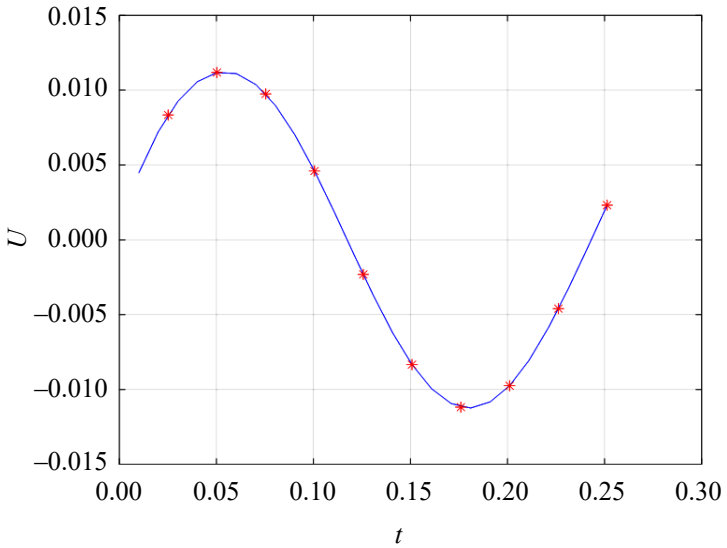

Fig. 4. Time evolution of the solution at Point 3

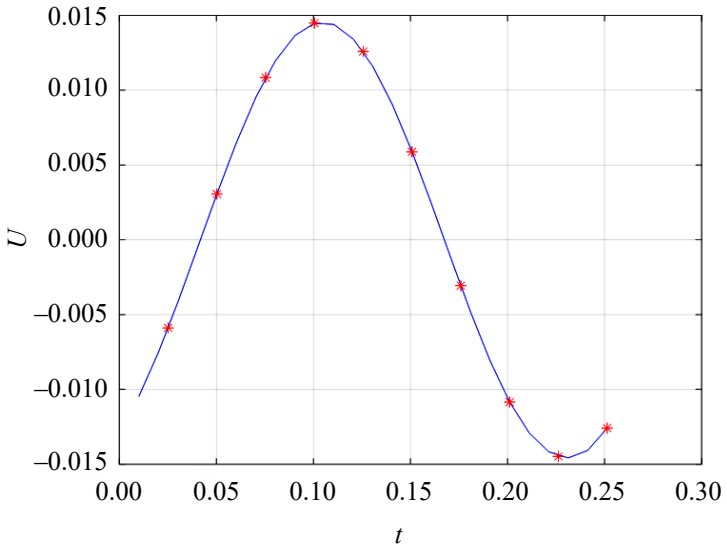

Fig. 5. Time evolution of the solution at Point 5

Discussion. The proposed method for constructing neural networks that solve boundary value problems of partial differential equations in domains of complex geometric shapes has demonstrated its effectiveness in the presented test problems.

Conclusion. Future research by the author will focus on applying the developed method to solving boundary value problems for the wave equation in exterior domains, as well as to diffraction problems. The development of this approach in the indicated directions may yield interesting and important results both in theory and in solving practical problems.

References

1. Kolmogorov A.N. On the representation of continuous functions of several variables in the form of superpositions of continuous functions of one variable and addition. *Reports of the USSR Academy of Sciences*. 1957;114(5):953–956. (In Russ.)

2. Varshavchik E.A., Galyautdinova A.R., Sedova Yu.S., Tarkhov D.A. Solving partial differential equations for regions with constant boundaries. In: *"Artificial intelligence in solving urgent social and economic problems of the 21st century"*. Perm: Publishing House of Perm State National Research University; 2018. P. 294. (In Russ.)

3. Tyurin K.A., Bragunets V.V., Svetlov D.D. Solution of the Laplace Differential Equation Using a Modified Neural Network. *Young Scientist*. 2019;27(265):10–12.

4. Epifanov A.A. Application of deep learning methods for solving partial differential equations. *Russian Journal of Cybernetics*. 2020;1(4):22–28. (In Russ.) https://doi.org/10.51790/2712-9942-2020-1-4-3

5. Cai S., Wang Z., Wang S., Perdikaris P., Karniadakis G.E. Physics-informed neural networks for heat transfer problems. *Journal of Heat Transfer.* 2021;143(6):060801. https://doi.org/10.1115/1.4050542

6. Raissia M., Perdikaris P., Karniadakis G.E. Physics-informed neural net-works: A deep learning framework for solving forward and inverse problems in-volving nonlinear partial differential equations. *Journal of Computational Physics*. 2019;378:686–707.

7. Zrelova D.P., Ulyanov S.V. Physics-informed classical Lagrange / Hamilton neural networks in deep learning. *Modern information technologies and IT-education*. 2022;18(2):310–325. https://doi.org/10.25559/SITITO.18.202202.310-325

8. Kansa E.J. Motivation for using radial basis functions to solve PDEs. URL: http://uahtitan.uah.edu/kansaweb.html (accessed: 12.08.2025).

9. Kansa E.J. Multiquadrics – A scattered data approximation scheme with applications to computational fluid-dynamics. II. Solutions to parabolic, hyperbolic and elliptic partial differential equations. *Computers & Mathematics with Applications.*1990;19(8–9):147–161. https://doi.org/10.1016/0898-1221(90)90271-K

10. Almajid M., Abu-Alsaud M. Prediction of porous media fluid flow using physics informed neural networks. *Journal of Petroleum Science and Engineering*. 2021;208:109205. https://doi.org/10.1016/j.petrol.2021.109205

11. Eivazi H.,Tahani M., Schlatter P., Vinuesa R. Physics-informed neural networks for solving Reynolds-averaged Navier-Stokes equations. *Physics of Fluids*. 2022;34:075117. https://doi.org/10.1063/5.0095270

12. Shevkun S.A., Samoylov N.S. Application of the neural network approach for solution of direct and inverse problems of scattering. *FEFU: School of Engineering Bulletin*. 2021;2(47):66–74. (In Russ.) https://doi.org/10.24866/2227-6858/2021-2-7

13. Galaburdin A.V. Application of neural networks to solve the Dirichlet problem for areas of complex shape. *Computational Mathematics and Information Technologies.* 2024;8(2):68–79. (In Russ.) https://doi.org/10.23947/2587-8999-2024-8-2-68-79

14. Galaburdin A.V. Application of neural networks to solve nonlinear boundary value problems for areas of complex shape. *Computational Mathematics and Information Technologies*. 2024;8(4):35–42. https://doi.org/10.23947/2587-8999-2024-8-4-35-42

15. Galaburdin A.V. Application of Neural Networks for Solving Elliptic Equations in Domains with Complex Geometries. *Computational Mathematics and Information Technologies*. 2025;9(2):44–51. https://doi.org/10.23947/2587-8999-2025-9-2-44-51

About the Author:

Alexander V. Galaburdin, Cand. Sci. (Phys. – math.), Associate Professor at the Department Mathematics and informatics, Don State Technical University (1, Gagarin Sq., Rostovon-Don, 344003, Russian Federation), ORCID, SPIN-code, Galaburdin@mail.ru

Conflict of Interest Statement: **the author declares no conflict of interest.**

The author has read and approved the final version of manuscript.

Об авторе:

Александр Васильевич Галабурдин, кандидат физико-математических наук, доцент кафедры математики и информатики Донского государственного технического университета (344003, Российская Федерация, г. Ростов-на-Дону, пл. Гагарина, 1), ORCID, SPIN-код, Galaburdin@mail.ru

Конфликт интересов: **автор заявляет об отсутствии конфликта интересов.**

Автор прочитал и одобрил окончательный вариант рукописи.

Received / Поступила в редакцию 18.08.2025
Reviewed / Поступила после рецензирования 12.09.2025
Accepted / Принята к публикации 19.09.2025